Binder Jetting of Aqueous Polyvinyl Alcohol for Additive Manufacturing of Inconel 718

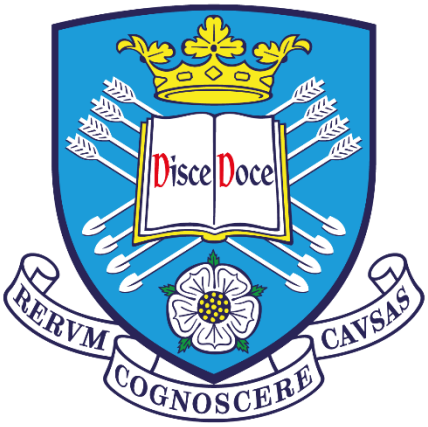

Sourabh Paul

Department of Mechanical Engineering

The University of Sheffield

A dissertation submitted for the degree of

Doctor of Philosophy

May 2022

Binder Jetting of Aqueous Polyvinyl Alcohol for Additive Manufacturing of Inconel 718

Sourabh Paul

Department of Mechanical Engineering

The University of Sheffield

A dissertation submitted for the degree of

Doctor of Philosophy

May 2022

'Tandem Felix'

- André-Marie Ampère

Declaration of Intent

All sentences or passages quoted in this document from other people's work have been specifically acknowledged by clear cross referencing to author, work, and page(s). Any illustrations that have not been generated by the author of this dissertation have been cited clearly with credit given to the illustrator. The contents of this dissertation have not been submitted in whole or in part for consideration for any other degree in any other university. The author understands that failure to abide the rules and regulations of the University of Sheffield regarding plagiarism would result in failure to complete the course.

Sourabh Paul

May 2022

Hatfield, Hertfordshire, UK

…Who then knows whence it has arisen

Whether God's will created it, or whether He was mute;

Perhaps it formed itself, or perhaps it did not;

The supreme Creator of the world, all pervasive and all knowing;

He indeed knows – or maybe not.

- Nasadiya Sukta, Rigveda

দাদু ও ঠামুর স্মৃতিতে

Acknowledgements

The author would like to thank his supervisor, **Dr Kamran Mumtaz** for the faith that was reposed on his capability. This journey started with an email which was sent to him on a hot and humid day in Madras in a moment of caffeine induced confidence.

The advice, encouragement and guidance of **Dr Patrick Smith** is humbly acknowledged. The project would not have been possible without the facilities of the Ink Jet Printing laboratory and the quiet, calm confidence which he instilled in the author with his kind words.

The role of **Wendy Birtwistle**, **Kurt Bonser** and **Jack Leach** was critical to the completion of the project without compromising the structural integrity of the university premises. The author also thanks them for their warm friendship along with the many cups of hot tea and discussions about cocktails, D&D and how the world would be a much better place with some 'fist'. In hindsight, these interactions were probably much more valuable in the grand scheme of life.

The author would like to thank **Chris Hill**, **Zhilun Lu**, **Prof Ian Reaney**, **Chris Todd, Richard Kay,** and **Tes Monaghan** for their help in the last stages of experiments.

The journey to a PhD has often been described as a dry one where solitude is one's best friend. The author gratefully acknowledges the part played by **Farshid**, **James**, **Ashfaque**, **Sirajum**, **Serena** and **Oliver** in proving it otherwise. The support of **Mohammed Al-Saddah**, **Ashfaq Khan** and **Zicheng Zhu** in and out of the workplace was instrumental in easing the difficulty.

The author salutes his parents for their infinite patience, sacrifice, and unconditional love while the author pretended to work on a wet rock, far away from the familiarity and verdure of home.

'Health is wealth' was a saying which was drilled into the author's mind from a young age. The profundity of this could not have been any starker for a person who struggled with chronic health issues during a pandemic. The capable staff of the **Royal Hallamshire Hospital, Sheffield** made sure that it did not break him.

Lastly, the author hails the spirit of Sheffield. The Steel City taught him that perfection and quirkiness can co-exist and that life, like chips; if taken with a generous dose of Henderson's relish, is beautiful.

ABSTRACT

Binder Jetting is an Additive Manufacturing technique which has been commercially available since 1996. It is characterised by the fabrication of three-dimensional components directly from a CAD model where the binder is selectively deposited on a powder bed repeatedly till the component is completely 'printed'. Commercial Binder Jetting systems use binders which are proprietary, typically resins that are difficult to handle and store due to safety and environmental concerns. This increases the costs of the manufacturing processes involving Binder Jetting and decreases its appeal to the manufacturing industry.

Binder Jetting of Inconel 718 has not been studied thoroughly till date. This thesis explores the feasibility of using aqueous solution of polyvinyl alcohol as liquid binders, for the first time, for Binder Jetting of Inconel 718, a precipitation strengthened nickel super alloy. Liquid binder was made using deionised water and polyvinyl alcohol of different molecular weights. The metal powder was mixed with dry polyvinyl alcohol powder to make a modified feedstock as a novel approach. Printability was established by printing small cubical samples, and the process was then scaled up by printing tensile specimens. The freshly printed green parts were cured and sintered in different gas purged atmosphere to investigate the role of sintering environments on product quality, focusing on porosity and mechanical strength. Hot isostatic pressing was performed on some of the samples to study the effect of post-processing on the sintered parts.

It was inferred that the polyvinyl alcohol, having a molecular weight of 26,000 g/mol was the most suitable candidate as the combination of the liquid binder and modified feedstock, yielded the highest green strength, lowest porosity. Tensile strength and hardness of all the sintered samples were found to be low, but the specimens sintered in an argon environment improved their tensile strength by a factor of 4.26 after post-processing. Phase analysis of the parts indicated the absence of deleterious phases like σ, δ and Laves phases in the specimens.

CONTENTS

List of Figures

List of Tables

List of Abbreviations

Additive Manufacturing	**AM**
Selective Laser Melting	**SLM**
Binder Jetting	**BJT**
Polyvinyl alcohol	**PVA**
Fused Deposition Modelling	**FDM**
Laminated Object Manufacturing	**LOM**
Electron Beam Melting	**EBM**
Ultrasonic Additive Manufacturing	**UAM**
Directed Energy Deposition	**DED**
Laser Engineered Net Shaping	**LENS**
Direct Metal Deposition	**DMD**
Hot Isostatic Pressing	**HIP**
Powder Bed Fusion	**PBF**
Continuous inkjet printing	**CIJ**
Drop on Demand	**DOD**
Body Centred Cubic	**BCC**
Hexagonal Close Packed	**HCP**
Face Centred Cubic	**FCC**
Particle size diameter	**PSD**
Scanning electron microscope	**SEM**
Thermogravimetric analysis	**TGA**
Variable Flow Rate	**VFR**
Programmable Logic Controller	**PLC**
Metal Injection Moulding	**MIM**
X ray diffraction	**XRD**
Ultimate Tensile Strength	**UTS**

CHAPTER 1: RESEARCH CHALLENGE & NOVELTY STATEMENT

'*You type words in an MS Word document, my toddler can do that and be cuter at it*' – ***a slightly irritated member of security staff upon discovering the author in the office at 01:30 AM***

1.1. Problem Statement

Additive Manufacturing (AM) is described as a process of joining materials to fabricate objects from 3D model data, usually layer upon layer, as opposed to subtractive manufacturing methodologies.

Polymer systems have traditionally dominated the consumer market and have an extensive role in making the technology 'visible' to people, metal additive manufacturing has been seen to be a keystone in solving the requirements of the aerospace, automotive, energy and bio-medical sector.

Nickel superalloys have been of interest to the aerospace industry because of its ability to retain its properties in high temperature conditions [1-3]. However, conventional manufacturing methods like casting, forming, and machining have proven to be cost prohibitive and wasteful for processing niche alloys like Inconel 625 and 718 [4-6].

Laser powder bed fusion techniques such as Selective Laser Melting (SLM) enjoys the confidence of the industry which had started taking baby steps towards incorporating AM in the manufacturing of their products when this PhD stated. Companies with manufacturing as their core competency have now started looking at AM, especially at SLM as a solution to maximise productivity while maintaining judicious use of resources and raw materials.

The process has its drawbacks in processing certain materials due to certain unique material characteristics. Aluminium and copper, as an example are difficult to process using SLM due to their low emissivity which causes the material to partially reflect the laser, reducing it melting

capability [7-9]. Inconel 718 is a precipitation strengthened alloy which derives its strength from niobium-nickel inter-metallics which are precipitated into the bulk of the medium. The rapid thermal inertia of SLM causes the niobium to separate out, which causes weakening of the alloy [10-11]. It is important to adopt a technique which can process Inconel 718 and is more material agnostic than SLM.

Binder Jetting (BJT) is a powder bed technique which prints a 'green part' by spreading a binder on every layer of powder. The green part is then sintered in a furnace using thermal cycles strategically to control the phases which develop during the sintering process. However, BJT is often marketed as an expensive AM technique owing to using expensive proprietary binders, which being a consumable, is a high recurring cost. The binders also require special storage conditions and require special handling overheads due to its toxic composition. Printheads are also customised and often are cost prohibitive, which discourage the industry from adopting it as the 'go-to' AM solution. The exploration and adoption of binders that are easy to manufacture, store and handle would open the AM market and increase the accessibility of the technology to industry. The novelty of the present work is the use of an aqueous PVA solution as a binder in a standard inkjet system for binder jetting of a niche strategic material Inconel 718. Binder jetting of Inconel 718 is, as such, a significantly less investigated process, even using commercial systems. For the first time, a unique approach has been attempted to dope the metallic Inconel 718 feedstock with PVA to facilitate synergic interaction between the modified feedstock and aqueous PVA binder.

1.2. Aim and Objectives of Research

1.2.1 Aim

The development of an aqueous polyvinyl alcohol-based binder and a modified feedstock which are simple to manufacture, handle, store, and dispose, specifically focusing on its composition, and looking at its effectiveness at being jetted from a capillary inkjet printhead, without compromising on effectiveness of the binder.

1.2.2 Objectives

- Investigating the role of composition of the binder on process responses such as green strength, porosity, and mechanical properties and comparing it with competing technologies.
- Investigating the role of sintering environment and its effect on process responses like porosity and mechanical properties and comparing it with competing technologies.

1.3. Thesis Structure

Chapter 2 will focus on the literature available of the following:

- Additive Manufacturing – definition and classification.
- General introduction to Binder Jetting and Ink Jetting
- Nickel superalloys processed by Binder Jetting

Chapter 2 is there to introduce the reader to the general principles of AM, stressing on the classifications of different AM techniques before focusing on Binder Jetting and Ink Jetting methods.

Chapter 3 will describe the experimental methodology followed throughout the study including elaboration on the choice of materials including metal powders and binders. The characterisation procedure and mechanical testing would also be discussed. The preliminary focus was to prepare water-based binders and test its jettability from the print head, which was done on a trial basis. It would also describe the process of making the different hybrid feedstock which were used throughout this investigation.

Chapters 4 – 7 each have an introduction section which would include a more focused literature review which is relevant to the chapter and topic under discussion. These chapters will focus on:

- **Chapter 4** – The first part of the chapter focuses on the powder rheology of the hybrid feedstock and compares it with the powder received as is from the manufacturer. It evaluates the suitability of the hybrid feedstock for Binder Jetting based on the process responses. The second part of the chapter looks at the rheological studies of the liquid binders developed and evaluates their jettability by calculating the Ohnesorge number.
- **Chapter 5** – This chapter discusses the interaction between the feedstock and the binder droplets by measuring the contact angle between the powder bed and the binder droplets. It explores the role played by the molecular weight of the polymer-based binders on their wettability and evaluates their suitability by measuring the flexural strength of printed green parts.
- **Chapter 6** – The chapter focuses on the porosity seen in parts which are printed using different PVA based binders and feedstock and sintered in different sintering environments. This is where the effectiveness of the jetting action of the print-head is investigated and how it is better than manual deposition of binders on a powder bed is analysed. The effect of post-processing strategies like HIP on porosity are also seen and discussed.
- **Chapter 7** – The results of mechanical testing including tensile testing and hardness are investigated here. The effect of different sintering environments is observed and a correlation between the mechanical properties and porosity is established.
- **Chapter 8** – All the results are summarised in the Conclusions chapter and future work is explored.

References

1. Akande IG, Oluwole OO, Fayomi OS, Odunlami OA. Overview of mechanical, microstructural, oxidation properties and high-temperature applications of superalloys. Materials Today: Proceedings. 2021 Jan 1; 43:2222-31.
2. Rame J, Utada S, Bortoluci Ormastroni LM, Mataveli-Suave L, Menou E, Després L, Kontis P, Cormier J. Platinum-containing new generation nickel-based superalloy for single crystalline applications. In Superalloys 2020 (pp. 71-81). Springer, Cham.
3. Perrut M, Caron P, Thomas M, Couret A. High temperature materials for aerospace applications: Ni-based superalloys and γ-TiAl alloys. Comptes Rendus Physique. 2018 Dec 1;19(8):657-71.
4. Zhang D, Feng Z, Wang C, Wang W, Liu Z, Niu W. Comparison of microstructures and mechanical properties of Inconel 718 alloy processed by selective laser melting and casting. Materials Science & Engineering A. 2018 May 2; 724: 357-367.
5. Hakeem AS, Patel F, Minhas N, Malkawi A, Aleid Z, Ehsan MA, Sharrofna H, Al Ghanim A. Comparative evaluation of thermal and mechanical properties of nickel alloy 718 prepared using selective laser melting, spark plasma sintering, and casting methods. Journal of Materials Research & Technology. 2021 June; 12: 870-881.
6. Gomes MC, dos Santos AG, de Oliveira D, Figueiredo GV, Ribeiro KS, Los Rios D, Barragán GA, da Silva MB, Coelho RT, Hung WN. Micro-machining of additively manufactured metals: a review. The International Journal of Advanced Manufacturing Technology. 2021 Sep 28:1-20.
7. Colopi M, Caprio L, Demir AG, Previtali B. Selective laser melting of pure Cu with a 1 kW single mode fiber laser. Procedia CIRP. 2018 Jan 1; 74:59-63.

8. Popovich A, Sufiiarov V, Polozov I, Borisov E, Masaylo D, Orlov A. Microstructure, and mechanical properties of additive manufactured copper alloy. Materials Letters. 2016 Sep 15; 179:38-41.
9. Ponnusamy P, Rahman Rashid RA, Masood SH, Ruan D, Palanisamy S. Mechanical properties of SLM-printed aluminium alloys: a review. Materials. 2020 Sep 26; 13(19):4301.
10. Tucho WM, Cuvillier P, Sjolyst-Kverneland A, Hansen V. Microstructure and hardness studies of Inconel 718 manufactured by selective laser melting before and after solution heat treatment. Materials Science and Engineering: A. 2017 Mar 24; 689:220-32.
11. Wang L, Cui R, Li BQ, Jia X, Yao LH, Su YQ, Guo JJ, Liu T. Influence of laser parameters on segregation of Nb during selective laser melting of Inconel 718. China Foundry. 2021 Jul;18(4):379-88.

CHAPTER 2: BACKGROUND AND LITERATURE REVIEW

'Tea first, cite later' – **a tea deprived author while compiling this review**

2.1. What is Additive Manufacturing?

2.1.1. Additive Manufacturing – Definition

Additive manufacturing is a term used to refer to a group of technologies which manufacture three dimensional, fully functionals parts, directly from a CAD model. The parts are usually made layer, upon layer. The CAD model is 'sliced' into several horizontal models using a specialised software. These slices are then replicated by the printer in an incremental manner.

AM has been defined officially as a process of joining materials to make objects from 3D model data, usually layer upon layer, as opposed to subtractive manufacturing methodologies by ASTM [1]. Subtractive methods like machining and grinding achieve dimensional and geometric tolerances by removing excess material in the form of chips. However, AM technologies build the part incrementally from the first to the final layer using a suitable raw material. This raw material can be in powder form (Selective Laser Melting, Electron Beam Melting and Binder Jetting), wire form (Fused Deposition Modelling and Wire Arc Additive Manufacturing) and even sheets (Sheet Lamination). The list of important parameters differs based on the additive manufacturing process used.

2.1.2. Classification of Additive Manufacturing Techniques

There are several ways in which AM techniques can be classified. The most conventional way it is usually done based on the form in which the material is deposited in every cycle. The material may be fed into the machine in the form of a wire and then be extruded out of a nozzle in molten form or may be used in granular form and be melted using a directed energy source. The following

section elaborates on some of the different AM processes which have a very different set of capabilities and advantages and are used either exclusively or inclusively for metals.

2.1.2.1. Melt Extrusion based Additive Manufacturing

These collection of AM processes would be characterised as deposition of molten material which is extruded via a nozzle. The material may be supplied to the machine in the form of a solid filament which is then molten by the aid of heaters and is then deposited as per the CAD model fed to the machine.

Fused deposition modelling (FDM) is an industrial translation of the melt extrusion-based AM which was trademarked by Stratasys Inc [2]. The material is supplied to a nozzle, usually in the form of a filament from a spool and is then heated inside the nozzle after which it is deposited in a molten state. The nozzle can move throughout the length and breadth of the substrate via a CNC enabled gantry system. Figure 2.1 represents the procedure schematically. The FDM process is a good choice for making inexpensive components which do not necessarily require high dimensional tolerances and surface finish. The nozzle follows the principle of Joules heating to melt the filament. The list of polymers which are processed by FDM is ever increasing, but some of the commonly processed polymers are nylon, acrylonitrile butadiene styrene and polylactic acid [3].

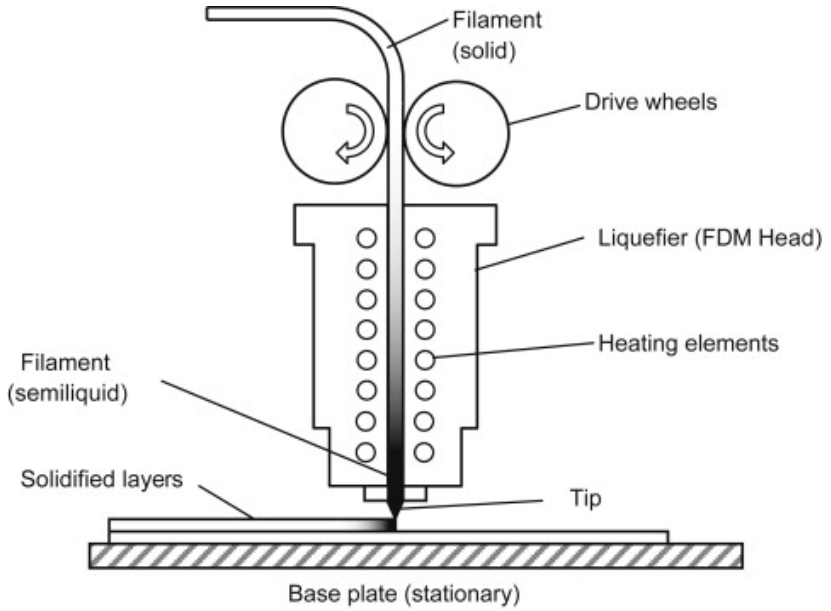

Fig 2.1 Schematic diagram of a Fused Deposition Modelling setup [4]

2.1.2.2. Sheet Lamination based Additive Manufacturing

Sheet lamination-based AM techniques share a common platform where each layer is a whole sheet or ribbon which is joined to the previous bulk of the component using joining techniques like solid state welding and adhesives. The sheet lamination technique is logistically easy to carry out, has low cost of operation and requires low energy as the material is not completely melted. The sheets can be separately cut into customised shapes and then be joined together, or the shape can be realised via a post processing method using wire cut electro discharge machine or end milling.

Laminated Object Manufacturing (LOM) involves the fabrication of parts by bonding sheets of paper using adhesive. This method is typically not suggested for making components for withstanding a structural load [5].

Ultrasonic Additive Manufacturing (UAM) is a sheet lamination-based AM technique that joins sheets of metal using ultrasonic welding. A sheet of metal, usually aluminium, copper, and stainless steel is laid onto the substrate bed and is vibrated ultrasonically. The heat generated melts the contacting interfaces leading to solid state welding. UAM is effectively used to make large parts in

an economical manner [5]. Complex geometries are realised with the aid of subtractive manufacturing processes, often as a post-processing feature.

2.1.2.3. Directed Energy Deposition

Directed Energy Deposition (DED) is an umbrella term which is used for defining a group of technologies which is characterised by the material being supplied either in the form of a wire or in the powder form and an energy source like an electron beam, laser or a plasma arc which is used to melt the material being fed. DED processes are done almost exclusively for metals and they have proved to be very useful in the repair and maintenance of existing parts which are difficult to replace. Figure 2.2 (a) and (b) are the schematic diagrams of the two different setups which use a metal wire and powder as the raw material of the DED process.

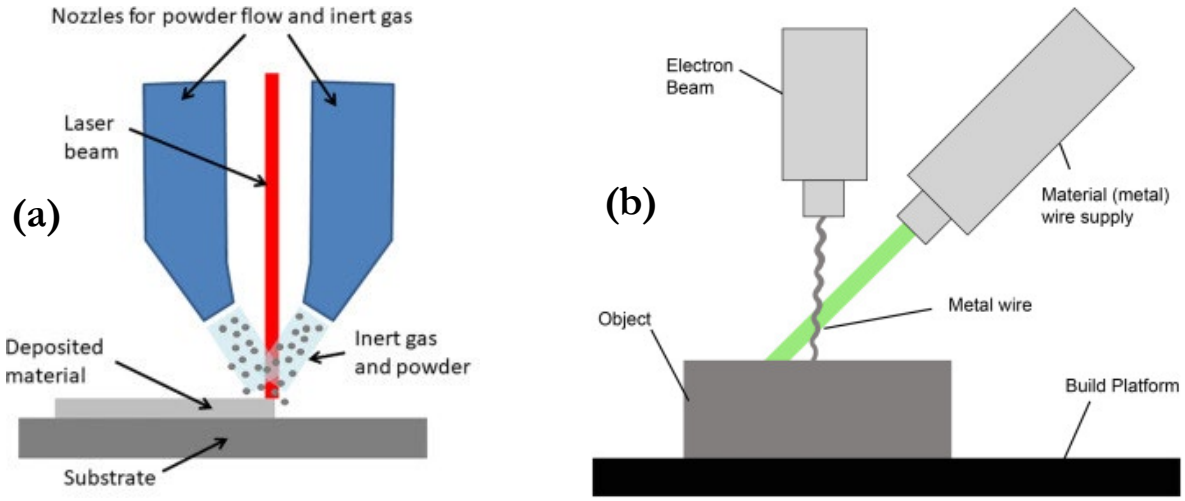

Fig 2.2 Schematic diagrams two different types of DED processes: (a) powder blown DED with laser melting [6] (b) wire fed DED with electron beam melting [7]

Some of the more particular terms used are Laser Engineered Net Shaping (LENS), Laser Cladding and Direct Metal Deposition (DMD).

DMD is a laser aided AM technique which was patented by the University of Michigan [8]. The process is started by directing a laser beam at the substrate/bulk of the component and creating a

melt pool in which a small amount of material in powder form is injected, thus creating a fresh layer. This process has proved to be useful in controlling the process parameters very precisely which resulted in components which had customised microstructure and mechanical properties, especially of those materials that cannot be cast, be thermos-mechanically processed or by powder metallurgy [9]. The same technique is referred to as LENS, mostly in academic circles.

Laser cladding, as the name suggests, is a technique which is used to coat or clad a substrate material with another material with the help of a laser source. The material may be fed in the form of an aerosol (hence also termed as a 'powder blown' technique) or a solid wire. An inert environment is maintained by argon flushing to prevent oxidation of the molten metal. The technique is useful because it can precisely control the coating rate which helps the operator to optimise between productivity and coating finesse and can be increased or decreased as per the localised demand in the component [10].

2.1.2.4. Powder Bed Fusion

The term 'Powder Bed Fusion' is used to define a set of AM technologies that is characterised by a flat powder bed where the material is arranged in the form of a static thin layer of powder and is then melted by using lasers or an electron beam as an energy source. Figure 2.3 is a schematic representation of a commercial SLM system. The powder is deposited in front of the wiper arm from the hopper which is then spread over the powder bed. The laser selectively scans regions according to the current horizontal plane which is obtained from the sliced CAD diagram and the build chamber platform moves down by a predetermined amount which is equal to the layer thickness of the build. SLM as a technology is very suitable for building prototypes very quickly. The manufacturing industry quickly realised that SLM as a process could compress manufacturing cycles and was valuable during the design phase where the iterative nature of designing would often prove to be very expensive using tradition manufacturing processes like casting, forming or

even metal injection moulding. However, SLM has several challenges when it comes to processing certain classes of materials like copper and aluminium alloys due to their reflective surfaces [11-13].

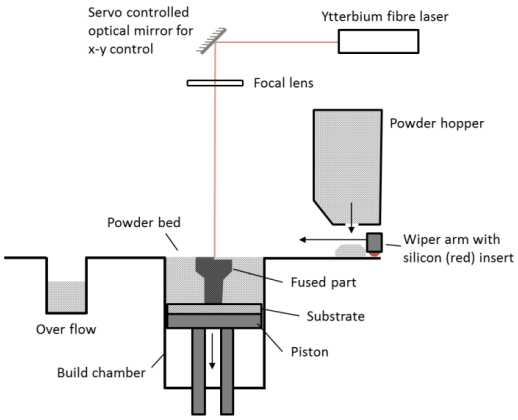

Fig 2.3 Schematic diagram of a commercial SLM system [14]

2.2 Inkjet Printing – an overview

2.2.1 Introduction

Inkjet printing is a technique in which a liquid is deposited on a substrate in a controlled manner using a printhead. The liquid is often referred to as an 'ink' which is 'jetted' from the printhead in the form of droplets having a pre-determined value, hence the name inkjet printing. The most visible example of an application area of this technology is the commercial desktop inkjet printer. The substrate in this case would be paper, where the ink is deposited in a controlled manner to produce a piece of text or an image, often using multiple inks of different colours. The printhead device ensures that the ink is jetted in the form of droplets of reliable volume and that this jetting process can be done repeatedly in a precise manner. When the printhead device is mounted on a 3D gantry system, one can control the rate of travel of the printhead and the height at which the droplet is released with respect to the substrate. The ink contacts the substrate (paper, glass), undergoes lateral spreading (assuming a solid substrate) and dries after some time.

The applications of Inkjet printing ranges from commercial desktop inkjet printers which are used to print documents to being used in printed electronics and making wearable bio-medical devices. Inkjet printing has been used to manufacture three dimensional components including integrated circuits and organic transistors [15-17].

2.2.2 Inkjet Printing - classification based on ink dispensing mechanism

2.2.2.1 Continuous Inkjet printing

Continuous inkjet printing (CIJ) is characterised by the continuous jetting of the ink onto a substrate. The continuous stream of ink follows the phenomenon also referred to as the Plateau-Rayleigh instability [18], where the stream of liquid breaks up into droplets of equal volume, minimising the effective total surface area. An electrostatic field is used to ensure that droplets are deposited only in the specified areas. It deflects the other droplets into a gutter reservoir from where the ink is often recycled. CIJ printing systems are associated with higher printing rates and is suitable for mass production requirements. However, it is considered as a wasteful technique where the ink is needlessly recycled, mandating complicated setups which put reliability and precision of the jetting process at risk [19]. The method is also restricted to being used with inks that are responsive to static electric charge, which compromises on its ability to be versatile in handling different liquids as inks. The Inkjet printing industry started out with CIJ printing but has now moved on to Drop on Demand (DOD) inkjet printing.

2.2.2.2 Drop on Demand Inkjet printing

Drop on Demand (DOD) inkjet printing is a process where a drop of ink is jetted from the printhead device only for the purpose of deposition on a substrate. This immediately makes DOD printing an economical process in comparison with CIJ printing. The formation of drops in a DOD printhead is achieved using a pressure pulse which propagates through the capillary tube which precedes the printhead device. When the pressure pulse is above the critical value which is needed for droplet formation, a drop of ink is jetted through the printhead nozzle. The pressure can be introduced using a piezoelectric actuator, cycling heating, and cooling of the ink (bubble jet technology) or using an electric field to overcome the surface tension of the droplet's meniscus at the printhead nozzle [20-21]. Figure 2.4 (a) and (b) illustrates the operation of a piezoelectric actuated printhead device in CIJ and DOD printing mode. For this investigation, we will only focus on piezoelectric printhead using a DOD printing strategy.

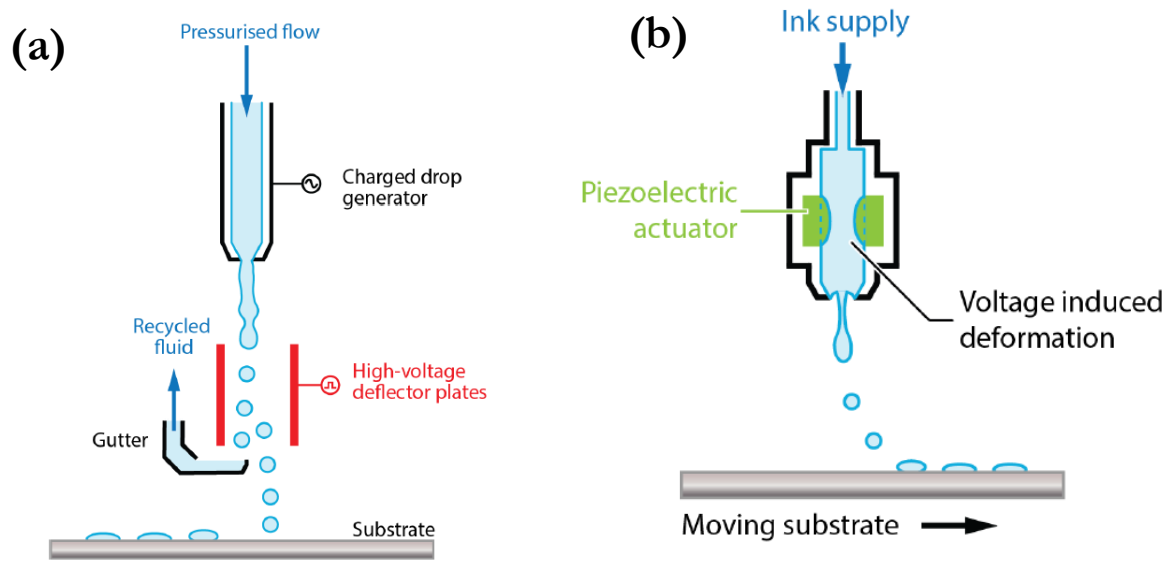

Fig 2.4 Schematic representation of Inkjet printheads in: (a) CIJ mode (b) DOD mode [22]

2.2.3 Inkjet Printing – A precursor to BJT?

One cannot help but notice the similarities between Inkjet printing and BJT. Both techniques are dependent on printhead devices for the repeated jetting of liquid in the form of droplets. The liquid is referred to as ink in Inkjet printing whereas it is termed as a binder for its adhesive action in BJT. The applications of the two technologies are very different and they operate at different scales. Inkjet printing is an older application which was first used by Baron Kelvin in his syphon recorder, where ink was selectively deposited on a roll of paper to be able to print messages in textual form. BJT was only patented as a technology in 1993, 126 years after the Baron used ink and a roll of paper to reinvent communications forever.

Sachs et al. used both CIJ and DOD printhead devices to print alumina powder using a tetraethyl orthosilicate binder [23]. Previously, the same research group had attempted using colloidal silica as a binder to print moulds for casting metals out of alumina [24]. One of the common observations in both studies was that using a CIJ printhead device for three-dimensional printing was preferable due to the faster build-up rate in comparison to using DOD printheads. It was only in 1996, that Z Corporation produced the first Binder Jetting prototype which included a table that could be controlled along the Z direction and an array of printheads which had a higher volume dispensing capability than a standard inkjet printhead device.

2.3. Binder Jetting – an overview

2.3.1. Introduction to Binder Jetting

Binder Jetting (BJT) was developed as a rapid prototyping technique at the Massachusetts Institute of Technology in 1989 by Sachs et al. [25]. It was an additive manufacturing process where a liquid binder is deposited in the selected areas of a powder bed from information acquired from a three-dimensional CAD model. The process is started with the spreading of a layer of powder and then

the binder is deposited selectively, in the form of droplets, using a printhead. The liquid binder infiltrates the powder bed and has an adhesive action on the powder particles, which bind together forming a 'green' part. This 'green' part is extracted carefully using brushes and pneumatic blowers to remove the dry powder leaving the part behind. The part is then put in an oven where the binder is cured, which increases the robustness of the 'green' part. Once the binder is cured, the part is taken out and sintered in a vacuum/gas purged environment after which further post processing stages may be carried out like heat treatment, hot isostatic pressing (HIP) and infiltration with other alloys to get better mechanical properties. Figure 2.5 is a schematic diagram of the printing process of parts in BJT.

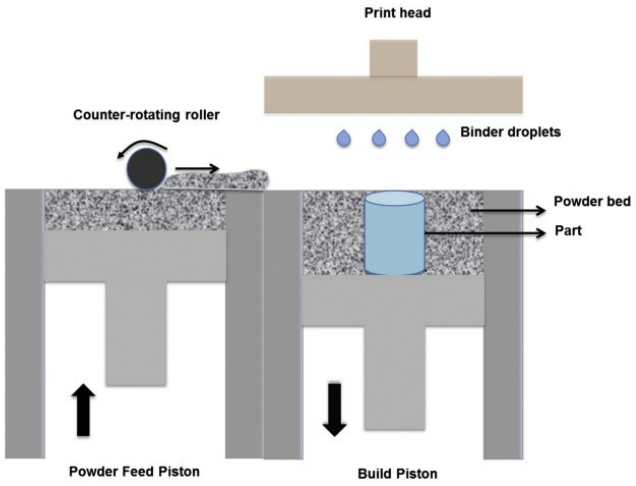

Fig 2.5 Schematic diagram of the BJT process [26]

BJT, as an AM technique offers advantages in the form of higher processing speeds, lower operating cost and being comparatively material agnostic over other methods like SLM. It is a process that does not extensively use support structures compared to other processes like SLM an EBM [27-30]. BJT has been considered as an AM process which is extremely scalable where any build size can be achieved if the number of printheads are scaled up along with the size of the build chamber.

Parts fabricated using BJT need to undergo multiple post-printing steps to ensure good mechanical properties including sintering, heat treatment and infiltration. These post-printing or post-

processing steps are time consuming and resource intensive in nature which often neutralises the high production rates of BJT. Metal and ceramic parts printed using BJT process had to be infiltrated with other materials to improve mechanical properties [31-33], which sometimes defeats the purpose of using niche materials for aerospace, automotive or bio-medical applications.

2.3.2. Effect of Process Parameters during BJT of Parts

2.3.2.1. Rate of Powder Spreading

In BJT, the powder is spread across the build platform using a rotating roller or a wiper. This is very similar to Powder Bed Fusion (PBF) processes like SLM and EBM. The spreading of powder should ideally be as fast as possible to increase the production time, but care should be taken to avoid improper, uneven spreading of powder which disrupts a uniform powder-binder interaction, leading to failed printing and poor part quality [34]. The spreading of powder also depends on the nature of the size and morphology of the powder particles. Powders having a smaller particle size diameter tend to form agglomerates due to the high Van Der Waals forces and need to be spread very slowly. Particles having a regular, spherical morphology spread easily with less effort and are stable to handle at higher spreading speeds. Irregularly shaped powders have poor flowability which hinders the printing process [35-36].

2.3.2.2. Rate of Binder deposition

The speed at which binder is deposited on the selected areas of the powder bed effects the printing quality and the powder-binder interaction. It affects the binder saturation level of the powder. Binder saturation is the amount of binder which is deposited on the powder bed via the printhead. It is calculated by finding out the void space (V_{air}), between the powder particles, which is filled with liquid binder (V_{binder}). The binder saturation level is calculated using the equations 2.1 and 2.2, as derived by Miyanaji [37]:

$$Binder\ saturation\ level = \frac{V_{binder}}{V_{air}}\ [Equation\ 2.1]$$

$$V_{air} = (1 - \zeta) * \left(V_{envelope}\right)\ [Equation\ 2.2]$$

the packing fraction of the powder bed is represented by ζ and $V_{envelope}$ is the product of the layer thickness (Z direction) and droplet spacings in the X and Y directions of the build platform.

A higher speed of the printhead would translate in lesser binder being deposited over the same distance which would translate into low values of binder saturation, leading to weak 'green' parts which may collapse immediately after printing, due to self-weight. Figure 2.6 (a) to (c) is a visual example of the same print with varying binder saturation. A slow deposition speed may increase processing time and can also lead to a high binder saturation. An oversaturation of binder often leads to weak structural strength of the 'green' part as the bulk of the powder starts tending towards behaving like a slurry. Oversaturation also leads to uncontrolled spreading of the binder into the powder bed which compromises on resolution of the printed parts. 'Feathering' occurs during binder oversaturation as is seen in Figure 2.6 (c), where geometrical features get distorted due to swelling at the circumference of the geometric features [38-39].

2.3.2.3 Layer thickness

The layer thickness is the size of the increment during a build while printing in any powder bed-based AM process. In BJT, it is the measure of the maximum amount of powder which needs to interact with the binder droplets. As discussed in Section 2.3.2.2, the binder saturation level is dependent on the $V_{envelope}$, which in turn is dependant on the layer thickness. A higher layer thickness would result in higher productivity but would also require greater control over the deposition process by the printheads. In the absence of such control, the resolution of the part would be affected.

The correlation between layer thickness and binder saturation level has been attempted in multiple cases. Fremond et al. attempted BJT of shape memory alloys, where they correlated dimensional resolution with layer thickness and binder saturation level [40]. An optimum layer thickness is important for the printing process as if it is too low, the binder tends to compensate of the lack of vertical infiltration with lateral spreading, which leads to non-uniform adhesion between particles. A large layer thickness translates into larger amount of binder which is deposited

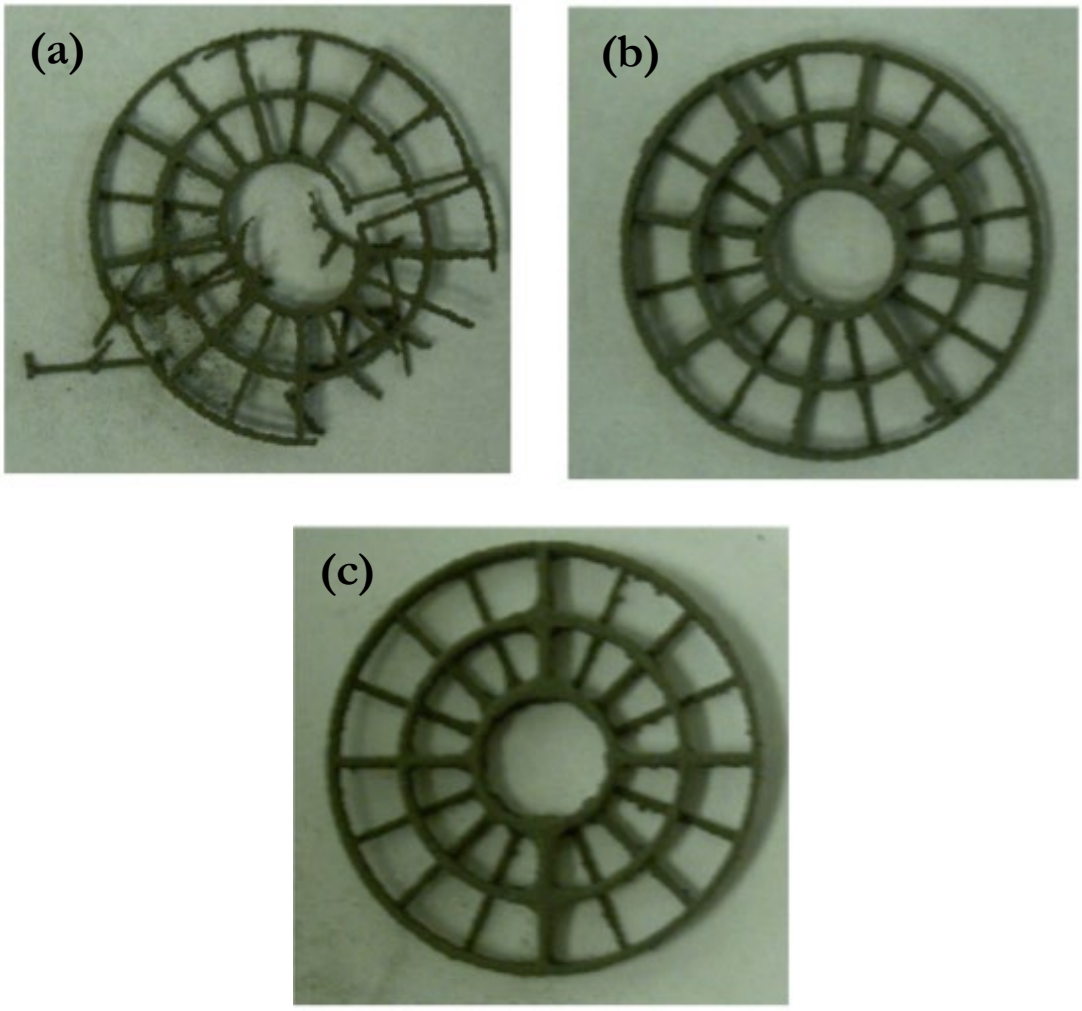

Fig 2.6 Effect of varying the binder saturation of the same print [38]: (a) 55% (b) 110% (c) 170%

into the powder which hinders good resolution. At an optimised layer thickness, the binder would infiltrate and laterally spread evenly, and both these processes would conclude at the same time.

2.3.3 Effect of choice of Materials during BJT of Parts

2.3.3.1 Particle Size Diameter and Morphology

The role of particle size and morphology has been discussed briefly in Section 2.2.2.1. Powder flowability is an important process response of these two parameters, which gets compromised when the parameters are less than ideal. Powders with smaller particle size diameter tends to form agglomerated which hinder proper flowability. The relationship between flowability and particle was best represented by Butscher et al [41]. Figure 2.7 represents the results from their study which implies a linear relationship between the particle size and powder flowability, where ff_c is the dependency of flowability on the median particle size.

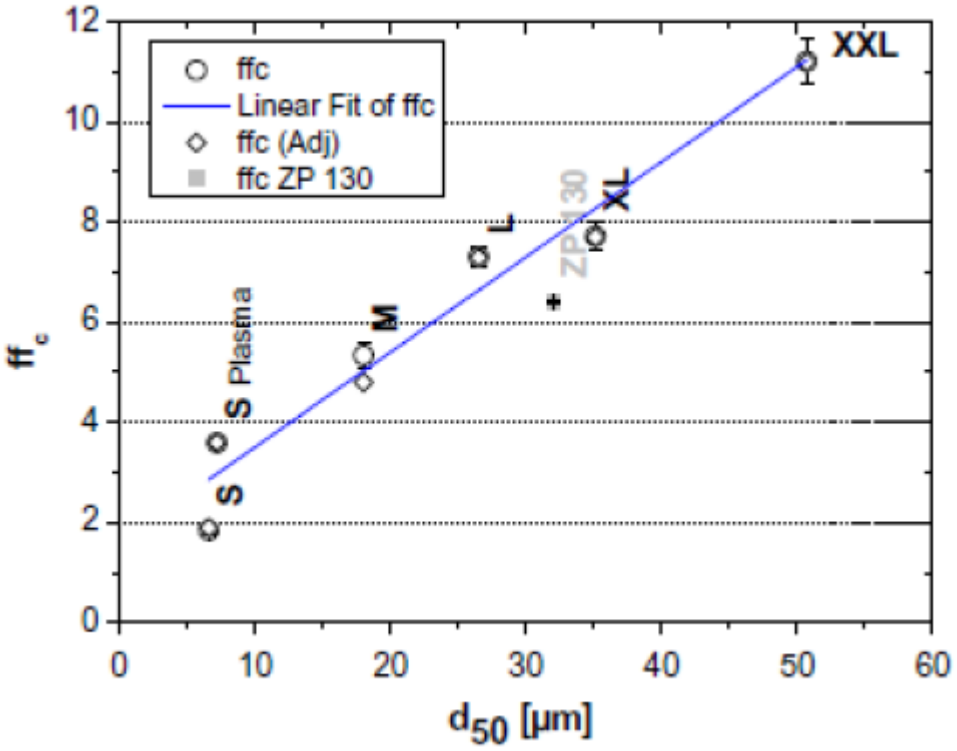

Figure 2.7 Relationship between particle size and flowability of powder [41].

The particle size also affects their ability to have a favourable packing fraction. The BJT process requires the powder bed to have a high packing fraction for higher green part strength, part density and mechanical properties. The high packing fraction also supports the green part being printed

mechanically and hence Binder Jetted parts often do not need mechanical supports like in other processes like SLM and EBM. Smaller powders tend to form agglomerates which negatively affects the packing fraction.

The shape of individual particles affects the flowability of the powder, which would influence the process responses of the printing process. Gas atomised powder particles usually have a regular, spherical shape whereas their water atomised counterparts tend to have a flaky, irregular morphology, which affects their flowability [42]. Powders with regular particle morphology offers less resistance to flow and is more stable when deposited [42].

2.3.3.2 Properties of the Binder

The interaction between the powder and the binder after the binder droplet contacts the powder bed is the core of the BJT process. The droplet infiltrates the powder bed due to capillary action and gravity. The direction of infiltration of the binder in the powder bed can be divided into two major components, vertical infiltration, and lateral spreading. The movement of binder into the powder bed is dependent on the physical properties of the liquid binder, mainly surface tension and dynamic viscosity [43-45]. If a binder droplet is not able to infiltrate the powder bed efficiently, it might create the need to use more binder to print a green part, which might create problems during the de-binding or burnout phase of part sintering. However, if a binder spreads too easily, it would be difficult to control the dimensional and geometric resolution of the part during printing [37, 46]. The ability of the binder to infiltrate the powder bed can influence the process parameters like layer thickness. The effectiveness of the binder infiltration also would affect the green strength of the printed part.

2.4 Superalloys – History & Development

2.4.1 The emergence of nickel-based superalloys.

The term 'superalloy' is an umbrella term used to refer to alloys which have nickel, cobalt and iron-nickel as base metals in the composition and retains its mechanical properties at temperatures above 540°C. The need for materials that could operate at high temperatures, without compromising on their mechanical properties was felt with the increasing role played by gas turbines in the areas of power generation, mechanical drives in the oil and gas sector and in-flight propulsion. Initially, it was thought that steels would be able to provide a solution but their tendency to deteriorate at elevated temperatures soon led to efforts at alloy development. The first cobalt-based superalloy was Vitallium, which was developed by Wojnar et al. in 1932 for manufacturing maxillary and hip replacement implants [47]. Nickel-chromium alloys, trademarked as Nimonic was first used to develop resilient toaster wires on account of its resistance to thermal fatigue [48].

Nickel based superalloys have now become the gold standard in industries which have high temperature applications. The success of nickel as a material of choice can be explained by having a look at the transition elements of the periodic table and observing the property trends exhibited by nickel and its neighbouring elements. The crystal structure of transition elements can be divided into three groups – Body Centred Cubic (BCC), Hexagonal Close Packed (HCP) and Face Centred Cubic (FCC). Elements having the same crystal structure are grouped together in the periodic table as observed in Figure 2.8. The BCC structured elements occupy the region of the 'd' block marked in purple, HCP elements are found in the centre (pink) and the FCC elements dominate the right-hand side of the 'd' block as shown in maroon. Zinc, cadmium are not atypical 'd' block elements as they have full d orbitals in their ground state and common oxidation state and do not

21 Sc 44.96	22 Ti 47.90	23 V 50.94	24 Cr 51.99	25 Mn 54.94	26 Fe 55.85	27 Co 58.93	28 Ni 58.71	29 Cu 63.54	30 Zn 65.37
39 Y 88.91	40 Zr 91.22	41 Nb 92.91	42 Mo 95.94	43 Tc 96.91	44 Ru 101.07	45 Rh 102.91	46 Pd 106.40	47 Ag 107.87	48 Cd 112.40
57* La 138.91	72 Hf 178.49	73 Ta 180.95	74 W 186.20	75 Re 186.20	76 Os 190.20	77 Ir 192.20	78 Pt 195.09	79 Au 196.97	80 Hg 200.59

Fig 2.8 Colour coded crystal structures of the transition elements and their position on the periodic table

have a dominant crystal structure and are coded in grey, along with mercury, which is a liquid at room temperature and manganese, which is an exception as well. The elements having BCC structure are brittle and are prone to having temperature dependent mechanical properties [49]. The elements in maroon have high toughness and ductility due to their FCC structure [49]. The FCC structure does not change with temperature in nickel and hence is an ideal choice for high temperature applications [50-51]. Elements having an HCP structure have similar properties and can technically be used in lieu of FCC elements [49, 50-51]. The platinoids consisting of ruthenium, rhodium, palladium, osmium, iridium, and platinum have high densities [52] which is discouraging for alloy development for aerospace applications. They are also cost prohibitive along with silver and gold. Rhenium is expensive because of its low availability and high demand in the petro-chemical industry as a catalyst [52]. From this method of elimination, nickel is a viable option to as a major component for making superalloys.

2.4.2 Metallurgy of Superalloys

2.4.2.1 Phases and microstructure

Phases are distinct materials that are composed of the elements present in the alloy. These materials have their own unique properties that affect the general properties of the alloy. Phases are

characterised by their composition, morphology, and location within the microstructure. Phases separate out in an alloy due to their different solidification temperatures. Phases in any alloy can be divided into the primary phase and the secondary phase(es). The primary phase forms the matrix in which the solvent element, in this case nickel will be present. It is conventionally referred to as the γ phase. Table 2.1 provides a description of the different phases found in superalloys, their chemical composition, and their contribution to the properties of the superalloys in general, as adapted from the ASM handbook on superalloys [48].

Table 2.1 Description of phases found in superalloys

Phase	Crystal structure	Chemical composition	Observations
γ	FCC	Solid solution	• It forms a continuous matrix in which the secondary phases reside. • Causes solid solution strengthening.
γ'	FCC	**$Ni_3Al/Ni_3(Al_xTi_y)$** with x and y varying between 0.5-1 and 0-0.05 wt.% respectively	• It forms precipitates withing the γ matrix, with cuboidal or spherical shape. • Principal strengthening phase of nickel-based superalloys. • Causes precipitation strengthening.
γ"	BCT	**Ni_3Nb**	• It forms precipitates within the γ matrix, in the form of coherent discs in alloys with Nb as a constituent element. • Causes precipitation strengthening and is the secondary strengthening phase after the γ' phase. • Principle strengthening precipitate in Inconel 718. • The phase is unstable at temperatures exceeding 650°C
η	HCP	**Ni_3Ti**	• It is an undesirable phase which is found in all superalloys. It increases the brittleness of the alloy in general.

δ	Orthorhombic	**Ni_3Nb**	• It's composition is identical to the γ" phase but the crystal structure is different and decreases the rupture strength of the alloy.
μ	Rhombohedral	**Co_2W_6 $(Fe,Co)_7(Mo,W)_6$**	• It is observed in Co based superalloys and have irregular platelet like shape at high temperatures. • It is not common in nickel-based superalloys
Laves	Hexagonal	**Fe_2Nb, Fe_2Ti, Fe_2Mo Co_2Ta and Co_2Ti**	• Commonly found in cobalt-based superalloys in the form of platelets or oblong globules. • May occur in Inconel 718 after long term exposure to high temperature.
Carbides phases are considered detrimental for the mechanical properties of superalloys, although they provide structure stabilisation at high temperatures in nickel-based superalloys in small quantities. M represents metal and C is carbon.			
MC	Cubic	**TiC, NbC**	• Found at the grain boundaries of the matrix in the form of globules and irregular platelets. • Causes grain boundary strengthening.
$M_{23}C_6$	FCC	**$Cr_{23}C_6$**	• They tend to accumulate at the grain boundaries after MC's decompose at lower temperatures. • Harmful for ductility and hot strength of superalloys.
M_6C	FCC	**Fe_3Mo_3C**	• Carbides are distributed randomly with no trend. They have a pinkish hue and tend to be stable at high temperatures.
M_7C_3	Hexagonal	**Cr_7C_3**	• Rarely found in most superalloys, unstable form and decomposes to $M_{23}C_6$ very rapidly.

2.4.2.2 Strengthening mechanisms in superalloys

Mechanical properties of superalloys can be controlled by tailoring the microstructure and the phases present in it. This control is established either by tweaking the chemical composition i.e., by introducing alloying elements and encouraging the formation of desirable phases and eliminating phases that are deleterious to the mechanical properties of the alloy. The role of alloying elements in getting desired mechanical properties in superalloys has been described in

detail in Table 2.1. Chemical based strengthening in superalloys occur in three major ways – solid solution strengthening, precipitation strengthening and grain boundary strengthening [53].

Processing based control is dependent on the manufacturing process used to make the alloy. Cast products are usually weak due to the columnar grain structure which is refined by forming [54]. The strength of metals is due to the presence of dislocations in the crystal structure, which can be introduced both in the form of processing (e.g., cold rolling) or by introducing alloying elements (TiC inhibits grain growth and causes grain hardening in superalloys) [54].

Solid solution strengthening

Solid solution strengthening occurs when the existing crystal lattice structure of the base material is distorted due to the introduction of an atom(s) of the alloying element as part of a solid solution. The size disparity between the atom(s) of the alloying element and the base material dictates the nature of strengthening which occurs in the solid solution.

When the atom(s) of the alloying element are big enough to replace the base material atom(s) in the lattice, it distorts the lattice structure and introduces stress in it and is referred to as Substitutional Solid Solution Strengthening [53]. This type of strengthening mechanism occurs when the disparity of size between the alloying element and base material atoms is less than 15% [53-54]. The region affected by the distortion induced stress is called the stress field and they are spherical in nature for substitutional solid solution strengthening. When the atoms of the alloying element are smaller than the atoms of the base material, they occupy the interstices of the lattice and cause tetragonal distortion within the lattice structure and this form of strengthening is called Interstitial Solid Solution Strengthening. Figure 2.9 is representative of a standard lattice structure with distortion based on substitutional solid solution strengthening and interstitial solid solution strengthening.

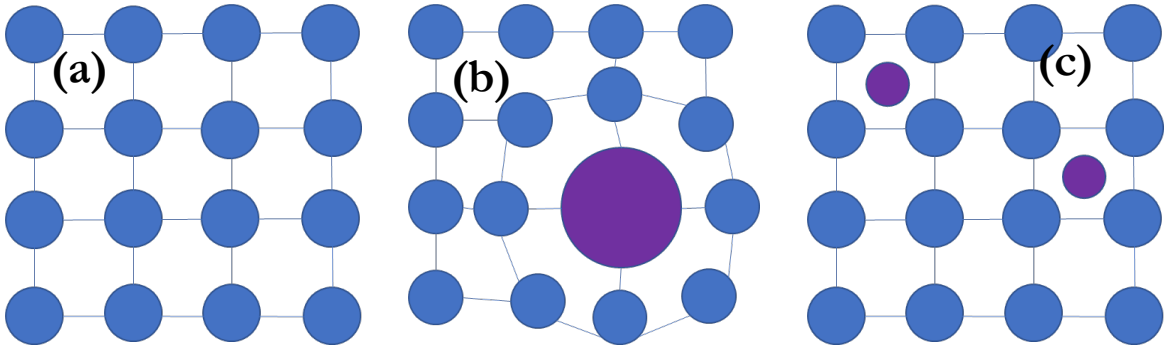

Fig 2.9 Different types of lattice structures: (a) Undistorted lattice (b) Substituional Solid Solution Strengthening (c) Interstitial Solid Solution Strengthening

Precipitation strengthening

Precipitation strengthening occurs due to the presence of precipitates in the primary, matrix phase. The precipitates are termed as secondary phases. In case of superalloys, the γ' and γ'' phases are responsible for precipitation hardening. These precipitates hinder the propagation of the dislocations, thus strengthening the alloy. The effectiveness of precipitation strengthening depends on the extent of coherency between the crystals of the precipitate and the base matrix material. The number of precipitates which can be packed into the lattice of the matrix increases with the coherency, which increases the probability of the precipitates acting as hurdles for the dislocation front.

The γ' and γ'' phases are precipitates that have a close packed crystal (CPC) structure which are more effective as hurdles for the dislocation front in comparison with tetragonally packed crystals (TCP). These CPC precipitates increase the amount of force or energy needed to overcome them, thus strengthening the material [55]. The size of the precipitates is an important criterion which affects their efficacy as strength enhancers. The precipitates would fail to stop the dislocation front in case their size is too small and would encourage dislocation bowing and reduce the mechanical strength of the material [53-54].

Grain boundary strengthening

Grain boundary strengthening depends on the grain boundaries to hinder the propagation of the dislocation front, thus contributing to the strength of the material. Grain boundaries are where most dislocations stop its propagation but causes stress in the region which causes deformation in neighbouring grains, thus forming a stress front which can propagate. If the grain boundaries are changes by controlling the grain size, one could control the number of dislocations present in every grain and stop the propagation of a dislocation or stress front. Specimens having a smaller average grain size would have a higher tensile strength in comparison to specimens which would have a larger average grain size. This can be achieved via process control (e.g., faster cooling rates during casting, faster scan rates during SLM) or through the composition route, where carbides are introduced in superalloys, especially in nickel and iron-nickel based superalloys.

The phenomenon of grain boundary strengthening is governed by the Hall-Petch equation which is provided as follows [56-58]:

$$\sigma = \sigma_0 + \frac{k_y}{\sqrt{d}} \quad [Equation\ 2.3]$$

where σ is the yield stress, σ_0 is the resistance of the lattice to the dislocation front, k_y is the material strengthening coefficient and d is the average grain size. The Hall-Petch equation can be misleading as it gives the impression that the strength of a material can be increased by plunging the value of the grain size. However, one cannot go lower than the size of the unit cell of the material. Schuh and Nieh experimentally determined that the average grain size at which nickel superalloys are at their strongest is 10 nm, below which there is a deterioration of mechanical properties due to grain boundary sliding [59].

Carbides are used to induce grain boundary strengthening but they also have an undesirable side effect of encouraging phase instabilities in the microstructure. The MC type of carbides form at

high temperatures and occur throughout the microstructure and often decompose to form intermediate and low temperature carbides like M_6C and $M_{23}C_6$, respectively.

$$MC + \gamma \rightarrow M_6C + \gamma' \text{ at 816-982°C [Equation 2.4]}$$

$$MC + \gamma \rightarrow M_{23}C_6 + \gamma' \text{ at 790-816°C [Equation 2.5]}$$

M23C6 is the most found form of carbide in nickel-based superalloys and has a blocky and irregular morphology.

2.5 BJT of Superalloys

BJT as an additive manufacturing technique was initially reserved for the processing of ceramics having application as refractory materials for casting of niche alloys. The material agnostic versatility of BJT was realised and commented on by many researchers who helped develop BJT as a technology and implement it in industry [60] but its use was restricted to processing ceramics. The first BJT prototype was tested in 1996 by Z Corporation, an MIT incubated company, who chose to focus on printing of ceramic moulds for the casting industry. In Europe at around the same time, VoxelJet AG started developing and testing commercial BJT systems which processed sand and fabricated moulds for casting of steel and aluminium alloys [61]. BJT was used for making casting moulds was its scalability and its quick build-up rate, which has been discussed in Section 2.2. Moulds of flexible size and geometry could be made very quickly using materials which are difficult to process in traditional PBF systems like SLM and EBM. In 2005, they expanded into systems that focused on polymers and the system, the VX800 found moderate commercial acclaim as an educational tool in universities.

It was only in 2005, when ExOne Ltd launched commercial systems which focused on Binder Jetting of metals. The R2 Metal 3D and X1 Lab were commercial systems which proved to be successful in being versatile systems [62], thus opening the gates to systematic research in Binder Jetting and its capability to process different materials. Figure 2.10 represents the commercial

journey undertaken by Binder Jetting technology. Mostafaei et al. successfully printed specimens of Inconel 625 using an ExOne M-Flex commercial system. They correlated the inverse

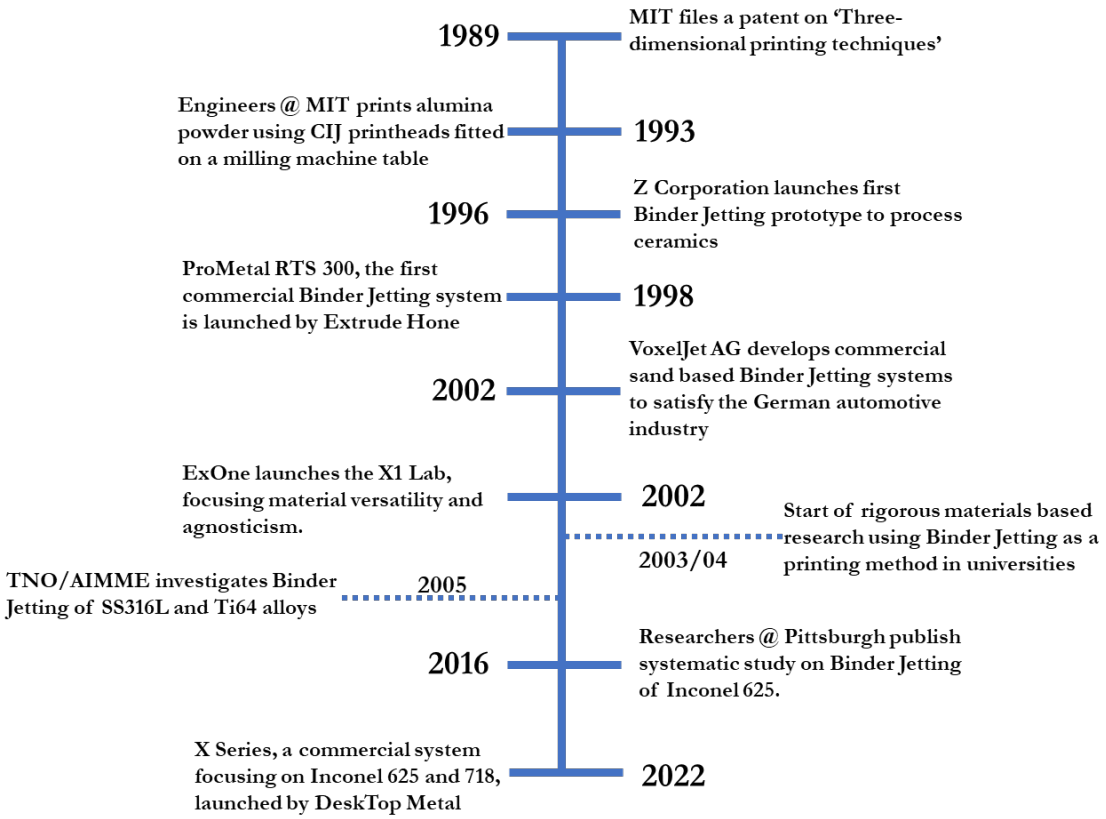

Fig 2.10 A timeline of the evolution of Binder Jetting as a technology

relationship between sintering temperature and porosity [63]. Heat treatment of these specimens improved the mechanical properties like hardness and tensile strength and caused refinement of the microstructure [64]. The printed and sintered specimens performed poorly in fatigue testing, which is contrary to the fact that Inconel 625 is high fatigue alloy. It was observed that surface grinding of the specimens could be used as a post-processing technique to tighten the dimensional tolerances and to improve the fatigue life of the specimens [65]. One trend which was noted was the substantial effect which post-processing had on the improvement of the mechanical properties of the Inconel 625 samples. Enrique et al. attempted to make metal matrix composites with Inconel 625 and adopted BJT as the processing technique [66]. They observed that the sintering cycle played an important role in the development of microstructure of the final part. The parts that were

sintered directly with no dedicated burnout/debinding had a Cr_3C_2 phase which was absent in the counterparts which had a debinding cycle prior to sintering.

There have been relatively less systematic studies of processing of Inconel 718 using Binder Jetting. The first reported systematic study in 2008 used a ProMetal RTS-300 system and focussed on the optimisation of parameters like layer thickness and particle size diameter [67]. The density observed was reported to be 99% when sintered at 1300°C which came at the expense of the Ni_3Nb precipitates dissolving into the γ matrix, reducing the strength of the alloy. It was found out that 1280°C was a better sintering temperature. Nandwana et al. did an extensive study on BJT of Inconel 718 and concluded that feedstock composition can be tweaked to assist the BJT process [26]. The study also observed that finer powders (7 μm and 21 μm particle size diameter) tended to have a higher binder saturation which discouraged the formation of carbides whereas coarser powders (70 μm) tended to have a mix of metal carbides with Laves phases.

2.6 Chapter Summary

Chapter 2 started with the introduction of Additive Manufacturing as group of technologies that are used to build three-dimensional, fully functional parts, directly from a CAD model. Emphasis was made on the different techniques of additive manufacturing with focused on the basic principle of operation, and the advantages and limitations of the various processes. After a preliminary background of the technology was introduced, the chapter focused on introducing the BJT process more extensively explaining the advantages and disadvantages of the process. Studies available in literature on process parameters and their effect on the process responses were discussed. Inkjet printing was discussed briefly due to the procedural similarities between inkjet printing and binder jetting, with the different mechanisms of the ink jetting being explained. Reported literature specific to BJT of superalloys was explored, starting with a timeline dedicated to the maturity of BJT as an additive manufacturing technique both at the prototype and commercial level. Studies on processing of superalloys using BJT as the choice of additive

manufacturing method were explored where it was inferred that Binder Jetting had certain advantages over SLM, its nearest competitor in terms of material agnosticism, production rates and lack of support structures which limit design flexibility. It was observed that not many systematic studies were conducted on Binder Jetting of Inconel 718 despite preliminary studies on Inconel 625 and CMSX 4 alloys being extremely promising.

References

1. International Organization for Standardization, ISO/ASTM 52900:2015(EN): Additive Manufacturing—General principles—Terminology. Berlin, 2015.
2. Crump SS, inventor; Stratasys Inc, assignee. Apparatus and method for creating three-dimensional objects. United States Patent US5121329. 1992 Jun 9.
3. Wickramasinghe S, Do T, Tran P. FDM-based 3D printing of polymer and associated composite: A review on mechanical properties, defects, and treatments. Polymers. 2020 Jul 10;12(7):1529.
4. Leong KF, Liu D, Chua CK. Tissue engineering applications of additive manufacturing. In: Hashmi S, Gilmar GF, Yilbas B, editors. Title: Comprehensive Materials Processing. Amsterdam: Elsevier; 2014.
5. Kumar SA, Prasad RVS. Basic principles of additive manufacturing: different additive manufacturing technologies. In: M. Manjaiah, K. Raghavendra, N. Balashanmugam, J. Paulo Davim, editors. Woodhead Publishing Reviews: Mechanical Engineering Series, Additive Manufacturing. Sawston: Woodhead Publishing; 2021.
6. Sing SL, Tey CF, Tan JHK, Huang S, Yeong WY. 2-3D printing of metals in rapid prototyping of biomaterials: Techniques in additive manufacturing. In: Narayan R, editor. Title: Rapid Prototyping of Biomaterials. 2nd Edition. Amsterdam: Elsevier; 2020.
7. Pontes AJ. Design for Additive Manufacturing. In: Pouzada AS, editor. Title: Design and Manufacturing of Plastic Products. Amsterdam: Elsevier; 2021.

8. Mazumder J, Morgan D, Skszek T, Lowney M, inventor; Dm3D Tech LLC, assignee. Direct metal deposition apparatus utilizing rapid-response diode laser source. United States Patent US200020065573A1. 2002 May 30.
9. Dinda GP, Dasgupta AK, Mazumder J. Laser aided direct metal deposition of Inconel 625 superalloy: microstructural evolution and thermal stability. Materials Science & Engineering: A. 2009 May; 509: 98-104.
10. Liu Y, Ding Y, Yang L, Sun R, Zhang T, Yang X. Research and progress of laser cladding alloys: a review. Journal of Manufacturing Processes. 2021 June; 66: 341-363.
11. Jadhav SD, Dadbakhsh S, Goossens L, Kruth JP, Van Humbeeck J, Vanmeensel K. Influence of selective laser melting process parameters on texture evolution in pure copper. Journal of Materials Processing Technology. 2019 Aug 1; 270:47-58.
12. Tran TQ, Chinnappan A, Lee JK, Loc NH, Tran LT, Wang G, Kumar VV, Jayathilaka WA, Ji D, Doddamani M, Ramakrishna S. 3D printing of highly pure copper. Metals. 2019 Jul;9(7):756.
13. Bhaduri D, Ghara T, Penchev P, Paul S, Pruncu CI, Dimov S, Morgan D. Pulsed laser polishing of selective laser melted aluminium alloy parts. Applied Surface Science. 2021 Aug 30; 558:149887.
14. Harrison NJ. Selective laser melting of nickel superalloys: solidification, microstructure and material response [dissertation]. Sheffield (UK): The University of Sheffield; 2016.
15. Kwon J, Takeda Y, Fukuda K, Cho K, Tokito S, Jung S. Three-dimensional, inkjet-printed organic transistors and integrated circuits with 100% yield, high uniformity, and long-term stability. ACS nano. 2016 Nov 22;10(11):10324-30.
16. Arai K, Iwanaga S, Toda H, Genci C, Nishiyama Y, Nakamura M. Three-dimensional inkjet biofabrication based on designed images. Biofabrication. 2011 Sep 7;3(3):034113.

17. Cui X, Gao G, Yonezawa T, Dai G. Human cartilage tissue fabrication using three-dimensional inkjet printing technology. Journal of Visualized Experiments. 2014 Jun 10(88): e51294.
18. Kull HJ. Theory of Raleigh-Taylor instability. Physics Reports. 1991 Aug; 206(5): 197-325.
19. Beedasy V, Smith PJ. Printed electronics as prepared by inkjet printing. Materials. 2020 Feb; 13(3): 704.
20. Shah MA, Lee DG, Lee BY, Hur S. Classifications and Applications of Inkjet Printing Technology: A Review. IEEE Access. 2021 Oct 8.
21. Chen PH, Chen WC, Chang SH. Bubble growth and ink ejection process of a thermal ink jet printhead. International Journal of Mechanical Sciences. 1997 Jun 1;39(6):683-95.
22. Beedasy V. Investigation into the effects of pulsed laser sintering on inkjet-printed functional materials for printed electronics [dissertation]. Sheffield (UK): The University of Sheffield; 2021.
23. Sachs E, Cima M, Williams P, Brancazio D, Cornie J. Three-dimensional printing: rapid tooling and prototypes directly from a CAD model. Journal of Engineering for Industry. 1992 Nov; 114: 481-488.
24. Sachs E, Cima M, Cornie J. Three-dimensional rapid tooling and prototypes directly from a CAD model. Annals of the CIRP. 1990 Jan; 39(1): 201-204.
25. Sachs EM, Haggerty JS, Cima MJ, Williams PA, inventors. Massachusetts Institute of Technology, assignee. Three dimensional printing techniques. US Patent US5340656A.
26. Nandwana P, Elliott AM, Siddel D, Merriman A, Peter WH, Babu SS. Powder bed binder jet 3D printing of Inconel 718: densification, microstructural evolution and challenges. Current Opinion in Solid State and Materials Science. 2017; 21(4): 207-218.
27. Bai Y, Williams CB. An exploration of binder jetting of copper. Rapid Prototyping Journal. 2015 Mar 16.

28. Gokuldoss PK, Kolla S, Eckert J. Additive manufacturing processes: Selective laser melting, electron beam melting and binder jetting—Selection guidelines. materials. 2017 Jun;10(6):672.
29. Mostafaei A, Stevens EL, Ference JJ, Schmidt DE, Chmielus M. Binder jetting of a complex-shaped metal partial denture framework. Additive Manufacturing. 2018 May 1; 21:63-8.
30. Gibson I, Rosen D, Stucker B, Khorasani M. Binder jetting. In Additive manufacturing technologies 2021 (pp. 237-252). Springer, Cham.
31. Elliott AM, Momen AM, Benedict M, Kiggans J. Experimental study of the maximum resolution and packing density achievable in sintered and non-sintered binder-jet 3D printed steel microchannels. In ASME International Mechanical Engineering Congress and Exposition 2015 Nov 13 (Vol. 57359, p. V02AT02A019). American Society of Mechanical Engineers.
32. Rishmawi I, Salarian M, Vlasea M. Tailoring green and sintered density of pure iron parts using binder jetting additive manufacturing. Additive Manufacturing. 2018 Dec 1; 24:508-20.
33. Zhang D, Kenel C, Dunand DC. Microstructure and properties of additively manufactured WC-Co microlattices and WC-Cu composites. Acta Materialia. 2021 Dec 1; 221:117420.
34. Miyanaji H, Zhang S, Lassell A, Zandinejad AA, Yang L. Optimal process parameters for 3D printing of porcelain structures. Procedia Manufacturing. 2016 Jan 1; 5:870-87.
35. Miyanaji H, Zhang S, Lassell A, Zandinejad A, Yang L. Process development of porcelain ceramic material with binder jetting process for dental applications. Jom. 2016 Mar;68(3):831-41.
36. Yang L, Zhang S, Oliveira G, Stucker B. Development of a 3D printing method for production of dental application. In2013 International Solid Freeform Fabrication Symposium 2013. University of Texas at Austin.
37. Miyanaji H. Binder jetting additive manufacturing process fundamentals and the resultant influences on part quality [dissertation]. Louisville (US): The University of Louisville; 2018.

38. Lu K, Reynolds WT. 3DP process for fine mesh structure printing. Powder Technology. 2008; 187: 11-18.
39. J.F. Bredt, Binder Stability and Powder\Binder Interaction in Three-Dimensional Printing, Dept. of Mechanical Engineering, Massachusetts Institute of Technology, Cambridge (US), 1995, p. 382.
40. Fremond M. Shape memory alloy. In Shape memory alloys 1996 (pp. 1-68). Springer, Vienna.
41. Butscher A, Bohner M, Roth C, Ernstberger A, Heuberger R, Doebelin N, von Rohr PR, Müller R. Printability of calcium phosphate powders for three-dimensional printing of tissue engineering scaffolds. Acta Biomateralia. 2012; 8(1): 373-385.
42. Koseski RP, Suri P, Earhardt NB, German RM, Kwon YS. Microstructural evolution of injection molded gas-and water-atomized 316L stainless steel powder during sintering. Materials Science and Engineering: A. 2005 Jan 15;390(1-2):171-7.
43. Washburn EW. The dynamics of capillary flow. Physical review. 1921 Mar 1;17(3):273.
44. Denesuk M, Smith GL, Zelinski BJ, Kreidl NJ, Uhlmann DR. Capillary penetration of liquid droplets into porous materials. Journal of colloid and interface science. 1993 Jun 1;158(1):114-20.
45. Denesuk M, Zelinski BJ, Kreidl NJ, Uhlmann DR. Dynamics of incomplete wetting on porous materials. Journal of Colloid and interface science. 1994 Nov 1;168(1):142-51.
46. Dini F, Ghaffari SA, Jafar J, Hamidreza R, Marjan S. A review of binder jet process parameters; powder, binder, printing and sintering condition. Metal Powder Report. 2020 Mar;75(2):95-100.
47. Wojnar L, Dabrowski JR, Oksiuta Z. Porosity structure and mechanical properties of vitalium-type alloy for implants. Materials Characterisation. 2001 March; 46(2-3): 221-225.
48. Donachie MJ, Donachie SJ. Superalloys: A Technical Guide. ASM international; 2002.
49. Mishra P. Physics of Condensed Matter. Delhi (India): Elsevier; 2011.

50. Owe Berg TG. On ferromagnetism, paramagnetism and cohesive energy of transition metals and their alloys. Journal de Physique et le Radium. 1951 March; 12(3):418-429.
51. Reed RC. The superalloys: fundamentals and applications. Cambridge (UK): Cambridge University Press; 2008 Jul 31.
52. Renner H, Schlamp G, Kleinwächter I, Drost E, Lüschow HM, Tews P, Panster P, Diehl M, Lang J, Kreuzer T, Knödler A. Platinum group metals and compounds. Ullmann's Encyclopedia of Industrial Chemistry. 2000 Jun 15:1-73.
53. Lakhtin Y. Engineering Physical Metallurgy. Moscow (USSR): Mir Publications; 1968.
54. Smith WF, Hashemi J. Foundations of Materials Science and Engineering. New York (US); 2009.
55. Petch NJ. The cleavage strength of polycrystals. Journal of the Iron and Steel Institute. 1953; 174:25-28.
56. Sylwestrowicz W, Hall EO. The deformation and ageing of mild steel. Proceedings of the Physical Society. Section B. 1951 Jun 1;64(6):495.
57. Hall EO. The deformation and ageing of mild steel: II characteristics of the Lüders deformation. Proceedings of the physical society. Section B. 1951 Sep 1;64(9):742.
58. Hall EO. The deformation and ageing of mild steel: III discussion of results. Proceedings of the Physical Society. Section B. 1951 Sep 1;64(9):747.
59. Schuh CA, Nieh TG. Hardness and abrasion resistance of nanocrystalline nickel alloys near the Hall-Petch breakdown regime. MRS Online Proceedings Library (OPL). 2002;740.
60. Hull C, Feygin M, Baron Y, Sanders R, Sachs E, Lightman A, Wohlers T. Rapid prototyping: current technology and future potential. Rapid Prototyping Journal. 995 March; 1(1): 11-19.
61. VoxelJet AG. The voxeljet history [Internet]. 2022 [cited 2022 May 20]. Available from: https://www.voxeljet.com/about-voxeljet/history.
62. ExOne Company. Our Story [Internet]. 2022 [cited 2022 May 20]. Available from: https://www.exone.com/en-US/About/Our-Story.

63. Mostafaei A, Stevens EL, Hughes ET, Biery SD, Hilla C, Chmielus M. Powder bed binder jet printed alloy 625: Densification, microstructure, and mechanical properties. Materials & Design. 2016 Oct 15; 108:126-35.

64. Mostafaei A, Behnamian Y, Krimer YL, Stevens EL, Luo JL, Chmielus M. Effect of solutionizing and aging on the microstructure and mechanical properties of powder bed binder jet printed nickel-based superalloy 625. Materials & Design. 2016 Dec 5; 111:482-91.

65. Mostafaei A, Neelapu SH, Kisailus C, Nath LM, Jacobs TD, Chmielus M. Characterizing surface finish and fatigue behavior in binder-jet 3D-printed nickel-based superalloy 625. Additive Manufacturing. 2018 Dec 1; 24:200-9.

66. Enrique PD, Mahmoodkhani Y, Marzbanrad E, Toyserkani E, Zhou NY. In situ formation of metal matrix composites using binder jet additive manufacturing (3D printing). Materials Letters. 2018 Dec 1; 232:179-82.

67. Turker M, Godlinski D, Petzoldt F. Effect of production parameters on the properties of In 718 superalloy by three-dimensional printing. Material Characterisation. 2008 Dec; 59(12): 1728-1735.

CHAPTER 3:

MATERIALS, METHODS & CHARACTERISATION

'My methodology is not knowing what I'm doing and making that work for me' **– Stone Gossard, Guitarist, Pearl Jam.**

3.1 Selection of Inconel 718

Inconel 718 is a nickel super alloy which is characterised by its austenitic nature containing nickel and chromium. It belongs to the Inconel family of nickel super alloys which also include Inconel 625, BS 3076 and Nicrofer 6020. Inconel 718, unlike most of its other solution hardened cousins is a precipitation strengthened alloy where the primary strengthening phase is Ni_3Nb, which is termed as the γ' phase. The presence of chromium is instrumental in the alloy having a considerable resistance to oxidation, even at elevated temperatures of 1500 K [1].

Inconel 718 powders are manufactured specifically for use in AM processes by commercial enterprises like Renishaw Plc, Aconity3D GmbH, and Carpenter Additive Ltd. The powders are usually used in powder bed fusion processes like SLM and EBM. The particle size of the powders depends on the process being used. Typically, lower particle size is chosen for SLM based processes as compared to EBM due to the disparity in the energy densities between lasers and electron beams used in commercial systems [2]. The powder which has been used and would be used during this investigation has been supplied by Carpenter Additive Ltd. The composition of the powder has been provided in Table 3.1, with the elements having a compositional percentage of > 10% weight highlighted in bold font.

Table 3.1- Composition of Inconel 718, supplied by Carpenter Additive Ltd.

Element	Min	Max	Element	Min	Max
Aluminium	0.30	0.70	Manganese	--	0.35
Boron	--	0.006	Molybdenum	2.80	3.30
Carbon	0.02	0.08	**Niobium + Tantalum**	4.75	5.50
Calcium	--	0.01	**Nickel**	50.0	55.0
Cobalt	--	1.0	Phosphorus	--	0.015
Chromium	17.0	21.0	Sulfur	--	0.015
Copper	--	0.30	Selenium	--	0.005
Iron	15.0	21.0	Silicon	--	0.35
Magnesium	--	0.01	Titanium	0.75	1.15

3.1.1 Particle size & morphology

The particle size diameter (PSD) of the Inconel 718 particles of the powder which was supplied by the manufacturer was measured using a laser diffraction particle size analyser [Malvern Mastersizer 3000, Malvern, UK]. Figure 3.1 represents the mean particle size diameter of the powder and its statistical distribution. The measurement was done three times to ensure precision and repeatability. It was observed that the median particle diameter (D50) was 75.5 μm which matched the PSD of the powder which was supplied by the manufacturer.

The particle size distribution was also visually analysed using micrographs taken using the help of a scanning electron microscope (SEM) [Tescan Vega 3, Tescan, Brno, Czechia] as seen as in Figure 3.2. The micrography was done in a high vacuum mode in a conventional scattered emission manner. Samples which were the feedstock which consisted of metallic powder and non-metallic PVA was coated with gold/palladium alloy to discourage charging when the sample was analysed

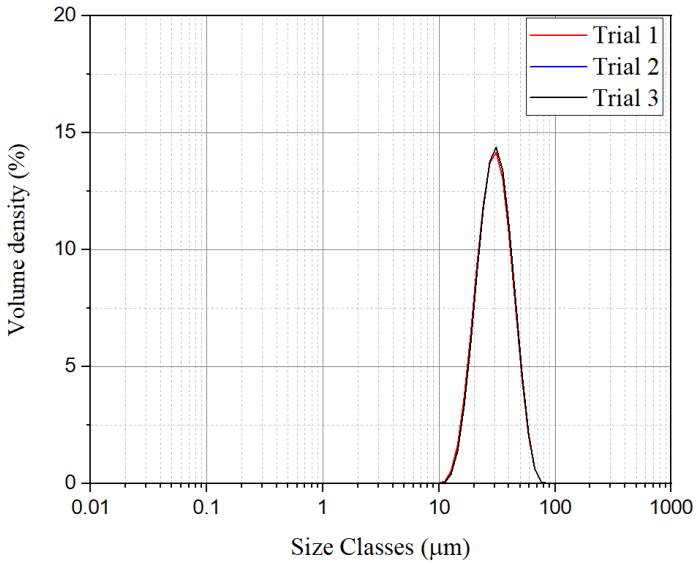

Fig 3.1 Measurement of particle size diameter and its distribution of Inconel 718 powder

under the electron beam.

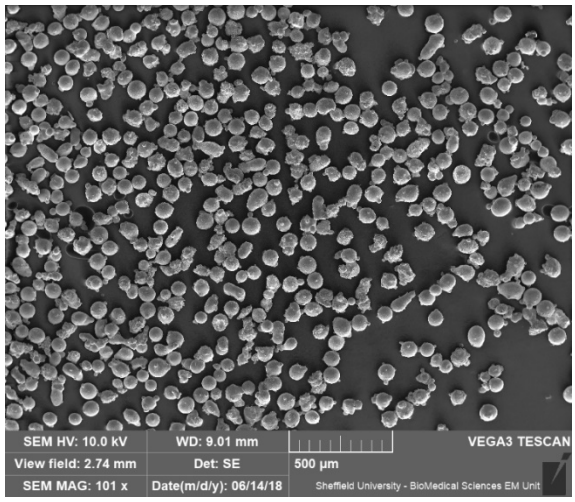

Fig 3.2 SEM micrograph of virgin Inconel 718 powder

3.2 Selection of Polyvinyl Alcohol

Polyvinyl alcohol (PVA) is a polymer which was discovered by Hermann Staudinger in 1924. It is a colourless, tasteless, and water-soluble synthetic polymer which has widespread applications, ranging from textiles industries to the niche biomedical industries [3]. The polymer is considered environmentally friendly and is nontoxic when used in solutions under concentration of 5% by weight and under. It is available commercially in the form of granules with a wide range of molecular weights, ranging from 30,000 to 200,000 g/mol [4]. PVA of three different molecular weights was purchased from Alfa Aesar [Alfa Aesar, Heysham, UK]. Table 3.2 describes the details of the different types of PVA which have been used in this body of work, including the nomenclature which has been used throughout this thesis. It was necessary to get PVA samples with a high degree of hydrolysis, which is a measure of a polymer's solubility in water. The degree of hydrolysis of PVA is inversely proportional to its ease of dissolution in water. PVA with high degree of hydrolysis, also termed as 'fully hydrolysed' PVA, tend to have dissolution temperatures

Table 3.2 Choice of different types of Polyvinyl Alcohol

Molecular weight (g/mol)	Degree of hydrolysis (%)	Nomenclature used
10,000	**95%**	**LMW**
26,000		**MMW**
84,000		**HMW**

greater than 80°C and require high dissolution time, especially for specimens with high molecular weight [5]. The high temperature of dissolution is needed to overcome the inter and intra hydrogen bonding in the PVA. However, after complete dissolution, the $-OH$ groups of fully hydrolysed PVA form strong hydrogen bonding with the water molecules as compared to PVA specimens having lower degree of hydrolysis [5-6]. The strong hydrogen bonding between the $-OH$ groups present in the polymeric chain of PVA, and the water molecules is important for the spreadability

of the aqueous binders as discussed in Chapter 5. The degree of hydrolysis for the PVA used in this study, regardless of molecular weight, was chosen to be greater than 98%.

3.3 Preparation of Feedstock and Binder

3.3.1 Pulverisation of polyvinyl alcohol

The PVA which was received from the manufacturer was in granular form. The granules were of irregular size and shape and were much larger that the Inconel 718 particles. The mismatch in size between the metal powder and the PVA granules discouraged homogenous mixing due to granular convection [7] and hence it was important to reduce the size of the PVA granules. PVA was initially ball milled at room temperature to obtain a fine, pulverised powder; but it was observed that the temperature inside the grinding jar became high enough to cause the PVA to melt and stick together, which defeated the purpose of the ball milling of the specimens. Ball milling of the PVA specimens was then done at -196°C to ensure that the PVA granules got pulverised into a fine powder after undergoing cryogenic embrittlement. A cryogenic ball mill [CryoMill, Retsch, Haan, Germany] was used to reduce the granules of PVA of different molecular weights into a fine powder. The details of the parameters are provided in detail in Table 3.3. After the PVA samples were reduced to fine powder, they were sealed in airtight jars and stored in a silica gel lined desiccators to prevent them from interacting with moisture and humidity. Once the powders were put inside the desiccators, they could be stored safely up to 15 days without any deterioration in sample quality.

Table 3.3 List of milling accessories and parameters used for pulverisation of polyvinyl alcohol

Milling Accessories	Description
Cryogenic coolant	liquid nitrogen
Grinding ball	Stainless steel, 2 pieces, Φ 2.5 mm
Grinding jar	25 mL, stainless steel
Cooling mode	Auto at -196 °C
Milling Parameters	**Value**
Milling time/cycle	120 s
Number of cycles per sample	02
Frequency of cycle	30 Hz (1800 RPM)

3.3.2 Preparation of modified feedstock

The modified feedstock or feedstock is the term which would be used to refer to the mixture of Inconel 718 powder and PVA of different molecular weights. The metal powder and a desired quantity of PVA was weighed into a jar, which was then mixed using a speed mixer [DAC 800 FVZ, Hauschild & Co KG, Hamm, Germany]. It was observed that the feedstock was a homogeneous mixture of dry PVA powder and metal powder when the rotational speed was maintained at 600 RPM. The maximum time limit of a cycle was 15 minutes, which was a feature of the speed mixer, and every sample went through 4 such cycles to ensure a homogeneous feedstock. For cohesive regimes where the feedstock contains metal powders, higher speeds improve the homogeneity of the feedstock due to more 'avalanches' experienced by the feedstock per rotation; where 'avalanches' denotes the vertical flow of small masses of powder which behave as a single unit during the mixing process [8]. The entire mixing process and the parameters used for it is described in tabular format in Table 3.4. The resultant feedstock was then stored in glass jars of 200 mL capacity with silica desiccant packets to reduce the effect of moisture on the

feedstock. A blend of ethylene glycol and iso-propyl alcohol was used in a ratio of 1:4 to prevent powder agglomeration due to accumulation of static charge in the powder during the mixing process. 50 mL of this blend was used in every jar.

Table 3.4 List of parameters used in the preparation of feedstock using a speed mixer

Mixing Parameters	Value
Weight of sample	**500 g**
Rotational speed	**600 RPM**
Mixing time/cycle	**15 minutes**
Cycles/sample	**4**

3.3.3 Preparation of liquid binder

The liquid binder, also referred to as binder throughout this body of work is an aqueous solution of PVA which was manufactured by mechanical agitation of PVA in de-ionised water using an overhead rotary stirrer [T25, Ultra Turrax, Oxford, UK]. The process setup is represented schematically in Figure 3.3. Three PVA specimens of molecular weights 10,000; 26,000 and 84,000 g/mol were chosen for experimentation. The molecular weights of the candidate PVA specimens were identical to the ones mentioned in Table 3.2. Molecular weight was considered as a relevant process variable throughout the thesis. An ideal binder used for processing materials using BJT would have high infiltration capability with optimum levels of vertical infiltration and lateral spreading, as discussed by **Leary** [9]. The extent of lateral spreading and vertical infiltration of a binder depends on the surface tension and viscosity of the binder during processing of material which can be directly attributed to the molecular weights for polymers like PVA [5,10]. A weighed sample of PVA is placed in a beaker and a calculated amount of de-ionised water [Alfa Aesar, Heysham, UK] is poured into it. The beaker is then placed on a hot plate with a magnetic stirring facility [CL464, Camlab, Over, UK] and is heated up to a suitable temperature and thermally agitated using the rotary stirrer for a set amount of time. After complete dissolution of the PVA

in the solvent, the setup is dismantled and the PVA solution, which is now considered as the binder, is allowed to cool down to room temperature. The binder is then stored in airtight glass jars and stored in a refrigerated environment of 6°C till it is used. Prepared binders, stored in this manner can be used for a period of 20 days, before the binder solution starts to deteriorate. The values of parameters which were used to prepare the liquid binders are provided in Table 3.5. The different grades of PVA had different times of dissolution which was linearly proportional to their molecular weights. The HMW PVA took more time to dissolve in comparison to MMW and LMW. This was attributed to the lengthier polymer chains which is associated with higher molecular weight which requires more energy to dissolve in the solvent. The temperature of the solution was kept constant throughout the dissolution process. The speed of the overhead stirrer was kept constant at 300 RPM.

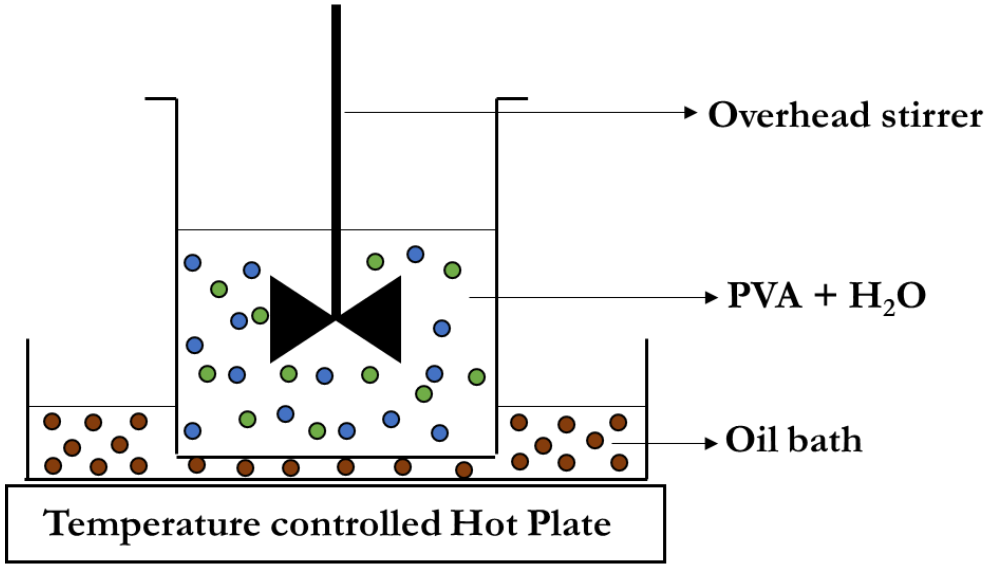

Fig 3.3 Schematic diagram of setup to make aqueous liquid binder

Table 3.5 List of parameters used for making liquid binders

Parameter	Type of PVA	Value
Dissolution temperature	All	80°C
Dissolution duration	LMW	60 min
	MMW	85 min
	HMW	105 min
Stirrer speed	All	300 RPM

3.4 Printability Trials

The effect of the composition of the modified feedstock and the liquid binder on the quality of printing and structural integrity of built parts was investigated by trial and error. The addition of an optimum amount of binder is important for the green strength of the printed green part. Table 3.6 tabulates the different combination of PVA concentrations used in the liquid binders and modified feedstock used in the experimental printability trials. A single drop on demand, piezoelectric glass capillary printhead device [MJ-AT-01, MicroFab Technologies Inc., Plano, US] was used for the printability exercise along with a commercial Inkjet printing system [JetLab 4xL, MicroFab Technologies Inc., Plano, US]. When the effective amount of PVA was deficient, the printed part collapsed under self-weight due to lack of adhesive action of the binder on the powder particles. When the effective amount of PVA was high, it often led to drying out of the green part due to a lack of water which cause it to crumble upon any attempts to handle it. This was seen in samples where the feedstock had 10% PVA by weight which was printed using 5% by weight PVA binder. The excessive PVA present in the green part would cause interchain crosslinking, especially after the thermal curing process [11]. The crosslinking process could make the cured part extremely brittle, which could cause the part to become extremely fragile and susceptible to crumbling. When the amount of PVA was above optimum in the liquid binder, the printhead would have problems in dispensing it in a reliable manner.

Table 3.6 Combination of molecular weights of polyvinyl alcohol, its concentration in the Liquid Binder and Modified Feedstock respectively

PVA Molecular Weight (g/mol)	**Different composition-based variations**
10, 000 (LMW) 26, 000 (MMW) 84, 000 (HMW)	LMW/MMW/HMW_5_5 LMW/MMW/HMW _5_10 LMW/MMW/HMW _10_5 LMW/MMW/HMW _10_10
PVA Concentration in Binder (% Wt.)	
5% 10%	
PVA Concentration in Feedstock (% Wt)	
5% 10%	

Table 3.7 tabulated the trials which were performed to obtain an optimum amount of PVA in the liquid binder and the modified feedstock. Once the printability trials were concluded, the feedstock and liquid binder, each containing 5% PVA by percentage of weight were prepared using the methodology described in Section 3.3. Considering the three different types of PVA which have been chosen, the final candidates were LMW_5_5, MMW_5_5 and HMW_5_5 respectively using the nomenclature used in Table 3.7. This concludes the section on binder and feedstock preparation and now characterisation of the binders and feedstocks would commence in the next few sections.

Table 3.7 Summary of attempts to print parts with variation in composition of PVA in the liquid binder and feedstock.

Binder → / Feedstock ↓	0% PVA	5% PVA	10%PVA
0% PVA	Green part disintegrated	Green part disintegrated	Liquid binder did not jet
5% PVA	Green part disintegrated	**Part printed, cured**	Liquid binder did not jet
10% PVA	Dried green part crumbled	Dried green part crumbled	Liquid binder did not jet

3.5 Thermal Characterisation of Feedstock and Binder

The green part, once printed and cured, underwent a thermal cycle which involved three main stages including binder burnout/de-binding, pre-sintering, and sintering. The cycle was concluded with furnace cooling or air cooling. Thermogravimetric analysis (TGA) was used to gauge the temperature at which the PVA starts to thermally decompose, indicating the burnout temperature and indicate the presence of any extraneous carbon formed due to formation of soot or due to charring of the sintered specimen. TGA of the PVA binders and the feedstock was carried out separately and have been represented in Figures 3.4 (a) and (b). The TGA of the PVA samples was done based on the ASTM E1131-20 standard for thermoplastics [12], where the maximum temperature was set at 600°C, following a ramping rate of 10°C/min in a nitrogen purged environment. TGA of the feedstock was done till 1260°C using the same ramping rate and purging environment. It was observed that the Inconel 718 component of the feedstock did not participate in any thermal decomposition in an inert nitrogen environment. Hence, its effect was subtracted from the decomposition behaviour to focus more on the PVA component of the feedstock using the proprietary software of the TGA setup [TGA 8000, Perkin Elmer, Massachusetts, US]. The TGA of the feedstock simulated the parameters of the actual sintering process including the final

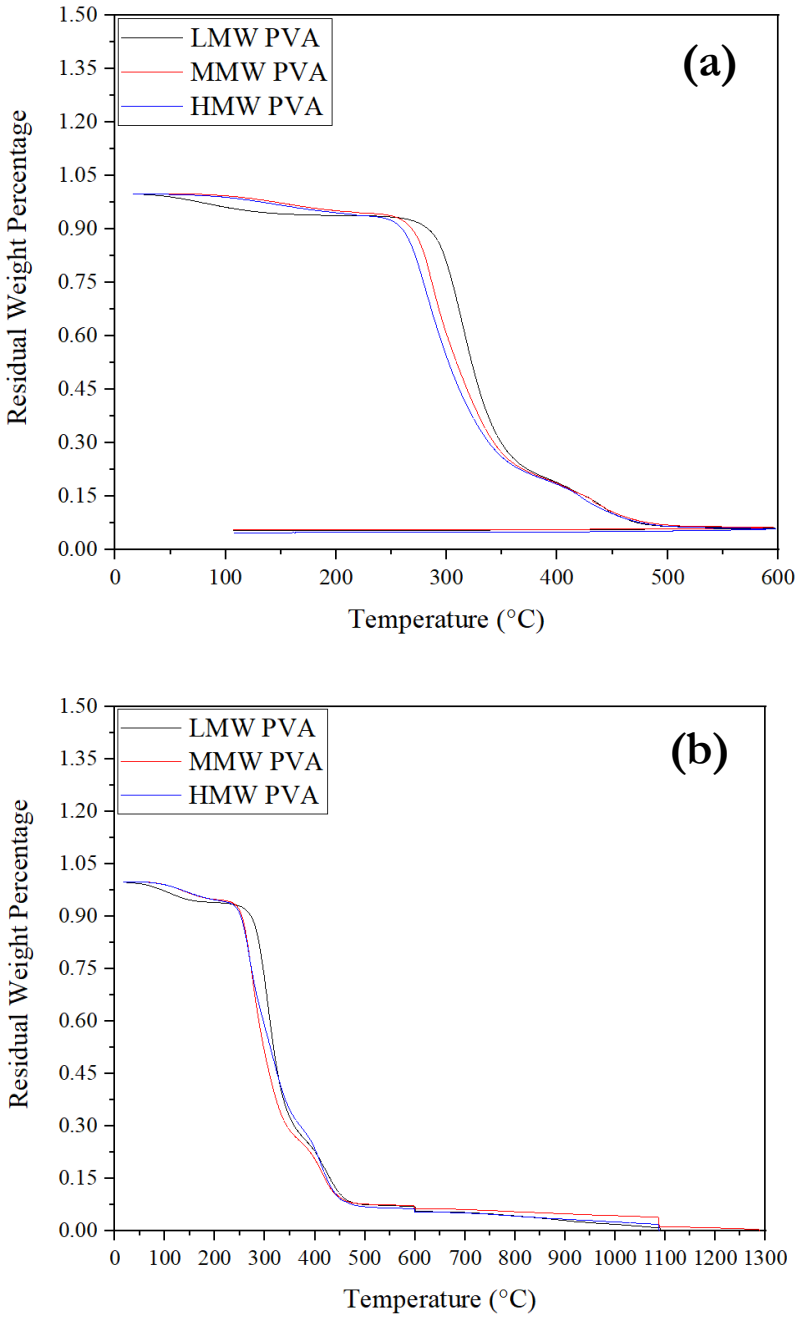

Fig 3.4 TGA plots to gauge thermal decomposition behaviour and extent of charring in (a) PVA granules (b) modified feedstock having Inconel 718 + PVA.

temperature and ramping rate. It was observed that 0.75% of the binder was what remained after the conclusion of the ASTM E1131-20 sanctioned TGA cycle whereas in case of TGA of the modified feedstock, very little of the binder was remaining after the burnout phase.

3.6 Rheological Characterisation of Powder and Binder

3.6.1 FT4 based powder rheology

The permeability, variable flow rate (VFR) and shear stress of the different feedstock were measured using an FT4 powder rheometer (Freemantech, Tewkesbury, UK). Virgin Inconel 718 was initially characterised as a benchmark to understand the effect of the addition of different polyvinyl alcohol powders on the spreadability of the modified feedstock. The rheological studies were based on the rotation of a stainless-steel blade which would be inserted into a cylindrical glass vessel of 25 mL containing a sample of the feedstock. The resistance to dynamic flow experienced by the rotating blade due to the powder present in the vessel would be directly proportional to the VFR. The methodology was best described by the work of Søgaard et al. [13], whose work evaluated the feasibility of using the FT4 rheometer as a reproducible characterisation method. The results of the FT4 based rheological evaluation of the feedstocks have been elaborately discussed in Chapter 4.

3.6.2 Surface tension and dynamic viscosity of the binder

The characteristics of an ideal binder which can be used to process materials using BJT have been discussed in Section 3.3.3. The ability of the binder to vertically infiltrate and laterally spread once it has contacted the powder bed is dependent on its physical properties like surface tension and viscosity. The effective surface tension and viscosity would be dependent on environmental factors like operating temperature, hence it is very important to measure the surface tension and viscosity of the binders at different temperatures to gauge their possible behaviour as binders during BJT of materials. The surface tension of the binder was measured using a tensiometer [K20, Krüss, Hamburg, Germany]. The tensiometer has a Wilhelmy plate which was slowly dipped vertically into the liquid, in this case being the PVA based binder. After contact is established, the surface tension, σ is calculated by the proprietary software, using Equation 3.1 [14]

$$\sigma = \frac{F}{L\ \cos\theta}\ [Equation\ 3.1]$$

σ is the calculated surface tension, F is the measured force which acts between the plate and the liquid, L is the contact length between the plate and the liquid, which is the width of the plate and θ is the contact angle formed between the liquid and the plate. The measurement process is preceded by a calibration step where the value of θ is calculated using a calibration liquid with known surface tension. The calibration was performed using distilled water at an ambient temperature of 30°C. The schematic figure of the working principle is described in Figure 3.5.

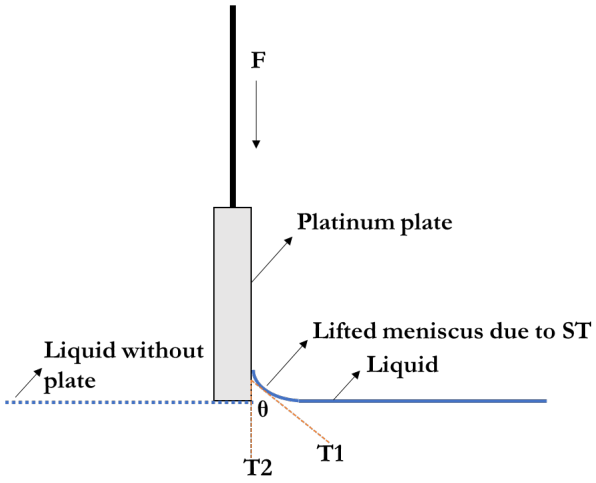

Fig 3.5 Wilhelmy plate setup used for calculating surface tension of a liquid. Θ is the angle made between T1 and T2, which are tangents to the plate surface and the liquid meniscus.

The dynamic viscosity of the liquid binders was measured using a temperature-controlled viscometer [ViscoLab 3000, Cambridge Viscosity, Boston, US]. The temperature was varied between 25-40°C at 25, 30, 35 and 40°C and the viscosity was measured at these points. All the experiments were done three times for maintaining repeatability. The results have been presented and discussed in Chapter 4.

3.7 Wettability Analysis – Measure of Powder-Binder Interaction

The wettability analysis was performed using static sessile drop testing method. The setup has been represented in Figure 3.6 (a) to (c) which schematically describes the three important stages of the experiment. A predetermined amount of binder (200 μL) is released from a micro-pipette which then impinges on the powder bed and is immediately imbibed by it. The digital microscope (in the same direction as the sight of the reader) starts recording the process at 100 fps and stops only when the droplet completely disappears because of its imbibition by the powder bed. The procedure and setup were adapted from the dissertation of Williams [15]. The frames were carefully observed, and every candidate liquid binder droplet was measured at the third second after the impingement of the droplet on the powder bed. This experiment was preceded by a benchmarking exercise where the powder bed was replaced by a solid substrate of Inconel 718. The experiment was conducted for every combination of PVA based binder and the corresponding feedstock consisting of Inconel 718 powder and PVA powder. The commercial binder was tested against virgin Inconel 718 powder, as in commercial systems, pure powder would be printed using commercially available binders. The experiment was conducted in a dark lit room with a LED light source fitted at the back of the micro-pipette as was described in the literature [15].

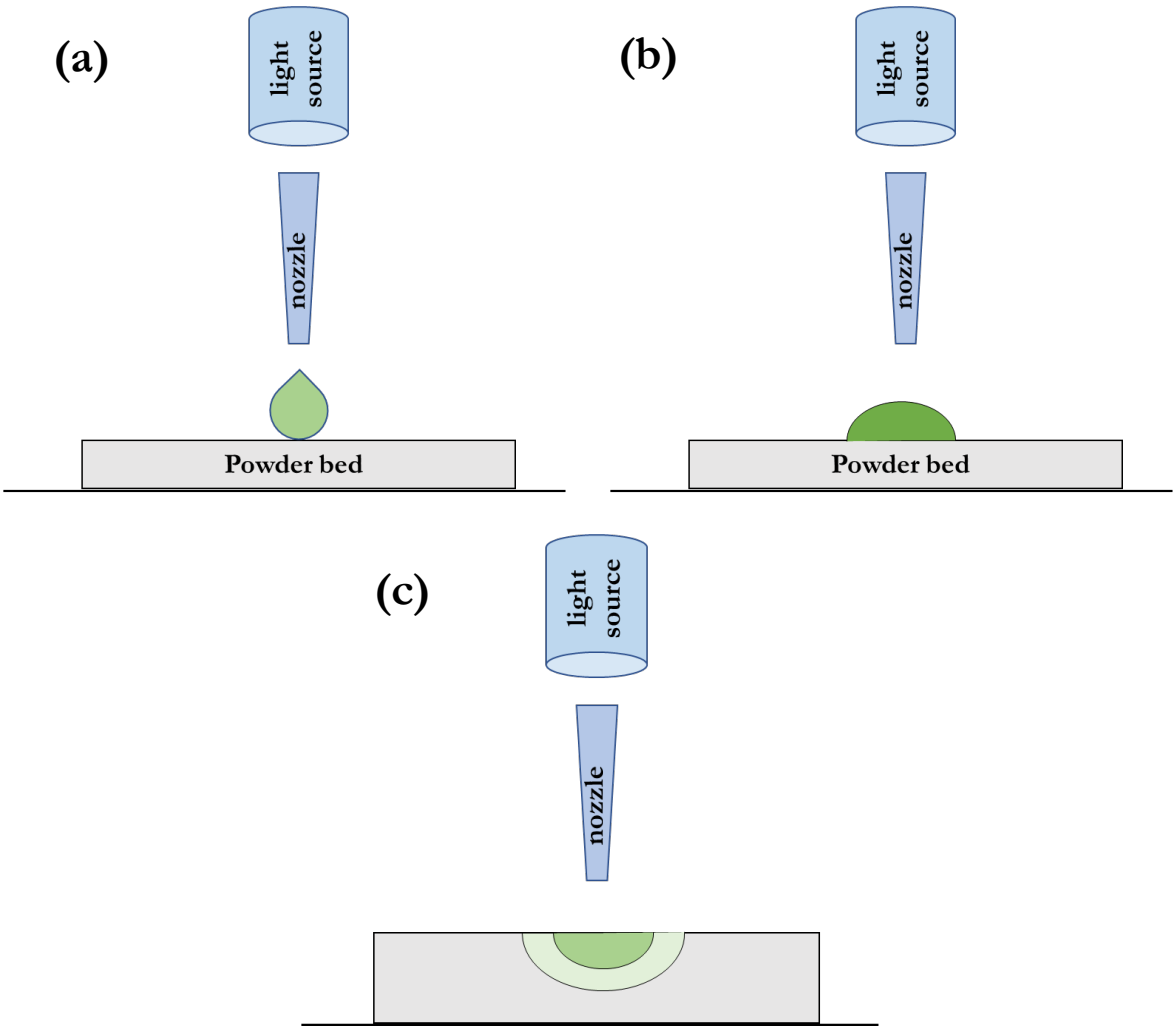

Fig 3.6 Schematic diagram of the three different stages of the sessile drop testing experiment : (a) liquid binder droplet contacts the powder bed (b) droplet starts to infiltrate the powder bed (c) droplet disappears from sight, forms nugget inside the powder bed.

3.8 Jetting of Binder and Printing of Parts

3.8.1 Droplet jetting parameters during printing

A drop on demand piezoelectric printhead was used to dispense binder as mentioned earlier. These printhead devices are characterised by the presence of a piezo-ceramic attachment. When a voltage is applied across the attachment, it deforms and introduces a pressure wave into the column of liquid binder which helps the nozzle of the printhead device to reliably dispense a single binder

droplet. The way the voltage is applied across the piezo-ceramic attachment dictates the formation and dispensing of droplets from the nozzle of the printhead onto the substrate. The piezoelectric attachment expands and contracts when voltage is applied and withdrawn from it, which causes pressure waves to form in the capillary column and dispense a droplet [16]. The time for which voltage is applied, withdrawn, and applied again are termed as the rise, fall and delay time of the droplet ejection process. The time between the rise and fall of the voltage is called the 'dwell time'. Figure 3.7 represents the phenomenon when the voltage is applied, held, and then withdrawn from the piezo-ceramic attachment. The voltage and the rise, fall and dwell times are initially set by trial and error with the objective of droplet ejection from the nozzle. The entire cycle of voltage rise, dwell and fall is called a waveform which physically signifies a single pulse typically causing a binder droplet to be ejected. Several such waveforms can be introduced per unit time, which increases the control on the droplet dispensation process and decreases the droplet volume.

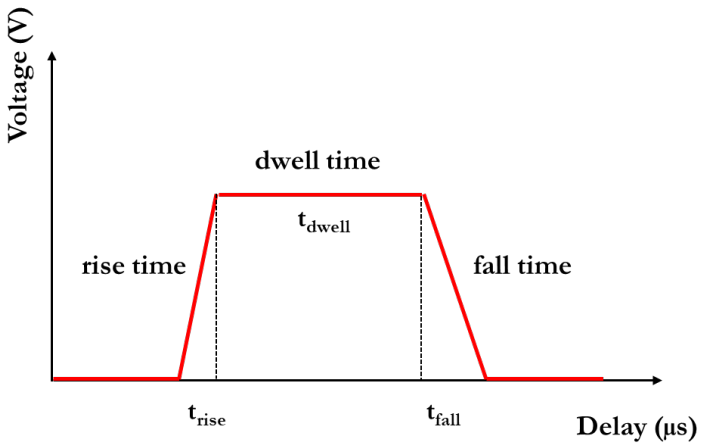

Fig 3.7 Stages of a generic waveform involved in the formation and ejection of a droplet from a piezoelectric printhead device. The t_{rise} and t_{fall} may be symmetric or asymmetric to ensure reliable ejection of droplets.

3.8.2 Droplet spacing during printing

Once the waveform parameters are set to ensure reliable ejection of droplets, the printhead moves around the powder bed on an 3D gantry system, selectively depositing droplets of binder. The

distance between two consecutive depositions of droplets along a rectilinear direction of movement is termed as the droplet spacing. Droplet spacing can be expressed as a function of the droplet diameter, d, which is always constant due to the nature of printhead device. The number of drops deposited in a unit area of the powder bed increases with the decreasing value of droplet spacing. One can control the amount of liquid binder being deposited per unit volume of the powder, thus controlling the binder saturation levels of the printing process. In commercial Binder Jetting systems, the desired binder saturation level is fed to the system which then calculates the droplet spacing based on other printing parameters like layer thickness. However, in the JetLab 4xL system, the input demanded by the user interface was droplet spacing in the form of steps in the X and Y direction of printing, which then led to the automatic calculation of print speed. In this work, the desired binder saturation level was kept at 110% to avoid poor particle adhesion and feathering as discussed in Section 2.3, Chapter 2, and the number of droplets per envelope was calculated and fed into the JetLab 4xL user interface. Table 3.8 elaborates on the parameters adopted for the printing process.

Table 3.8 Summary of parameters adopted during the printing process. The parameters highlighted in green are calculated by the user interface

Controllable and Calculated Parameters for Ejection of Droplets from the Printhead			
Frequency	60 Hz	**Rise time**	3 μs
Voltage	25 V	**Dwell time**	25 μs
Echo Voltage	-25 V	**Fall time**	3 μs
Droplet volume	10 pL	**Final rise time**	3 μs
Controllable and Calculated Printing Parameters			
Binder Saturation	110%	**Printhead distance**	1000 μm
Layer thickness	200 μm	**X/Y spacing**	30 μm
Volume/envelope	80 pL	**Droplets/spacing**	8

3.8.3 Printing setup

Figure 3.8 represents the setup which was used to print the green parts. A smooth, polished glass platform was used as a substrate for all builds in this body of work. Glass was the material of choice as it is chemically inert, relatively unresponsive to heat during the curing process and is easy to remove from the cured part due to its polished surface. Templates were placed on the substrate, which acted as a mechanism to ensure uniform layer thickness as the feedstock was wiped over it with a knife edge wiper. A fresh template was placed after a layer was processed, and fresh powder was wiped onto the template, effectively following the 'layer-by-layer' action of any powder bed technique. The parts being printed were kept well away from the walls of the template to avoid any structural support. After the conclusion of the printing process, the templates were cut in several places with a hot scalpel and removed.

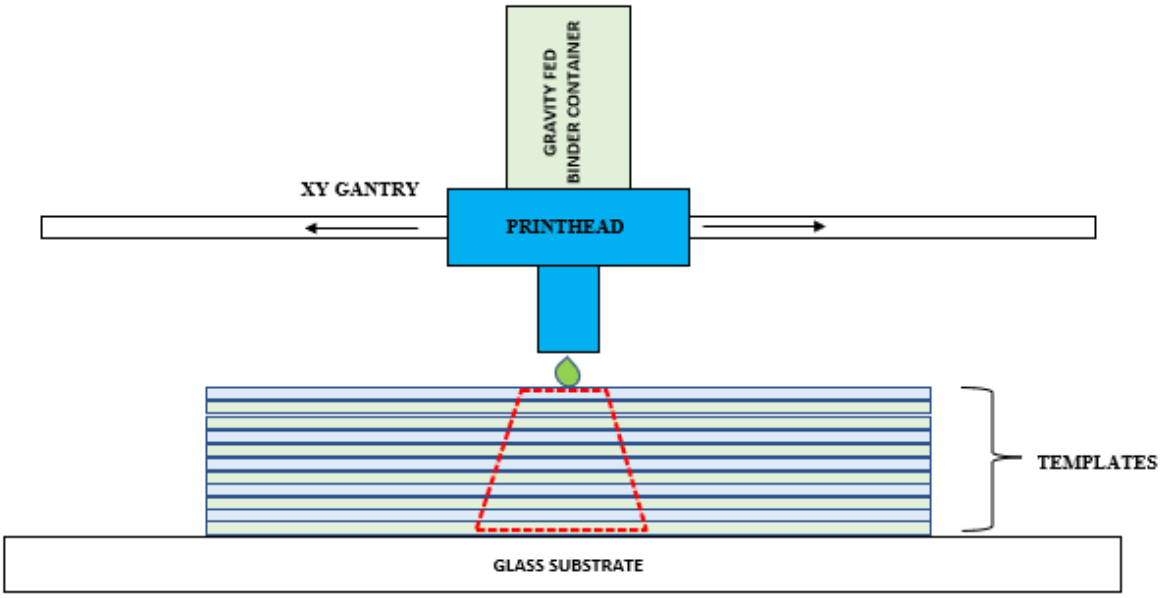

Fig 3.8 Schematic representation of the printing setup. The dotted red line indicates the part being printed

The green part was then carefully extracted from the mass of powder using a brush and then transferred to the curing oven, where it was kept at a constant temperature of 60°C for twelve hours. The curing atmosphere enabled the excess water to evaporate and the PVA present in the binder and the feedstock to strengthen the now cured green part.

3.9 Post-processing of Green Parts – Sintering and HIP

The cured parts were sintered in a horizontally mounted tube furnace [TF1400, Carbolite Gero, Hope, UK]. Figure 3.9 shows the thermal cycle which was programmed into the tube furnace feedback system using a programmable logic controller (PLC). This cycle was followed for all parts which were sintered throughout the study. The binder burnout was done at 600°C, which was

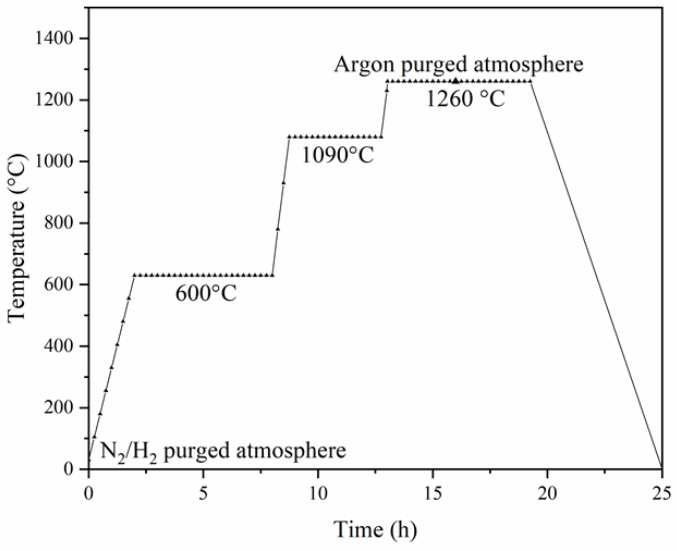

Fig 3.9 Thermal cycle including the binder burnout, pre-sintering, and sintering stages of the post-processing of the printed part [17].

maintained for four hours, after which it was pre-sintered at 1090°C before being sintered at 1260°C. After the conclusion of the sintering process, the furnace was switched off to cool down naturally. The gas purged environment was maintained till the temperature of the furnace cooled down to 100°C. The cycle was carried out in two different purged atmospheres to investigate the role of sintering environments on the part quality. Table 3.9 tabulates the details for the sintering

Table 3.9 Description of sintering variables in tabulated format

Sintering Stages and Duration		
Burnout stage	600°C	4 hours
Pre-sintering	1090°C	4 hours
Sintering stage	1260°C	6 hours
Sintering Atmosphere		
99.98% argon for burnout, pre-sintering, and sintering stages and furnace cooling	95% N_2 + 5% H_2 mixture for burnout and pre-sintering stages. 99.98% argon for sintering and furnace cooling.	

process. The gauge pressure of the gas cylinders [BOC, Guildford, UK] was maintained at 1.5 bar with a flow rate of 10.5 m^3/minute.

HIP was done on some of the samples to investigate its effect on the porosity and mechanical properties of the sintered parts. The post-processing was done using a hot isostatic press [AIP8-45H, AIP HIP, Columbus, US] at 1200°C for three hours, maintained at a pressure of 1200 bar. Fig 3.10 (a) to (c) are some of the parts that were printed and sintered.

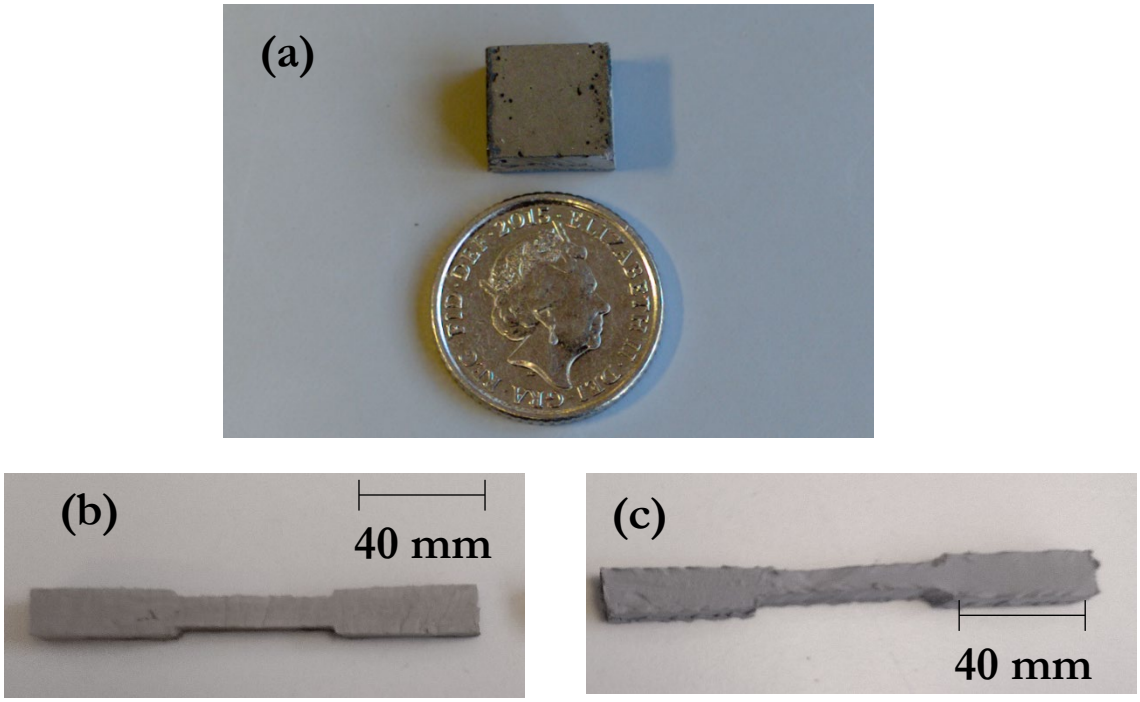

Fig 3.10 Parts that were processed using PVA based binder and feedstock: (a) sintered cubical sample (b) sintered tensile specimen (c) green tensile specimen.

3.10 Porosity Analysis

The porosity of the samples was evaluated using ImageJ, an open-source image processing software, which calculated the porosity by recognising the pores on SEM micrographs of polished samples of the transverse section of the samples. The SEM micrographs were converted to 8-bit greyscale images and the contrast threshold was measured using ImageJ. The 8-bit image converted the image into a black and white image where the contrast was dependent on the topographical features of the micrograph, which in this case were the pores and holes on the surface. This method was adopted from the dissertation work of Zavala-Arredondo [18]

3.11 Mechanical Testing of Parts

3.11.1 Measurement of green strength

Green strength is a qualitative measure of the robustness of green parts which are either freshly printed or which have undergone curing to activate the adhesive action of the binder. Parts with poor green strength often collapse under self-weight or are difficult to handle during the extraction and transfer process to the curing oven. A high green strength is indicative of a good interaction between the binder and the powder which translates into good, sintered parts with minimal porosity. A universal tensile testing machine [10ST, Tinius Olsen Ltd, Redhill, UK] was used to measure the flexure suffered by the green parts before failure. The parts were printed in accordance with ASTM B312 [19] and were cured in the curing oven for twelve hours as discussed in Section 3.8. The top ram was located at the middle of the sample and was given a clearance of 1-2 mm from the surface of the sample. The approach speed of the top ram was kept at a constant of 1 mm/min and the pre-load condition was reset to zero after adjusting the ram, before every experiment. The experiment was stopped when a drop in the reading was observed which was indicative of the flexural failure of the sample. Figure 3.11 (a) and (b) are indicative of a 'before and after' photo of a sample at the conclusion of a flex test. The results of the green strength tests have been discussed in Chapter 5.

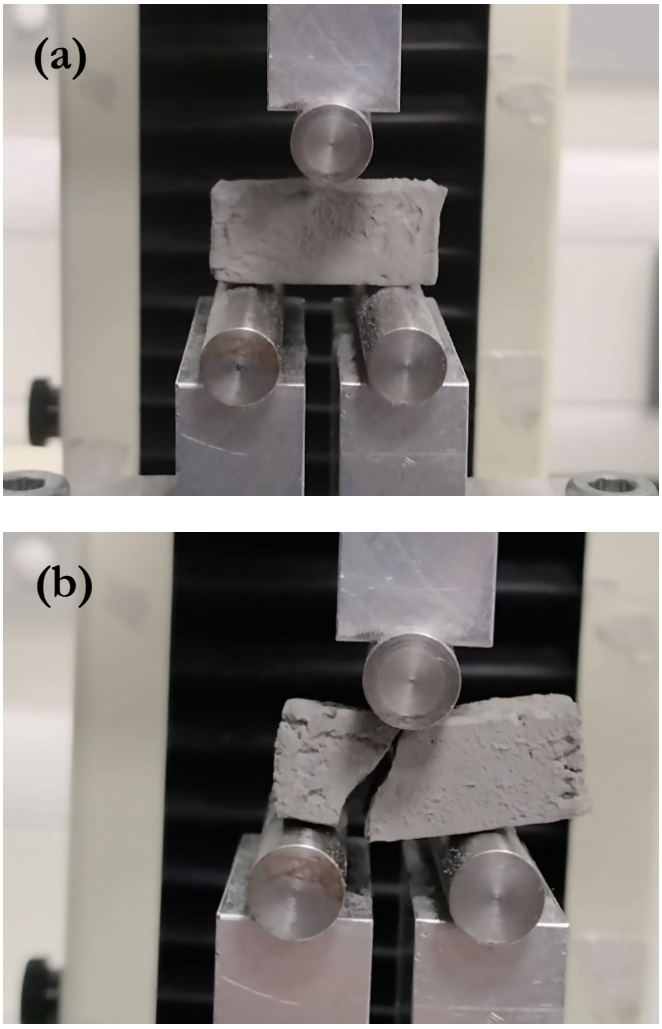

Fig 3.11 Images of printed and cured green part undergoing green strength measurement at (a) commencement (b) conclusion of experiment

3.11.2 Measurement of tensile strength and hardness

Measurement of the tensile strength was done using a universal tensile strength [50ST, Tinius Olsen Ltd, Redhill, UK] with a 50 kN load cell which was supplied by the manufacturer. A clip-on axial extensometer [Model 3542, Epsilon Technology Corp., Jackson, US] was used to measure the strain until the point of rupture. The strain rate was measured in accordance with ASTM F3055-14a, and its range was kept within 0.003-0.007 mm/mm/minute [20] to ensure that the sample failed under one minute.

The hardness was measured on hot mounted and polished samples using a microhardness tester [HM210, Mitutoyo, Kawasaki, Japan] with an incident load of 10 kgf. Every sample had ten indentations performed on them to ensure repeatability and the process was conducted in SI units for its universal acceptance.

3.11.3 Miscellaneous experimental details

3.11.3.1 Sample preparation protocol

Experimental procedures for measurement of hardness, SEM micrographs and XRD phase analysis require polished samples which guarantee the flatness of the sample. The sample preparation can be divided into (a) sectioning (b) hot mounting (c) grinding (d) polishing (e) cleaning and storage. The sectioning process is where a portion of sample, often containing the area of interest (fracture site, corrosion site etc) is separated from the main part. This was relevant in this work while working on the fractographs of the tensile test samples. The sectioning process carried out using a precision cutting machine [Secotom 10M, Struers Ltd, Rotherham, UK] with an abrasive SiC based wheel operating at a speed of 3000 RPM and a feed of 0.02 mm/s.

The hot mounting process involves putting the sample inside a compression based hot mounting press [SimpliMet, Buehler UK Ltd, London, UK], where a conductive thermoset polymer engulfs the sample at a temperature of 600°C and pressure of 7 bar.

The grinding process is done to ensure that the surface is flat. This is achieved by maximising the material removal of the sample in a uniform manner to achieve a flat surface. The grinding and polishing were achieved in an automated grinder polisher [AutoMet 250, Buehler UK Ltd, London, UK] where the sample is rubbed against different grades of SiC paper (P240, P300, P500). The grinding process is followed by the polishing process where the aim is to improve the surface finish of the surface and remove any scratches which were introduced on the surface of the mounted

sample during the polishing process. This is achieved in a similar process by using polishing pads and corresponding polishing suspensions [21].

After the polishing process, the virgin surface of the sample is prone to oxidation due to the presence of moisture in the air. The polished samples are immediately cleaned in a fast stream of iso-propyl alcohol and dried using a hot air gun. It is then stored in a desiccator with the surface protected using a metallographic cap.

3.11.3.2 X ray diffraction methodology

The phase analysis of the samples was completed using an X-ray diffractometer (Empyrean system, Panalytcal BV, Almelo, Netherlands). Cu-Kα radiation was used with the Cu tube set at 40 kV and 45 mA. An X ray mask of 1 mm width was used to filter the incoming X rays which were then sent outwards via a divergent slit having a width of 2 mm. The scanning was performed between 30 to 100° with an incremental step of 0.1°. The X ray beam was passed through a parallel plate collimator after diffraction and its intensity was monitored by a PIXcel detector which was set at 0D mode

3.12 Chapter Summary

Chapter 3 elaborates on the different experimental procedures which were adopted throughout this body of work. The initial part of the chapter focuses on the characterisation of the raw materials including the Inconel 718 and PVA. The preparation of the feedstock and binders are described followed by the thermal and rheological characterisation to gauge the suitability of the PVA based binders and feedstock in terms of charring and increased carbon content. The powder-binder interaction process was described with schematics. The droplet dispensing and printing parameters were also elaborated upon with the printing process being described with the help of a schematic representation. The sintering and post-processing techniques were described in tabular

form. Mechanical testing of the parts was mostly done according to international standards which were mentioned.

References:

1. Greene GA, Finfrock CC. Oxidation of Inconel 718 in Air at Temperatures From 973k to 1620k. Brookhaven National Lab., Upton, NY (US); 2000 Oct 1.
2. Spierings AB, Herres N, Levy G. Influence of the particle size distribution on surface quality and mechanical properties in AM steel parts. Rapid Prototyping Journal. 2011 Apr 26; 17(3): 195-202.
3. Lovell PA, Young R. Introduction to Polymers. 3rd Edition. Manchester (UK): CRC Press; 2011.
4. DeMerlis CC, Schoneker DR. Review of the oral toxicity of polyvinyl alcohol (PVA). Food and Chemical Toxicology. 2003 Mar; 41(3): 319-326.
5. Finch CA. Polyvinyl alcohol: properties and applications. London (UK): Wiley; 1973.
6. Rumyantsev M. Influences of co-solvent on hydrogen bond reorganisation in ternary poly (vinyl alcohol) solutions. European Polymer Journal. 2013 Aug; 49 (8): 2257-2266.
7. Jaeger HM, Nagel SR, Behringer RP. Granular solids, liquids, and gases. Reviews of modern physics. 1996 Oct 1;68(4):1259.
8. Sudah OS, Coffin-Beach D, Muzzio FJ. Effects of blender rotational speed and discharge on the homogeneity of cohesive and free-flowing mixtures. International Journal of Pharmaceuticals. 2002 July 5; 247: 57-68.
9. Leary M. Design for Additive Manufacturing. Kidlington (UK): Elsevier; 2020
10. Schlachter DA, Lennox MD, Favis BD, Therriault D, Tavares JR. Physicochemical Limitations of Capillary Models Applied to High-Concentration Polymer Solutions. ACS omega. 2022 Feb 11;7(7):5636-45.

11. Sonker AS, Rathore K, Nagarale RK, Verma V. Crosslinking of polyvinyl alcohol (PVA) and effect of crosslinker shape (aliphatic and aromatic) thereof. Journal of Polymers & Environment. 2017 July 5; 26: 1782-1794.
12. ASTM, ISO/ASTM E1131-20:2020(EN): Standard Test Method for Compositional Analysis by Thermogravimetry. West Conshohocken, 2020.
13. Søgaard SV, Allesø M, Garnaes J, Baldursdottír S, Rantanen J. Development of a reproducible powder characterization method using a powder rheometer. Annual transactions of the nordic rheology society (submitted). 2012.
14. Kruss K20: User Guide & Instruction Manual (English Edition). Hamburg (Germany): Kruss, 2013.
15. Williams RJ. The application of halloysite nanotubes in epoxy resin nanocomposites [dissertation]. Sheffield (UK): University of Sheffield; 2019.
16. Bogy DB, Talke FE. Experimental and theoretical study of wave propagation phenomena in drop-on-demand ink jet devices. IBM Journal of research and development. 1984 May;28(3):314-21.
17. Valencia JJ, Spirko J, Schmees R. Sintering effect on the microstructure and mechanical properties of alloy 718 processed by powder injection molding. In: E.A. Loria (Ed.), Superalloys 718, 625, 706, and Various Derivatives, TMS, 1997.
18. Zavala Arredondo MA. Diode area melting use of high-power diode lasers in Additive manufacturing of metallic components [dissertation]. Sheffield (UK): University of Sheffield; 2017.
19. ASTM. ASTM B312 (2020). Standard test method for green strength of specimens compacted from metal powders. West Conshohocken, US: ASTM International. 2020: 1-14.
20. ASTM. ASTM F3055-14a (2021). Standard specification for additive manufacturing nickel alloy (UNS N07718) with powder bed fusion. West Conshohocken, US: ASTM International. 2020: 1-5.

21. Vander Voort G, Manilova E. Metallographic techniques for superalloys. Microscopy and Microanalysis. 2004 Aug;10(S02):690-1.

CHAPTER 4:

EVALUATION OF FEEDSTOCK & BINDER

'Binders coming out of nozzles, how is that interesting? It's not like they glow in the dark or smell nice or whatever'

– an unconvinced housemate on a Friday evening over sushi and plum tea.

4.1. Introduction

The ability of the powder to spread uniformly and consistently is important for the printing process to be smooth and to prevent interruptions and failed prints. Any resistance offered by the feedstock would be detrimental to the entire printing procedure, resulting in failed prints or a compromise with the tight dimensional and geometrical tolerances expected from most AM methods. Clayton et al. suggested that the suitability of a feedstock for any AM process required its rheological study [1] including measurement of permeability and specific energy. The FT4 rheometer has been used as an experimental tool to measure the suitability of a powder feedstock, for its use in AM processes [2-4].

Permeability of a powder is the resistance of a powder bed towards an air flow passing through. It is a measure of the extent to which an amount of powder can be compacted [5]. A lower value of permeability would indicate that powder compaction is too high and that would restrict outgassing of the binder during the thermal cycle, which may cause irregular porosity within the bulk of the printed part. An optimum permeability would ensure that the individual powder particles are not too compacted, which offers the opportunity for the gases to escape the part. Permeability would also help the liquid binder to penetrate the bulk of the powder layer deposited and wet all the particles, leading to a better inter-particle binding which would result in more robust green parts [6].

Specific energy is a measure of the resistance offered by the bulk of the powder to flow. A high value of specific energy indicates poor spreading of the feedstock due to the combined effect of inter-particle friction, interlocking and cohesion, which is detrimental to the free-flowing action of the powder. The term 'Variable Flow Rate' or VFR has been used extensively in available literature to study the spreadability of different powders. The relationship between specific energy and VFR of a sample of given mass, say m is provided by Equation 4.1.

$$Specific\ Energy = \frac{VFR}{m} \text{[Equation 4.1]}$$

Shaheen et al. in their numerical studies predicted that large particles having a diameter of 75-79 μm would have strong cohesive forces which would lead to the formation of powder 'heaps' which would cause non-uniform spreading [7]. Increased resistance to powder flow would result in non-uniform layer thickness. The VFR of the feedstock consisting of the metal powder and the dry PVA binder was measured to compare its resistance to bulk flow with virgin metal powder. The VFR of dry PVA powder was not performed we were primary interested its effect on the entire feedstock as a whole.

Rheological analysis of the liquid binders involved measurement of surface tension and dynamic viscosity. Sessile drop testing was also performed to better understand the interaction between the binder and the metal powder on the powder bed and its effect on wetting.

The combination of an aqueous binder with 5% PVA by weight and a feedstock containing 5% PVA by weight in the form of granular powder was found to be a suitable combination in the printability trials. The role played by molecular weight of the PVA towards this choice of combination was unknown. Lewandowska et al. concluded that aqueous solutions of PVA are non-Newtonian in nature and are rheologically stable over the variation of time and temperature [8]. Mohsen-Nia et al. observed that the rheological properties of aqueous solutions of PVA depended on the molecular weight and degree of polymerisation of the polymers [9]. The

rheological evaluation of the binder was to primarily identify whether the binder could be jetted reliably over time by the inkjet printhead. This can be done by calculating the Ohnesorge number (Oh), a dimensionless number which is defined by Equation 4.2.

$$Oh = \frac{\mu}{\sqrt{\sigma \rho L}} \quad [Equation\ 4.2]$$

μ is the dynamic viscosity, σ is the surface tension, ρ is the density of the liquid being jetted by the printhead and L is the diameter of the printhead nozzle. The reciprocal of Oh is often used instead to indicate stability with which a liquid can be jetted successfully by a printhead. This reciprocal is termed as the Z number. The studies of Derby *et al.* suggested that the range of the Z number for stable jettability should be such that $Z \in [1,10]$ [10]. However, instances of successful jetting outside this window have also been reported [11-12]. The measurement of surface tension and dynamic viscosity of the binder has become a standardised practice across all groups investigating BJT [13-15].

4.2. FT4 based Rheological Evaluation of Feedstock

Fig. 4.1 depicts the variation of permeability of different feedstock with pure Inconel 718 being used as a benchmark. The permeability is measured as a function of pressure drop across the bulk of the powder which was compacted using a standardised packing stress. Air is blown from the bottom of the compacted powder at a standardised pressure and the difference of pressure at the bottom and the top of the compact is termed as the pressure drop. The fundamental law that governs permeability is Darcy's equation, which assumes that the permeating fluid, air in this case flows through a cylinder, which would be an approximation because of the inter-particle gap [16]. Darcy's approximation is provided as Equation 4.3. It can be concluded that the flow rate of the fluid through the porous media is directly proportional to the pressure drop across the compacted

sample, which is represented by Equation 4.4. It is easier to experimentally measure the pressure drop across the specimen and develop an understanding of its permeability.

$$Q = \frac{kA(P_i - P_o)}{\mu L} \; [Equation\ 4.3]$$

$$\Rightarrow Q \propto (P_i - P_o) \; [Equation\ 4.4]$$

where Q is the flow rate of the permeating fluid, P_i and P_o are the inlet and outlet pressure of the permeating fluid, μ is the dynamic viscosity of the fluid, L is the length of the tube, k is the permeability of the specimen and A is the area of the specimen.

The addition of PVA, regardless of molecular weight increased the permeability of the feedstock in comparison to virgin Inconel 718. Metal powder particles are prone to agglomeration due to large amount of surface charges present on the surface of a single particle. The addition of PVA increases the separation between two adjacent Inconel 718 powder particles and discourages agglomeration, which in turn increases the permeability. No correlation could be made in between the molecular weight of the dry granular PVA and its role in increasing the permeability of the modified feedstock. After the measurement of permeability, it was concluded that feedstock containing Inconel 718 and PVA of different molecular weights needed to rheologically evaluated further.

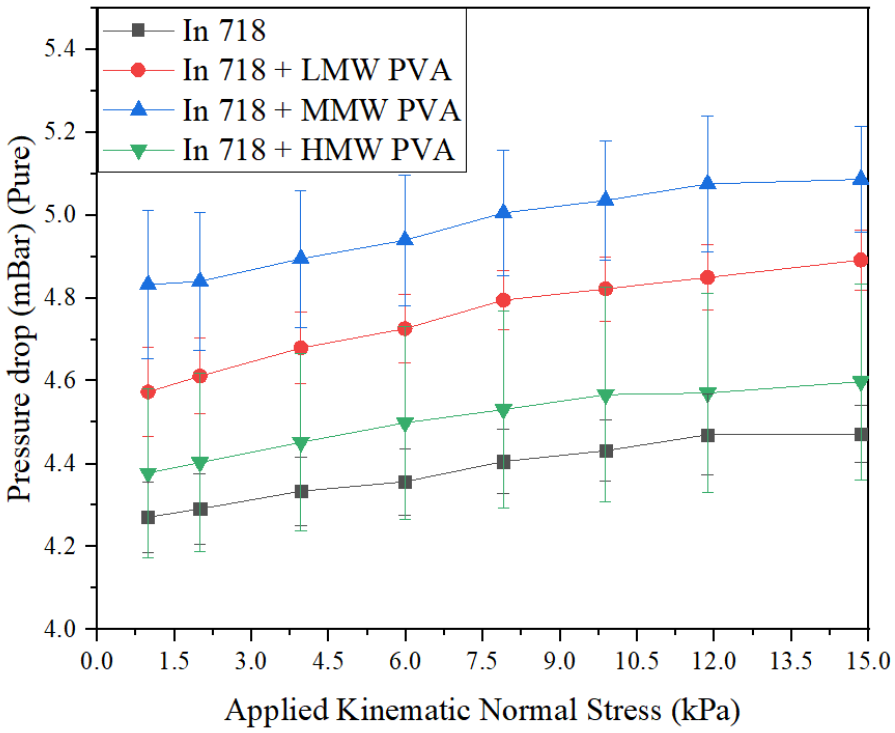

Fig 4.1. Measurement of permeability of different feedstock containing Inconel 718 including (a) pure Inconel 718 (b) Inconel 718 + LMW PVA (c) Inconel 718 + MMW PVA (d) Inconel 718 + HMW PVA

Fig. 4.2 represents the response of the different feedstock when the total energy was measured repeatedly by the FT4 system. The total energy of pure Inconel 718 became high with increasing number of iterations. There was no specific trend followed the feedstock composed of Inconel 718 and PVA. The total energy of all these feedstocks starts higher in comparison to that of pure Inconel 718 and were comparatively more volatile. But there was a drop in total energy for all the feedstocks at around the 7-8th iteration which then started climbing up till the 12th and final iteration. The blade tip speed was maintained at 100 mm/s till the 8th iteration so change of blade speed was not responsible for any sudden changes in the total energy. The sudden drop in total energy could be attributed to the disparity of particle size in the feedstocks and the nature of the FT4 test to measure specific energy. The rotating blade gradually comes down and enters the cylinder, shifting the feedstock continuously and redistributing the Inconel 718 and PVA particles,

which are of different sizes. Similar material responses were noted by Madian et al. [17], who observed an increase in localised compressibility around the rotating blade, while processing uranium dioxide feedstocks having different particle sizes. Another explanation is that smaller particles would settle down at the bottom due to the vigorous stirring action of the blade and would act as a stand-alone material. Some of the PVA granules were smaller than the Inconel 718 particles and would settle at the bottom and would provide a lower value of total energy.

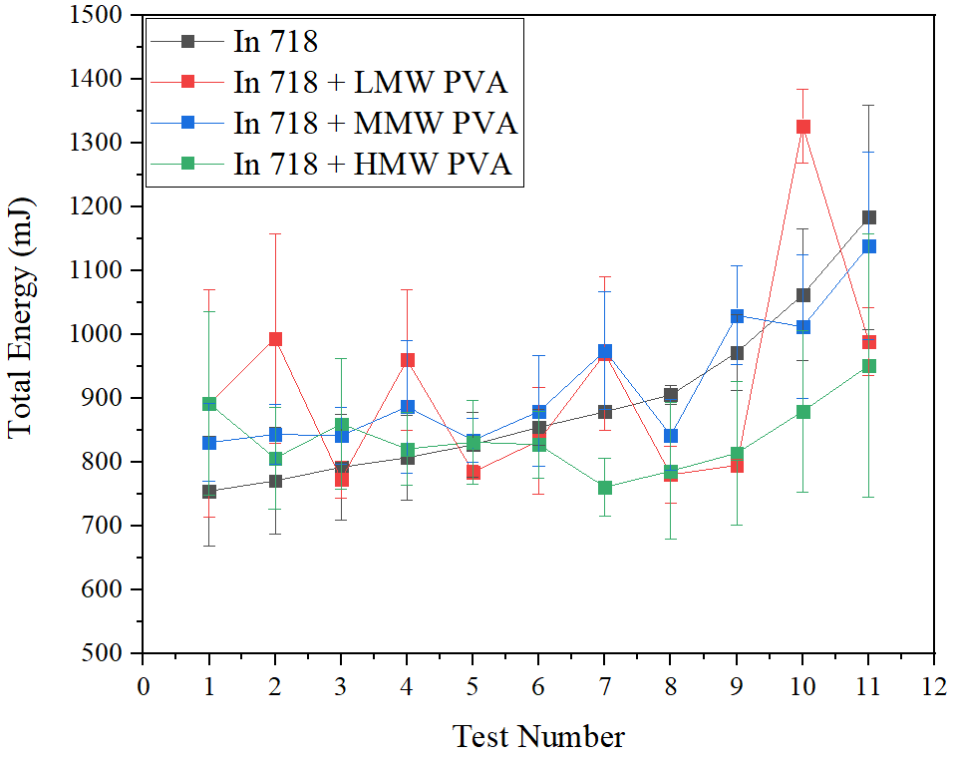

Fig 4.2. Measurement of VFR of different feedstock containing Inconel 718 including (a) pure Inconel 718 (b) Inconel 718 + LMW PVA (c) Inconel 718 + MMW PVA (d) Inconel 718 + HMW PVA

The feedstock consisting of metal powder and LMW PVA consistently displayed unsteady trends especially during the 8-12th iterations. The relative unsteadiness was expected, as it has been observed for the other samples and in other independent work as well [17]. It was the magnitude of change per iteration which was of interest. Sources of systematic errors were identified as potential slippage between the FT4 blade and the driving motor where the detrimental effect of the slipping was exaggerated due to the change of blade speed after the 8th iteration, which would have

seemingly increased the resistance faced by the FT4 blade to go through the bulk of the powder, thus registering a jump in the reading. The trends shown in the feedstock containing LMW PVA were the most unstable so it might suggest the effect of moisture or accidental contaminants which might have affected the powder batch that was prepared for the testing.

The combination of high permeability and low VFR should have helped identify which feedstock was more suitable for powder bed applications. But the combination of Inconel 718 and MMW PVA displayed an inconsistent and inconclusive VFR while having the highest permeability. The HMW PVA counterpart had a relatively stable VFR trend but offered limited improvement in permeability as compared to pure Inconel 718. These conflicting values led to the measurement of the shear stress of the different feedstocks. Shear stress indicated how the powder would behave as part of a consolidated powder bed when a fresh layer of powder is spread.

Fig. 4.3 shows the variation in shear stress over a range of standardised normal stresses. The shear stress of pure Inconel 718 and feedstock with LMW PVA have lower values of shear stress in comparison to the feedstock with MMW and HMW PVA for the same values of applied normal stress. Both feedstocks consisting of MMW and HMW PVA showed similar shear stress behaviour throughout the range of different normal stresses.

The conclusion from the rheological evaluation was not straight forward as one would have thought. The addition of PVA granules to pure Inconel 718 increased the permeability. There was no conclusive trend observed in the variation of VFR and the feedstocks containing MMW and HMW PVA granules showed higher values of shear stress than feedstock containing LMW PVA and no PVA., indicating that spreading of MMW and HMW feedstock would be more difficult in comparison to LMW feedstock and pure Inconel 718. We had hoped to eliminate some of the feedstock combination which we had chosen but we would proceed with printing with all the combinations to experimentally verify if they are able to spread properly during Binder Jetting.

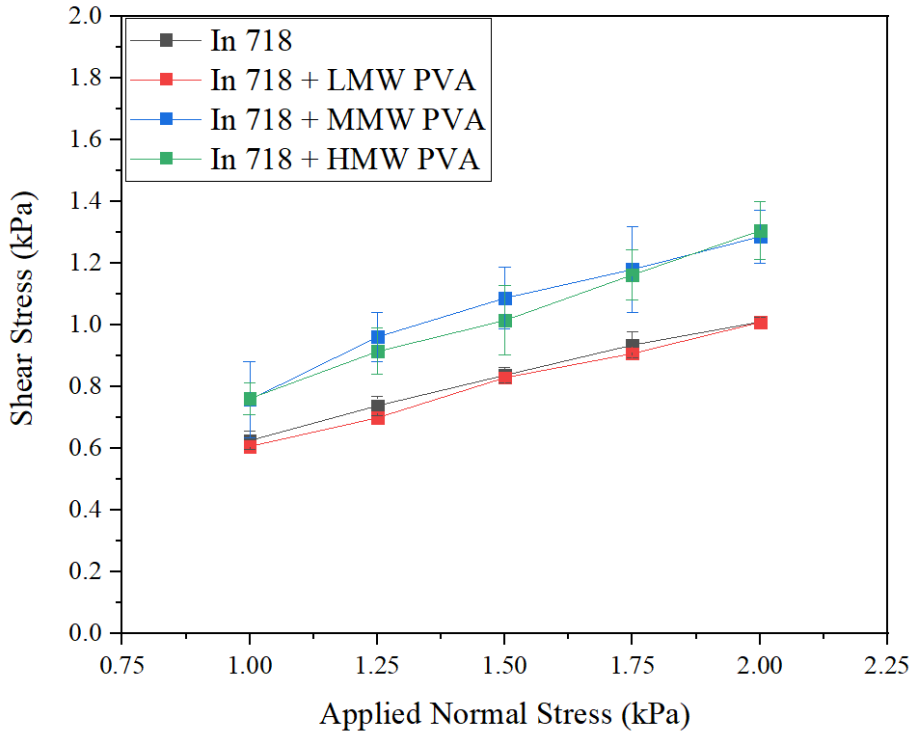

Fig 4.3. Measurement of shear stress of different feedstock containing Inconel 718 including (a) pure Inconel 718 (b) Inconel 718 + LMW PVA (c) Inconel 718 + MMW PVA (d) Inconel 718 + HMW PVA

4.3. Rheological Evaluation of Binders

The rate of change of dynamic viscosity with temperature is shown in Fig. 4.4. The bench marking was done using de-ionised water and the value of dynamic viscosity was found to be matching standardised values within experimental limits. The decline in deionised water was the most visible, changing by 30% over a range of 15°C. The LMW PVA binder had lower values of dynamic viscosity for every temperature point compared to the MMW and HMW PVA binders. The low viscosity would suggest better penetration of the binder into the powder bed. The behaviour of the MMW and HMW PVA binders with change in temperature was very similar, with the net decrease in the viscosity of all the binders was within 13.5%. The positive outtake here is the stability shown by the aqueous binders over a range of temperature, which indicates that the binder is not susceptible to small temperature changes. However, a cause of concern was that the values of viscosity measured for the PVA solutions over a range of temperatures, especially at 25°C; did

not agree with the similar work which was available over literature. Vikingsson et al studied PVA based hydrogels where the viscosity of a 4% by weight PVA solution was (56 x 10^{-3}) Pa.s at room temperature [18]. Salaoru et al. prepared aqueous PVA solutions of 4% by weight which were used as inks for inkjet printing and the viscosity was measured to be (4.9 x 10^{-3}) Pa.s at room temperature [19]. A similar work was done by Monne et al., where the viscosity of a 4.5% by weight solution was found to be (9 x 10^{-3}) Pa.s [20]. The values of viscosity which have been presented in Figure 4.4 are much lower in comparison to the studies which have been mentioned. The molecular weights of the PVA samples in all these studies were much higher than that of the PVA which have been used in this study, but the difference in values of dynamic viscosity by a factor of 0.1 between experimentally obtained results and literature was found to be an anomaly, irrespective of the molecular weights of the PVA which have been used.

Fig. 4.5 depicts the change in surface tension of the different binders with change in temperature. Deionised water has a very gradual declining trend which is consistent with literature. The LMW and HMW PVA based binders exhibit steep change in surface tension from 25°C to 40°C. The binder composed of MMW PVA showed a trend like deionised water with only the surface tension at 30°C being the outlier. The actual values of surface tension were also found to be at odds with values of similar PVA samples, as available in literature [19-20]. The reported values of 4% by weight PVA solution were lower than the experimentally obtained values.

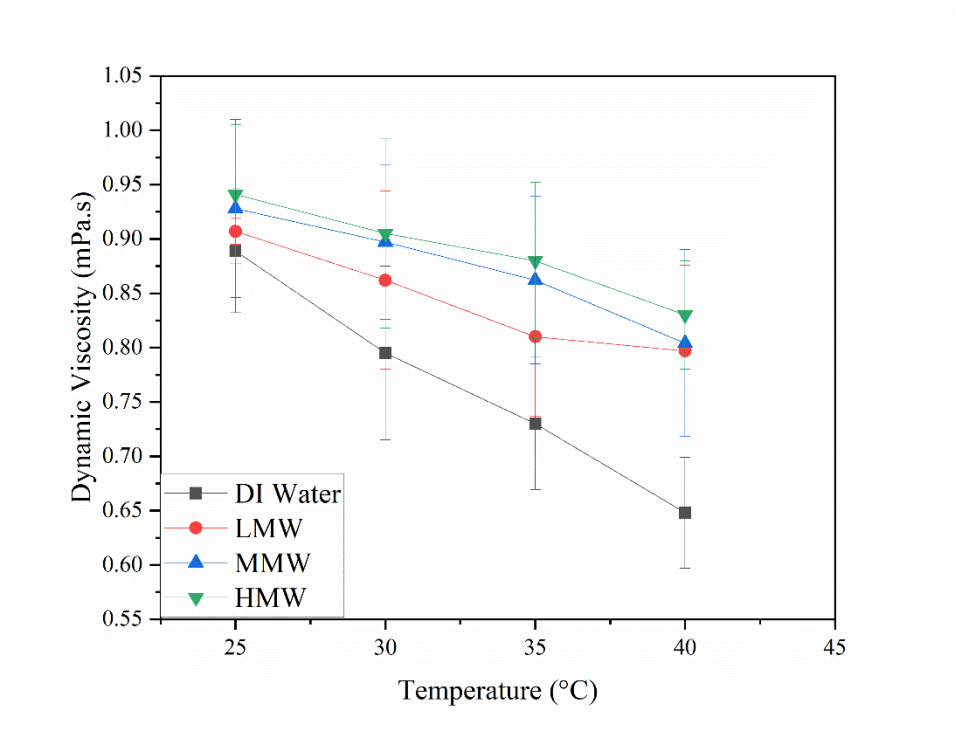

Fig 4.4. Measurement of dynamic viscosity of liquid binders composed of deionised water and PVA of different molecular weights. Deionised water has been used as a benchmark here.

The Z number of the different binders at 30°C is shown in the Fig. 4.6. The range of Z number was observed to be above the maximum value of Z number which was suggested by Derby et al. as a good measure of reliable jetting [10]. As mentioned in Section 4.1, successful jetting has been reported in literature where the Z number was not in the conventional jetting window [11-12]. The high values of Z can be attributed to the high values of surface tension and low values of viscosity which were experimentally obtained.

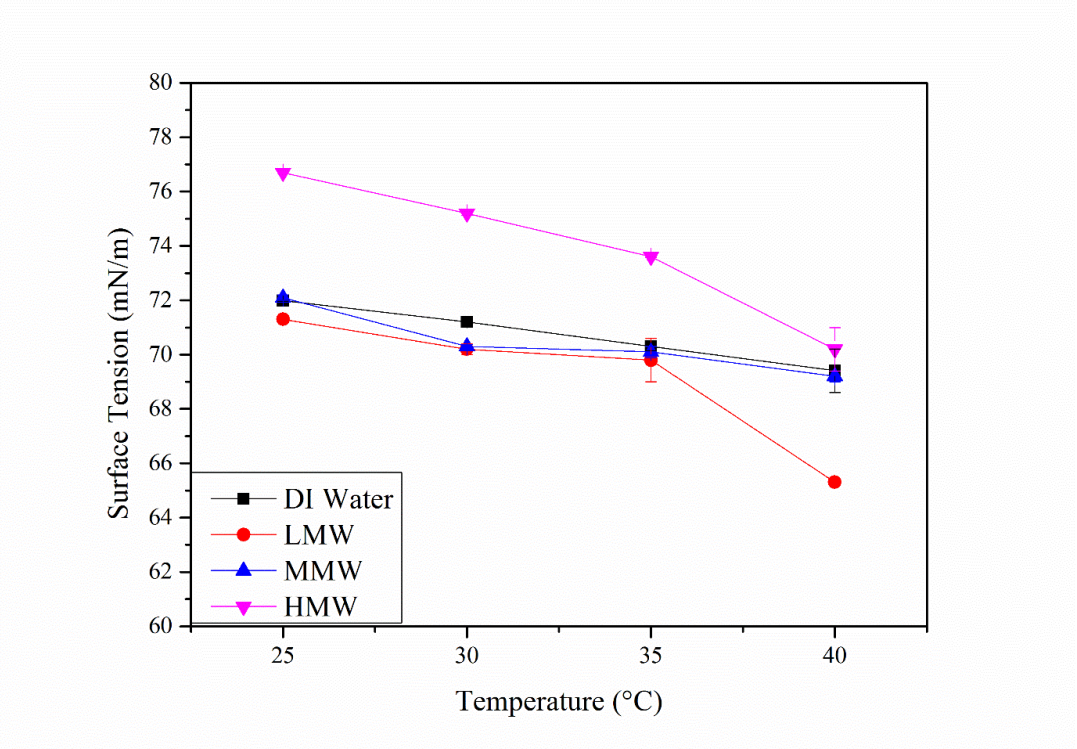

Fig 4.5. Measurement of surface tension of liquid binders composed of deionised water and PVA of different molecular weights. Deionised water has been used as a benchmark here

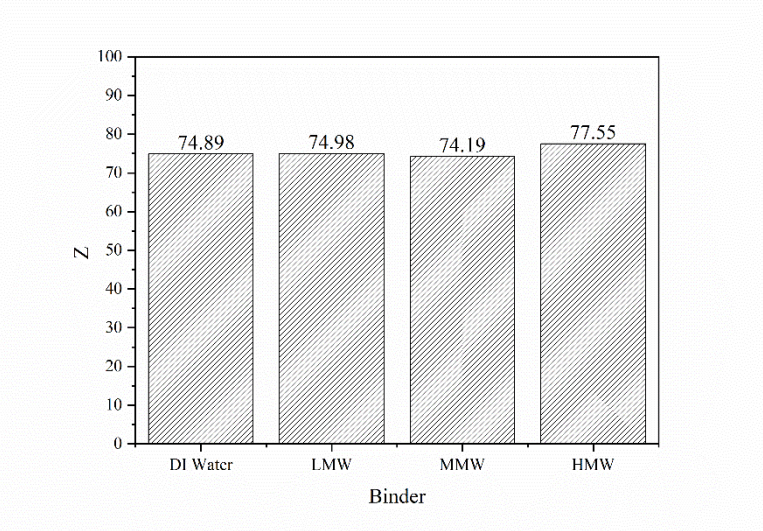

Fig 4.6. Z number of the binders being jetted at 30 °C. Jetting of fluid was possible despite Z>10 in all the cases.

4.4 Chapter Summary

Chapter 4 elaborates on the rheological characterisation of the feedstock and liquid binder and analyses their effect on the printing process. Separate specific literature reviews were done to understand which properties of the feedstock and liquid binder needed to be evaluated. It was concluded that an FT4 based measurement of the permeability, variable flow rate and shear stress of the feedstocks is relevant as these properties are indicative of powder flowability and stability, especially in powder bed applications like Binder Jetting. A study of the available literature on binders suggested that their jettability was a common constraint, and the calculation of the Ohnesorge number (or the reciprocal, the Z number) was necessary to ensure that the binders would be jetted reliably over the course of the work that has been undertaken. It was concluded that the Z numbers of all the binders were outside the normal jettability window as defined by Derby et al. [10] but the phenomenon of jetting outside this window had also been reported in literature [11-12].

The FT4 rheological evaluation revealed that the addition of the PVA granules increased the permeability of the feedstocks in comparison to the virgin Inconel 718 powder. The feedstock with MMW PVA had the highest value of permeability but had an inconclusive VFR. The feedstock which had HMW PVA had a lower value of permeability but exhibited a stable trend when its VFR was measured. The shear stress tests indicated that virgin Inconel 718 and the feedstock with LMW PVA would be more amenable to being spread across the powder bed. Due to the indeterminate nature of the FT4 evaluation of the powders, it was decided that all the feedstocks would be considered for further testing via printing of actual specimens.

The surface tension and dynamic viscosity of the different liquid binders were measured over a range of different temperatures to gauge the stability of the binders over a reasonable temperature range. The Ohnesorge number of the binders were calculated at room temperature, and it was

found that all the binders were jettable and could be dispensed reliable over a period without the problem of satellitation or unequal droplet formation.

References:

1. Clayton J, Millington-Smith D, Armstrong B. The application of powder rheology in additive manufacturing. JoM. 2015 Mar;67(3):544-8.
2. Mellin P, Lyckfeldt O, Harlin P, Brodin H, Blom H, Strondl A. Evaluating flowability of additive manufacturing powders, using the Gustavsson flow meter. Metal powder report. 2017 Sep 1;72(5):322-6.
3. Snow Z, Martukanitz R, Joshi S. On the development of powder spreadability metrics and feedstock requirements for powder bed fusion additive manufacturing. Additive Manufacturing. 2019 Aug 1; 28:78-86.
4. Lefebvre LP, Whiting J, Nijikovsky B, Brika SE, Fayazfar H, Lyckfeldt O. Assessing the robustness of powder rheology and permeability measurements. Additive Manufacturing. 2020 Oct 1; 35:101203.
5. Mussatto A, Groarke R, Ahmed A, Ahad IU, Vijayaraghavan RK, O'Neill A, McNally P, Delaure Y, Brabazon D. Evaluation via powder metallurgy of nano-reinforced iron powders developed for selective laser melting applications. Materials & Design. 2019 Nov 15; 182:108046.
6. Liravi F, Vlasea M. Powder bed binder jetting additive manufacturing of silicone structures. Additive Manufacturing. 2018 May 1; 21:112-24.
7. Shaheen MY, Thornton AR, Luding S, Weinhart T. The influence of material and process parameters on powder spreading in additive manufacturing. Powder Technology. 2021 May 1; 383:564-83.
8. Lewandowska K, Dąbrowska A, Kaczmarek H. Rheological properties of pectin, poly (vinyl alcohol) and their blends in aqueous solutions. e-Polymers. 2012 Dec 1;12(1).

9. Mohsen-Nia M, Modarress H. Viscometric study of aqueous poly (vinyl alcohol) (PVA) solutions as a binder in adhesive formulations. Journal of adhesion science and technology. 2006 Jan 1; 20(12):1273-80.
10. Derby B. Inkjet printing of functional and structural materials: fluid property requirements, feature stability, and resolution. Annual Review of Materials Research. 2010 Aug 4; 40:395-414.
11. Tekin E, Smith PJ, Schubert US. Inkjet printing as a deposition and patterning tool for polymers and inorganic particles. Soft Matter. 2008; 4: 703-713.
12. Vadillo DC, Tuladhar TR, Mulji AC, Mackley MR. The rheological characterisation of linear viscoelasticity for ink jet fluids using piezo axial vibrator and torsion resonator rheometers. Journal of Rheology. 2010; 54:781.
13. Mostafaei A, Elliott AM, Barnes JE, Li F, Tan W, Cramer CL, Nandwana P, Chmielus M. Binder jet 3D printing—Process parameters, materials, properties, modeling, and challenges. Progress in Materials Science. 2021 Jun 1; 119:100707.
14. Parab ND, Barnes JE, Zhao C, Cunningham RW, Fezzaa K, Rollett AD, Sun T. Real time observation of binder jetting printing process using high-speed X-ray imaging. Scientific reports. 2019 Feb 21;9(1):1-0.
15. Bai Y, Wall C, Pham H, Esker A, Williams CB. Characterizing binder–powder interaction in binder jetting additive manufacturing via sessile drop goniometry. Journal of Manufacturing Science and Engineering. 2019 Jan 1;141(1).
16. Zhou H, Lai Z, Lv L, Fang H, Meng H, Zhou M, Cen K. Improvement in the permeability of sintering beds by drying treatment after granulating sinter raw materials containing concentrates. Advamced Powder Technology. 2020 Aug; 31 (8): 3297-3306.
17. Madian A, Leturia M, Ablitzer C, Matheron P, Bernard-Granger G, Saleh K. Impact of fine particles on the rheological properties of uranium dioxide powders. Nuclear Engineering and Technology. 2020 Aug 1;52(8):1714-23.

18. Vikingsson L, Vinals-Guitart A, Valera-Martinez A, Riera J, Vidaurre A, Ferrer GG, Gomez-Ribelles JL. Local deformation in a hydrogel induced by an external magnetic field. Journal of Materials Science. 2016; 51: 9979-9990.
19. Salaoru I, Zhou Z, Morris P, Gibbons GJ. Inkjet Printing of polyvinyl alcohol multileyers for additive manufacturing solutions. Journal of Applied Polymer Science. 2016; 133 (25): 43572-43581.
20. Monne MA, Howlader CQ, Mishra B, Chen MY. Synthesis of printable polyvinyl alcohol for aerosol jet and inkjet printing technology. Micromachines. 2021; 12: 220-235.

CHAPTER 5:

INTERACTION BETWEEN POWDER AND BINDER - WETTABILITY ANALYSIS

'Use slo-mo cameras like they do on the Discovery Channel, upload the videos on YouTube and then bosh…. influencer innit' **– an enthusiastic cab driver, on how to 'monetise' my research.**

5.1 Introduction

The ability of the powder to wet the surface of the powder bed is important for printing robust green parts without any inconsistencies. A droplet of binder has a two-fold behaviour when it encounters the powder bed – it starts to radially spread and penetrate the powder bed at the same time. The spreading and subsequent wetting of the binder liquid occurs due to the lowering of the surface tension of the binder droplet whereas the penetration occurs because of capillary action and gravity. Miyanaji et al. established a relationship between capillary pressure and binder saturation level at the point of equilibrium for binder permeation [1]. Studies on the role of capillary action on the binder interaction with the porous powder bed have agreed that after contact between the droplet and the powder bed, the spread can be divided into primary and secondary spread, where the primary spread is when the sessile volume is greater than zero and secondary spread is when its equal to zero [2-3]. There have been attempts to deconstruct the process of droplet interaction with the powder bed. Hapgood et al. observed droplet coalescence and collapse when they were slow to penetrate porous granular media [4]. It was a generic study on the physics governing the interaction between droplets with granular media. Bai et al investigated this further with special focus on Binder Jetting, and stated that the droplet undergoes initial contact, spreading, imbibition along with drainage (powder bed penetration) with formation of the 'nugget' or 'primitive' as the concluding step [5]. Fig. 5.1 is a faithful reproduction of their study.

Sessile drop goniometry is used to measure the contact angle made by the droplet with the surface it is interacting with. The droplet encounters the surface, spreads and on reaching equilibrium, has three surface tension vectors which interact simultaneously. This has been schematically shown in Fig. 5.2. The angle made between the surface tension vectors Υ_{LV} and Υ_{SL} is termed as the contact angle of the droplet with the surface, where the subscripts L, V and S are for liquid (the droplet), vapour (the surrounding air) and S (the surface).

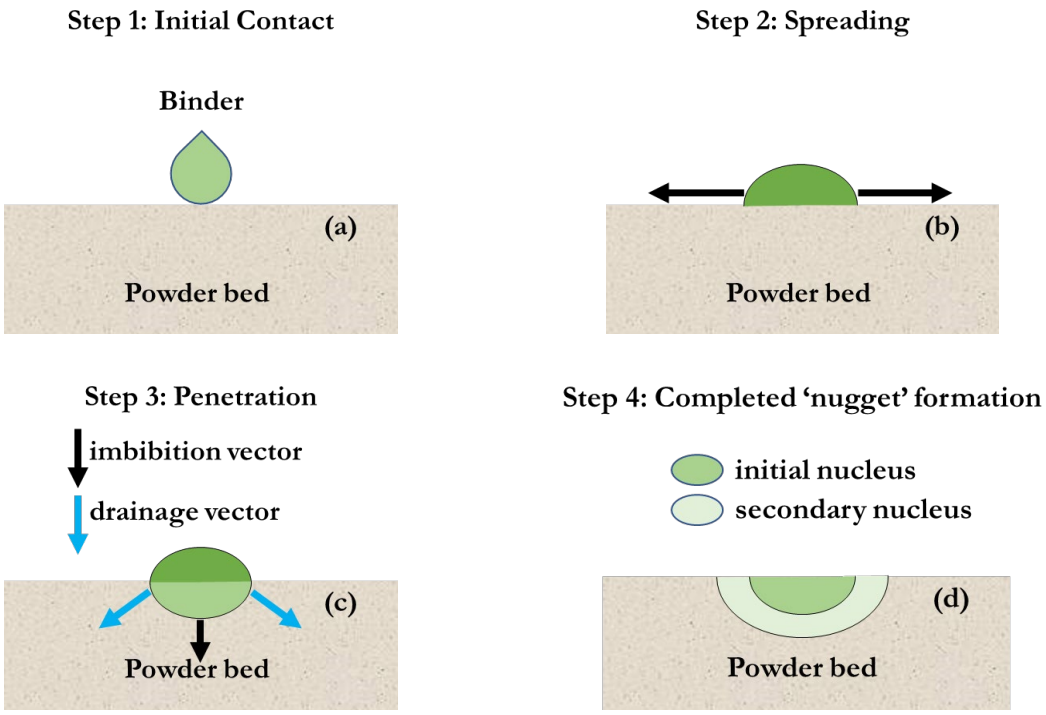

Fig 5.1. Reproduced diagram schematically explaining binder-powder interaction and 'nugget' formation

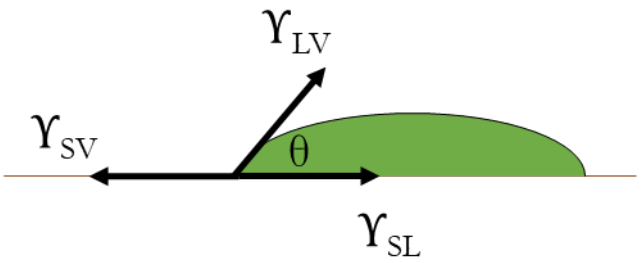

Fig 5.2. Contact angle formed between the surface tension vectors Υ_{LV} and Υ_{SL}

The sessile drop experiment as depicted in Fig. 5.2 has been described as a static contact angle measurement test as the droplet comes to a state of equilibrium when its interacting with a solid surface. As discussed, the nature of interaction between the binder and powder bed in case of BJT is not static as it involves gradual imbibition of the droplet into the bulk of the powder bed. Bai et al. calculated the dynamic contact angle, which is the angle formed between the droplet and the capillary pores formed in the powder bed [5]. The dynamic contact angle was argued to be a more accurate representation of the interaction between the droplet and the powder bed as it considered the binder rheology along with the particle dimensions.

The equation was represented as:

$$\theta = \cos^{-1}\frac{4.05\mu(1-\varphi)V^{\frac{2}{3}}}{T\varphi^{3}\gamma_{LV}d} \quad [Equation\ 5.1]$$

where μ, φ, V, T, γ_{LV} and d are dynamic viscosity, packing fraction, droplet volume, droplet penetration time, binder surface tension and particle diameter. However, the static contact angle has been used in many studies as a measure of wettability of the powder by the binder [6-8] and that has been continued in this study as well.

5.2 Results & Discussions

5.2.1 Sessile drop testing

Figure 5.3 represents the sessile drop test which was conducted on the modified feedstock composed of Inconel 718 and granulated PVA, respectively. It was observed that the droplets upon impacting the powder bed, started spreading rapidly and had asymmetrical shapes, given that the contact angles were not identical. Sessile drop testing of a commercial binder used in commercial Binder Jetting machines was done for the purposes of comparison. It was observed that the PVA binders had much lower contact angles on the powder bed in comparison to the solid surface due to the simultaneous spreading and penetration of the binder droplet on the porous surface. The MMW and HMW PVA binders had lower contact angles in comparison to the commercial binder, which meant that the spreading and penetrating capacity of the PVA binders was better in a time frame of 2 s.

5.2.2 Role of Molecular Weight on Wetting Behaviour of Binder

The interaction between the binder droplets and the powder bed can be explained based on the molecular weight and the length of the polymer chains of the PVA which was used in the binder. The molecular weight of the monomeric unit of PVA is $[CH_2 - CH(OH)]$ is 44 g/mol. The molecular weights of LMW, MMW and HMW PVA is 10,000; 26,000 and 84,000 g/mol as previously mentioned. The number of basic monomeric units in these polymers would be 227, 590 and 1909 respectively, forming a polymeric chain of different lengths. When PVA is dissolved in an aqueous solution, there are different types of interactions which occur simultaneously –

(a) intra chain H bonding between two adjacent $-(OH)$ groups

(b) H bonding between the $-(OH)$ group and the surrounding water molecules

(c) Van der Waals interaction between the $[CH_2 - CH(OH)]$ monomer where the H atom donates its sole electron to the C atom

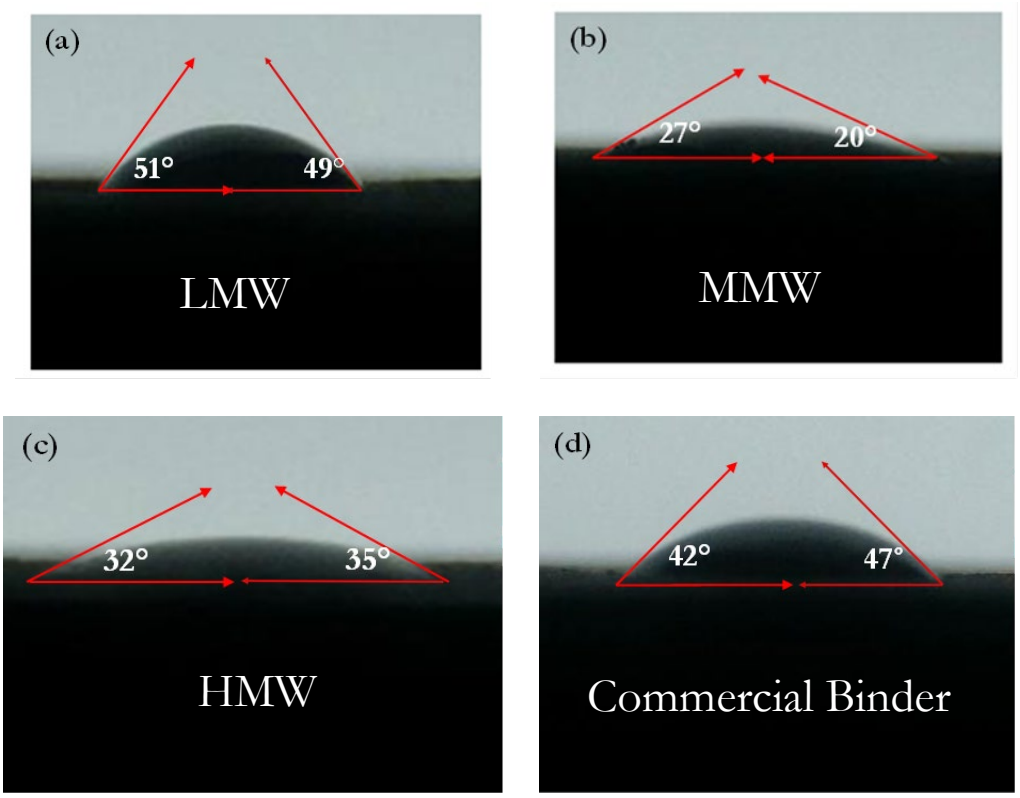

Fig 5.3 Contact angle between the binder droplet and the powder bed: (a) LMW (b) MMW (c) HMW (d) Commercial binder

studies have indicated that the intra chain H bonding dominates over the H bonding between the monomer and the water molecules, encouraging cross linking within the chain itself [8-9]. This decreases the interaction between the dissolved polymer and the solvent (distilled water) and does not hinder the water from spreading and penetrating the powder bed. Increasing length of the chain also leads to chain curling which increases the H bonding between the outer $-(OH)$ groups and the water molecules, which leads to decreased spreading of the water component of the binder [9]. The chain length of the polymer would have to be optimum to get the binding action of PVA and the spreading action of water.

5.2.3 Role of Powder Bed on Penetration Behaviour of Binder

Figure 4.1 as described in Chapter 4 measured the permeability of different feedstock. It was observed that the addition of PVA granules improved the permeability of the feedstock in comparison to virgin Inconel 718 powder. The feedstock which was composed of Inconel 718 and MMW PVA had exhibited the highest levels of permeability. A high permeability of the powder bed would indicate reduced agglomeration between the metal particles and increased inter particle spacing. Both these factors would encourage better binder powder interaction and better binder spreading and penetration.

The role of the presence of PVA granules in the feedstock could influence the penetrability of the binder by immediately dissolving with the aqueous component. However, it was found that no immediate dissolution of the granular PVA present in the feedstock would occur due to its interaction with a binder droplet. Their interaction is captured by the Flory-Huggins equation [10-11].

$$\Delta G_m = RT[n_1 \ln \phi_1 + n_2 \ln \phi_2 + n_1 \phi_2 \chi_{12}] \text{ [Equation 5.2]}$$

$\Delta G_m, R, T, n_1, n_2, \phi_1, \phi_2, \chi_{12}$ are the Gibbs free energy, universal gas constant, quantity of solvent in moles, quantity of solute in moles, solvent volume fraction, solute volume fraction and mixing parameter, respectively. The calculations indicated that the value of ΔG_m is very low for all the molecular weights of PVA used and hence, immediate dissolution of the PVA granules with the binder would not occur at room temperature. The calculations have been made available in the appendix.

The dissolution of the PVA granules present in the feedstock occur at elevated temperatures when exposed to the curing stage in the oven and provide adhesive effect to the printed part.

5.2.4 Green Strength

The green strength is a quantitative way to judge the robustness of printed parts. Miyanaji et al. emphasised on the importance of green strength of printed parts and their effect on the mechanical properties once the parts are sintered [12]. The parts printed using MMW and HMW PVA showed similar flexural deformation behaviour with the part printed using MMW capitulating at a higher load of 140 N in comparison to the HMW counterpart, which failed at 115 N. The robustness of the part printed using MMW is due to its better wetting behaviour which promoted better inter-particle bonding in comparison to the HMW binder. The LMW binder deformed extensively at lower loads and was able to absorb much less energy before breaking.

Fig. 5.4 represents the deflection vs compressive load plot of the green parts that were printed using different PVA based binders.

The part printed using MMW had the highest flexural strength of 3.46 MPa whereas the LMW and HMW counterparts had very similar flexural strengths of 2.8 and 2.7 MPa, respectively.

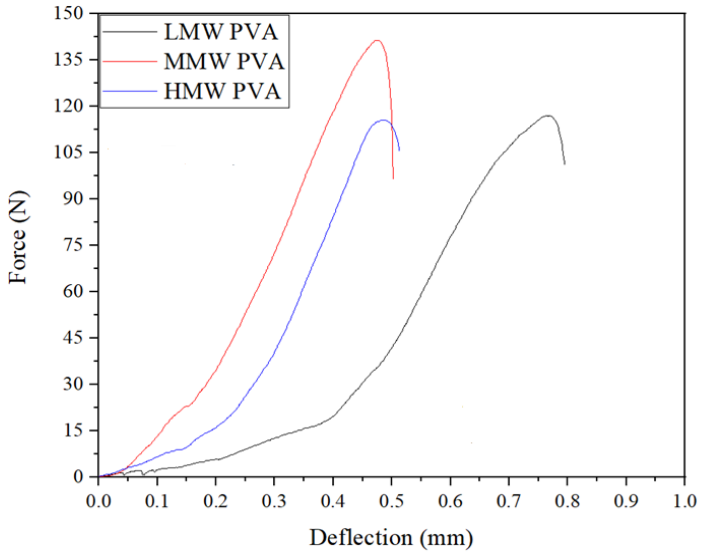

Fig 5.4 Deflection of green parts printed using different PVA based binder, under compressive load

5.3 Chapter Summary

Chapter 5 focuses on the powder-binder interaction which occurs when the binder droplet contacts the powder bed. The mechanism of the interaction was mapped from the previous studies that were reported, which focused on the binder propagation in the bulk of the powder bed. The contact angle of the binder droplets was initially measured on a solid substrate made of Inconel 718 as a benchmark and it was observed that the all the PVA based liquid binders had high contact angles, indicative of poor wetting action between the solid substrate and the binder. Literature suggested that the contact angle measured between the binder and the powder was a better measure of the wetting compatibility of the binder with the powder bed.

Sessile drop testing of binder droplets on the powder bed was conducted for three different types of PVA based liquid binders based on their molecular weight. A commercial binder was also trialled for the sake of comparison. It was observed that the MMW PVA based binder had the lowest contact angle of 27° with the powder which outperformed the commercial binder. The optimal polymer chain of the MMW PVA and the relative inviscid nature of the water base of the binder was attributed as the cause for its better wetting action in comparison to the commercial binder and the other PVA based binders.

The powder-binder interaction is best manifested in the green strength of the printed parts. Samples were printed in accordance with the ASTM B312-20 and were flexed to the point of failure using a UTM. The approach speed of the top ram was kept at a constant of 1 mm/min and the clearance between the ram and the top surface of the sample was maintained at 1-2 mm so that the approach speed of the top ram was constant when it came into contact with the test specimen. The parts that were printed using a combination of MMW PVA based binder and feedstock had the highest flexural strength of 3.46 MPa, whereas the parts which were printed using LMW and HMW inks had very similar values of 2.8 and 2.7 MPa respectively.

References

1. Miyanaji H, Zhang S, Yang L. A new physics-based model for equilibrium saturation determination in binder jetting additive manufacturing process. International Journal of Machine Tools and Manufacture. 2018 Jan 1; 124:1-1.
2. Denesuk M, Smith GL, Zelinski BJ, Kreidl NJ, Uhlmann DR. Capillary penetration of liquid droplets into porous materials. Journal of colloid and interface science. 1993 Jun 1;158(1):114-20.
3. Markicevic B, D'onofrio TG, Navaz HK. On spread extent of sessile droplet into porous medium: Numerical solution and comparisons with experiments. Physics of Fluids. 2010 Jan 8;22(1):012103.
4. Hapgood KP, Litster JD, Biggs SR, Howes T. Drop penetration into porous powder beds. Journal of Colloid and Interface Science. 2002 Sep 15;253(2):353-66.
5. Bai Y, Wall C, Pham H, Esker A, Williams CB. Characterizing binder–powder interaction in binder jetting additive manufacturing via sessile drop goniometry. Journal of Manufacturing Science and Engineering. 2019 Jan 1;141(1).
6. Miyanaji H, Momenzadeh N, Yang Li. Effect of printing speed on quality of printed parts in Binder Jetting Process. Additive Manufacturing. 2018 March; 20:1-10.
7. Barui S, Ding H, Wang Z, Zhao H, Marathe S, Mirihanage W, Basu B, Derby B. Probing ink–Powder interactions during 3D binder jet printing using time-resolved X-ray imaging. ACS applied materials & interfaces. 2020 Jun 22;12(30):34254-64.
8. Sengwa RJ, Kaur K. Dielectric dispersion studies of poly (vinyl alcohol) in aqueous solutions. Polymer International. 2000 Nov; 49(11):1314-20.
9. Kozlov M, McCarthy TJ. Adsorption of poly (vinyl alcohol) from water to a hydrophobic surface: effects of molecular weight, degree of hydrolysis, salt, and temperature. Langmuir. 2004 Oct 12; 20(21):9170-6.

10. Flory PJ. Thermodynamics of high polymer solutions. The Journal of Chemical Physics. 1941 Aug;9(8):660
11. Huggins ML. Some properties of solutions of long-chain compounds. The Journal of Physical Chemistry. 1942 Jan; 46(1):151-8.
12. Miyanaji M, Orth M, Akbar JM, Yang L. Process development for green part printing using binder jetting additive manufacturing. Frontiers of Mechanical Engineering. 2018 Nov; 13(4): 504-512.

CHAPTER 6:

EVALUATION OF POROSITY IN SINTERED PARTS

'Without porosity, we metal AM guys wouldn't have much to talk about really. I sometimes wonder if some of us are scared that solving porosity would diminish our relevance in this dynamic field' – ***a delirious postdoc at a pub, after too many beers***

6.1. Introduction

6.1.1. Porosity – a consistent issue in Additive Manufacturing

Porosity is a phenomenon which has defined as the presence of voids and cavities within the bulk of a material making it less than fully dense [1]. It has traditionally been a problem observed during manufacturing processes like casting and joining processes. All these manufacturing and joining processes involve the solidification of a melt pool, which can be large for castings or small for most welding processes. The formation of voids in cast products and weldments is usually due to the freezing in of the gas released from the molten pool of metal as it solidifies. Katayama et al. studied laser welding of stainless steel and concluded that the porosity was caused due to the entrapment of bubbles in the weld pool by the solidifying front [2]. The bubbles were caused due to evaporation of metals which was a side effect of the interaction between the metal and the laser. Continuing their studies on laser welding, Katayama reported lack of fusion during laser welding of aluminium alloys and low carbon steel [3]. The conclusion was that the laser parameters could not be optimised for both the materials simultaneously and led to unequal melting of the dissimilar materials. Matsunawa et al concluded that porosity during laser welding happened due to unstable keyhole phenomena and correlated the formation of voids to the choice of shielding gas [4]. The physics of porosity is similar in PBF processes like SLM, and initial investigation of porosity was heavily inspired by laser welding [5-7]. Kasperovich et al. investigated porosity during SLM of Ti-6Al-4V and reported that laser energy density had to be optimised perfectly to prevent porosity [8].

A low energy density would result in insufficient fusion whereas an excessively high energy density would encourage metal evaporation causing gas porosity and would also cause keyholing. Further studies on porosity during SLM of titanium alloys concluded that 90% of porosity can be eliminated by careful consideration of processing parameters like laser power, scanning speed and emissivity of the powder used [9].

Binder Jetting is a process where porosity is not introduced into the part being manufactured during the actual printing process. Any residual porosity in Binder Jetted components can be attributed to the sintering cycle. It does not involve the solidification of metal melt pools so porosity mechanisms which were valid for processes like SLM, and EBM are not valid for Binder Jetting. The sintering cycle is an important step for manufacturing components successfully using Binder Jetting which is very similar to Metal Injection Moulding (MIM). Both processes involve the use of binders and post-processing includes de-binding (also termed as binder burnout), sintering and further heat treatments. Sung et al. studied the effect of sintering temperature on porosity while processing stainless steel using MIM [10]. The porosity ranged from 39% of parts sintered at 900°C to 1% when sintered at 1350°C. The pore distribution was found to become more isolated with an increase in sintering temperature. Increased sintering temperatures were credited for better necking action among adjacent particles which resulted in overall improved quality of sintering and reduced porosity. Machaka et al. studied the role of particle size on powder-binder interaction during MIM of stainless steels [11]. Extremely fine powders having a PSD of 5 μm were prone to agglomeration when they interacted with the binder which caused an uneven de-binding process, resulting in formation of voids across the bulk of the manufactured samples. Studies have also investigated the role of the binder's stability in maintaining low levels of porosity while processing metals in MIM [12-13]. The consensus was that binder stability over range of temperature was necessary to ensure that the powder behaviour did not change over different stages of processing.

6.1.2. Porosity during Binder Jetting

Porosity in Binder Jetting so far has been attributed to the sintering cycle and literature has strongly suggested that the physics of sintering is similar in MIM and BJT. However, there are multiple parameters which are not factors in Binder Jetting in comparison to MIM. Parameters like extrusion temperature, flow activation and slurry rheology are extremely important and are extensively studied in MIM, but they are absent in Binder Jetting. A common cause of porosity in parts manufactured due to MIM is the improper mixing of powder and binder creating 'powder rich zones' and 'binder rich zones', which sinter differently [14-15]. This problem is avoided in Binder Jetting due to the jetting of the binder on the powder bed. In MIM, the mould often acts as a heat sink, which causes the extruded mix of powder and binder to shrink unevenly causing porosity [15-18]. The process of printing in Binder Jetting is done at room temperature and these issues, mentioned earlier do not arise or influence the printed part.

Mirzababaei et al., focused on the issue of porosity during BJT of 316L stainless steels [18]. Their review revealed that porosity in Binder Jetted parts was usually due to insufficient fusion of the particles during sintering. However, some other studies concluded that porosity in Binder Jetted parts were also attributed to inter-layer spacing, powder morphology and voids left behind after binder burnout [19]. The review of Du et al. focused on porosity of ceramic components printed using BJT and reported that an excessive binder saturation resulted in high levels of porosity [20].

The effect of particle morphology on densification was investigated during Binder Jetting of Inconel 625 [21-22]. Powders having higher particle size diameter showed higher densification in both their green and sintered forms and had lower shrinkage in the Z direction. Spherical gas atomised particles of Inconel 625 resulted in better densification and better mechanical properties than their irregularly shaped counterparts that were atomised in water. Nandwana et al. advocated for using coarser particles during BJT of Inconel 718 to avoid higher binder saturation and porosity as a

result, thus agreeing with previously mentioned literature which focussed on effect of binder saturation during processing of ceramics.

6.1.3. Strategies to eliminate porosity

Porosity is unavoidable in additively manufactured components [1]. Voids in the bulk in of a component may act as stress concentration sites which may encourage and propagate cracking, regardless of process or material used [23-26]. Postprocess HIP has been considered an effective way to reduce porosity and consolidate parts fabricated by AM [27]. It has been used reliably to reduce porosity during SLM of steels, titanium alloys and nickel super alloys [28-31]. The consolidating and packing action of HIP was used to reduce the porosity of sintered components which were printed via Binder Jetting in materials like copper [32-34], WC-Co cermets [35-36] and nickel super alloys [37-38].

6.2 Results & Discussions

6.2.1 Role of mode of binder deposition

Fig. 6.1 represents the SEM micrographs and their corresponding porosity maps of the transverse cross section of cubical parts which were printed with the binder deposited manually. The corresponding porosity maps have been calculated using an image processing software, ImageJ. This was an attempt done to understand the effect of the liquid binder alone on part quality. The specimen that was printed using LMW showed partial sintering with particle pull out. This increased the porosity and the LMW specimen reported a high porosity of 20.39%. The specimens that used MMW and HMW PVA as part of the feedstock and the liquid binder showed lower porosities of 9.78% and 10.97% respectively. The image processing software was able to report levels of porosity very well but was not able to identify the partial sintering which was the main failure here. The lack of a contiguous surface was not encouraging, and further mechanical testing of these parts was found to be futile and was not attempted.

Fig. 6.2 showcases the micrographs and porosity maps of parts that were printed on the JetLab 4xL printer using piezoelectric inkjet printheads. The distribution of liquid binder was much uniform and consisted in this method. The sintered parts showed a lower level of porosity and a consistent, contiguous surface. The parts printed using LMW, MMW and HMW PVA binders exhibited a porosity of 17.61%, 3.84% and 5.98%.

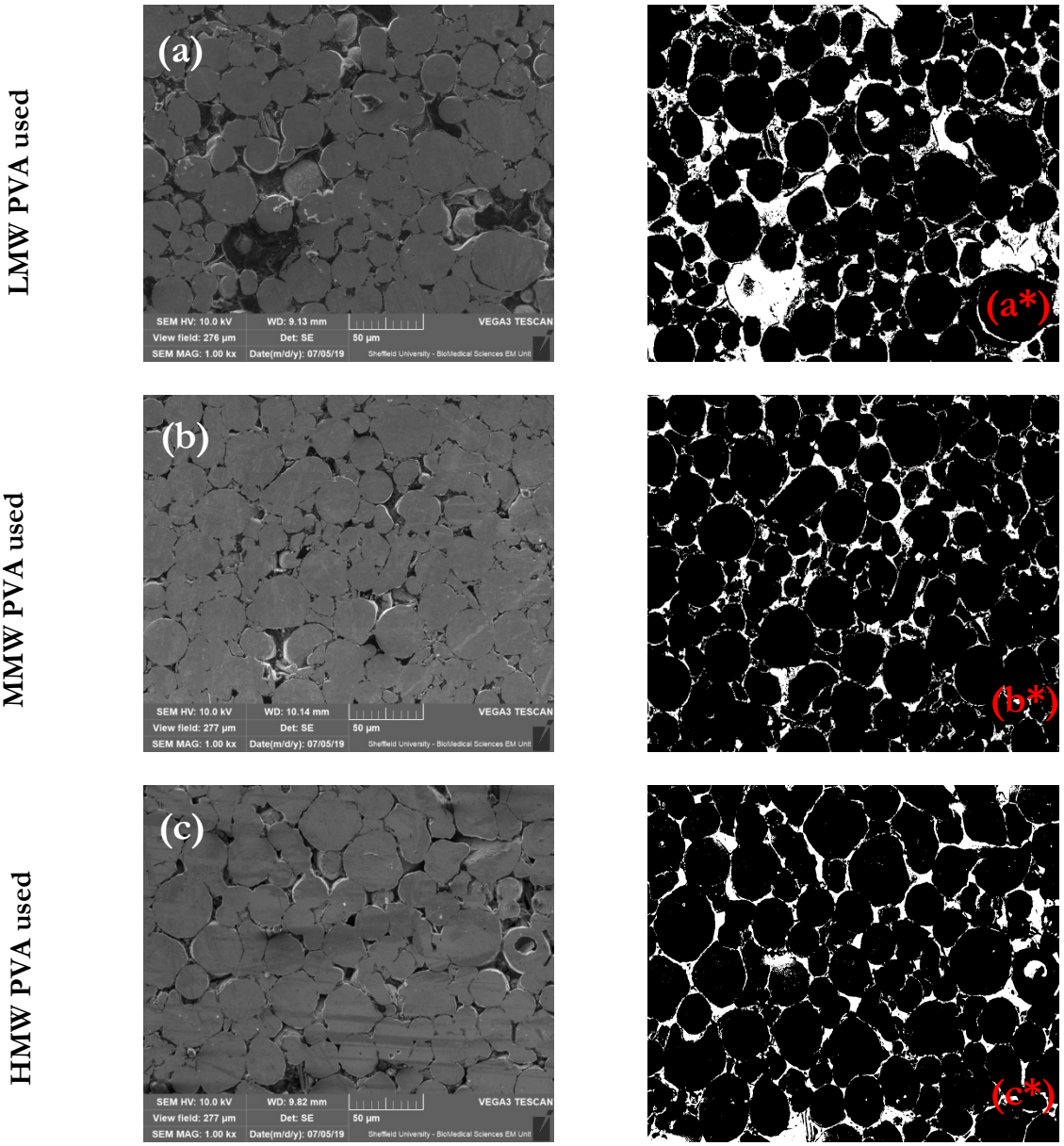

Fig 6.1 SEM micrographs and corresponding porosity mapping of manually deposited and sintered specimens: (a&a*) LMW; porosity of 20.39% (b&b*) MMW; porosity of 9.78% (c&c*) HMW; porosity of 10.97%.

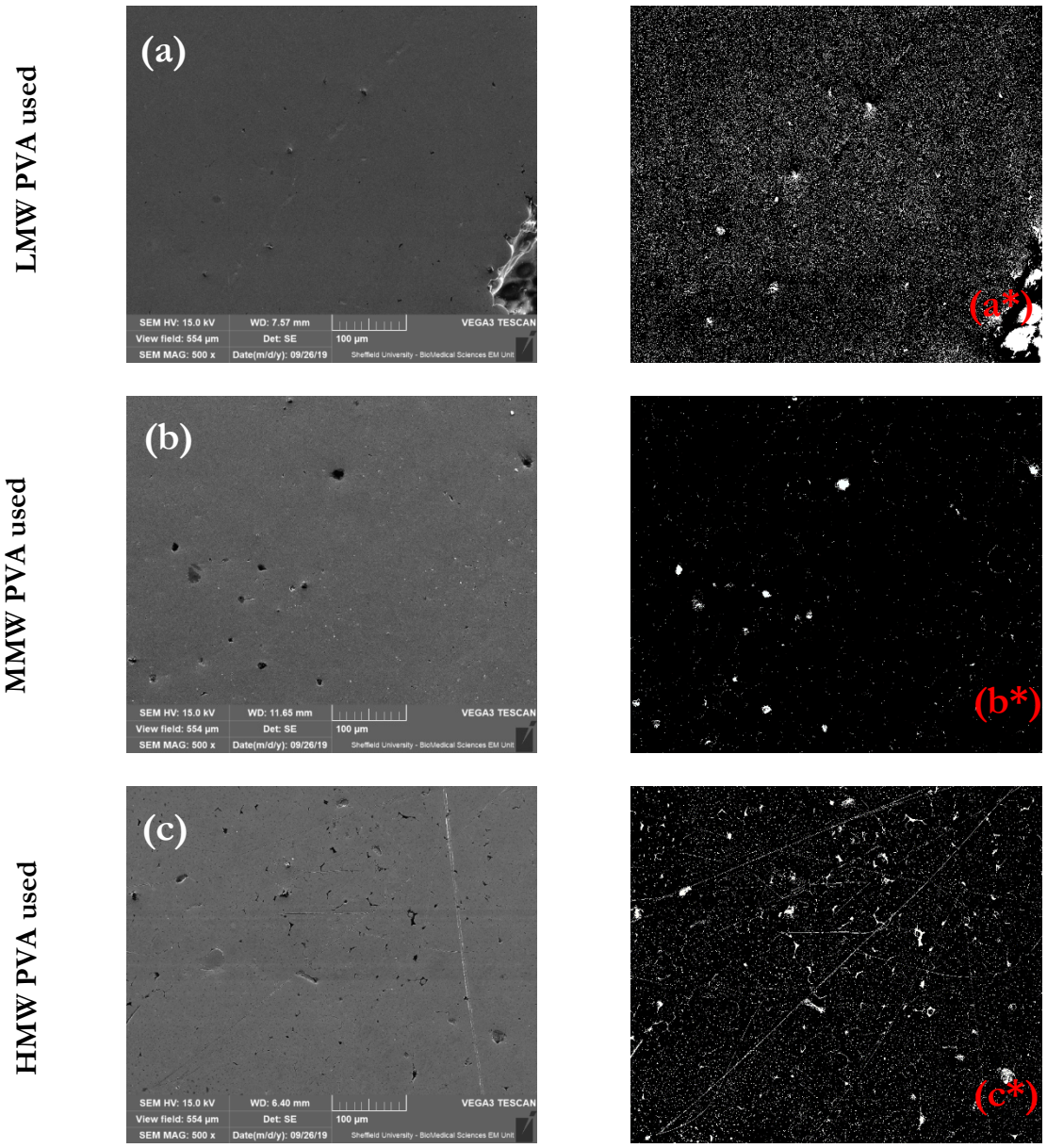

Fig 6.2 SEM micrographs and corresponding porosity mapping of specimens printed using jetting action of a piezo-electric printhead: (a&a*) LMW; porosity of 17.61% (b&b*) MMW; porosity of 3.84% (c&c*) HMW; porosity of 5.98%.

The lowered porosity as seen in the porosity mapping in Fig. 6.2 was due to better wetting of the feedstock by the binder. The manual deposition of the PVA based binder using a micro-pipette was characterised by the deposition of a large volume of liquid binder on the feedstock in a single step which led to the surface tension of the liquid dominating over the capillary action of the

porous feedstock and gravity [39]. The jetting action of the printhead was more consistent and it spread uniform droplets over the surface of the powder bed which encouraged better wetting, allowing the droplets to penetrate the powder bed causing better interaction between the particles of the feedstock and binder.

6.2.2. Role of Sintering Environment.

Fig. 6.3 and Fig. 6.4 represents the micrographs and their corresponding porosity maps for parts that were sintered in solely in an argon atmosphere throughout and in a mixture of H_2/N_2 gas followed by argon, respectively. Visual inspection of the micrographs indicated that the parts sintered in argon throughout, as shown in Fig. 6.3 had contiguous surface with full particle sintering. The parts printed using LMW, MMW and HMW binders, when sintered in an argon environment, exhibited porosities of 7.21%, 5.34% and 9.77% respectively with the part printed using MMW PVA in the feedstock and the binder having the lowest level of porosity. The mixture of H_2/N_2 gas followed by argon provided an environment which caused poor, inconsistent sintering along with particle pull out from the surface. Porosity mapping suggested that the parts printed using LMW, MMW and HMW binders had relatively high porosity levels of 17.58%, 11.31% and 10.37% respectively.

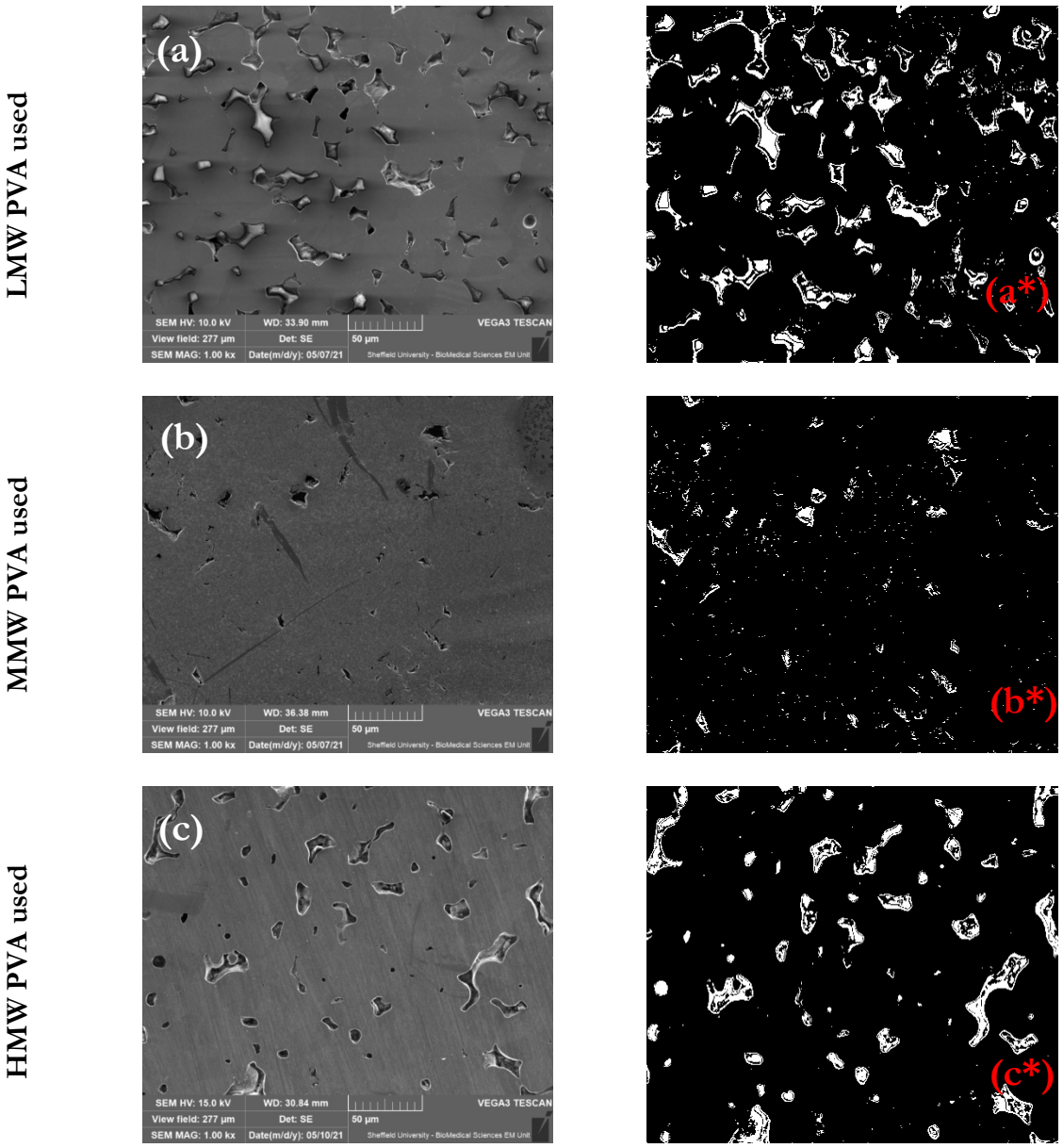

Fig 6.3 SEM micrographs and porosity mapping of tensile specimens sintered in 99.98% Argon environment: (a&a*) LMW; porosity of 7.21% (b&b*) MMW; porosity of 5.34% (c&c*) HMW; porosity of 9.77%.

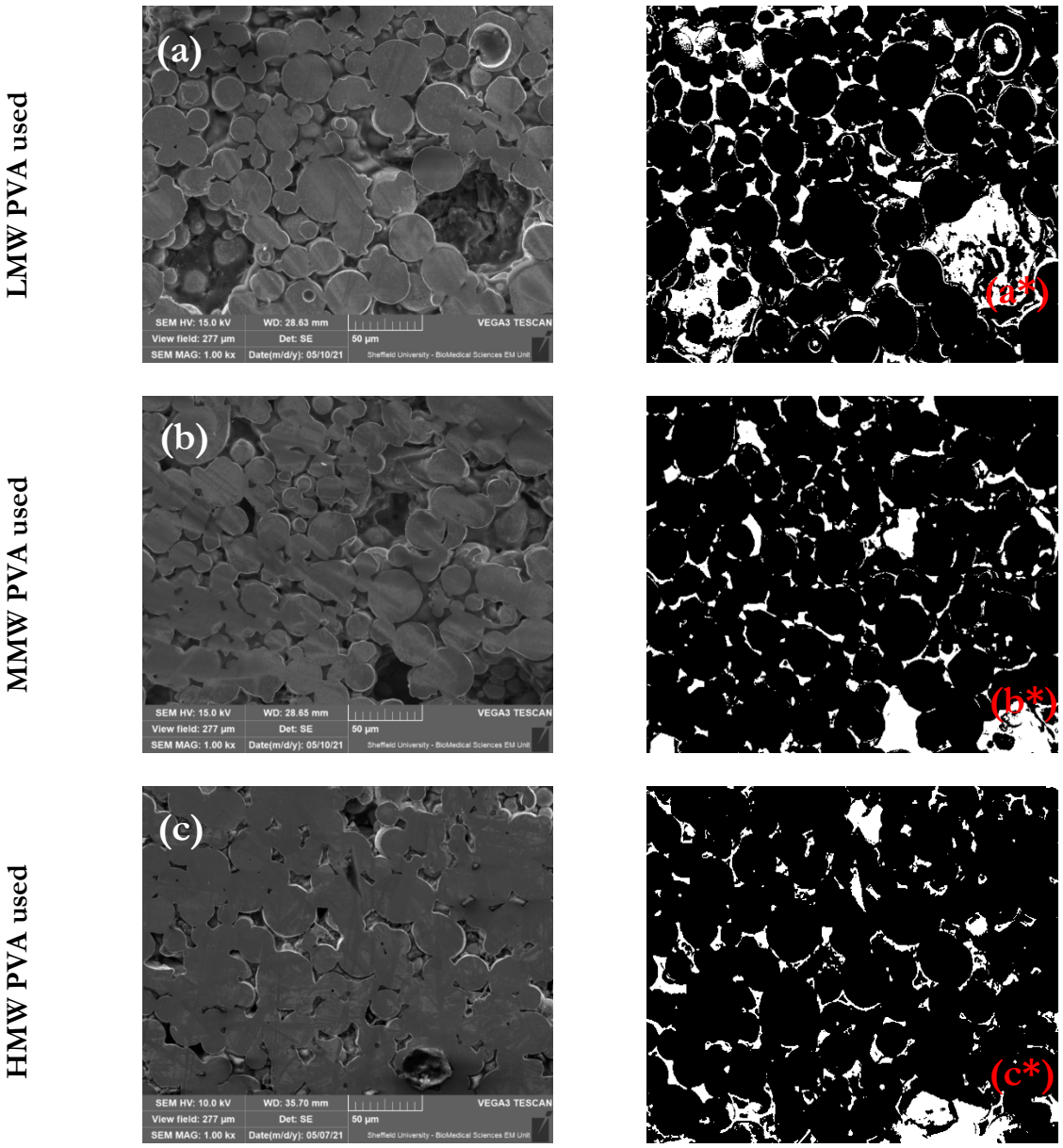

Fig 6.4 SEM micrographs and porosity mapping of tensile specimens sintered in a gas mix of N_2/H_2 followed by Argon: (a&a*) LMW; porosity of 17.58% (b&b*) MMW; porosity of 11.31% (c&c*) HMW; porosity of 10.37%.

The N_2/H_2 mixture was used as purging gas till the temperature reached 1260°C to prevent evaporation of chromium, after which argon was used during the sintering process. However, the same gas mixture would have led to nitrogen uptake by the chromium present in the Inconel 718 alloy to form hard, brittle Cr_2N phases. The removal of chromium reduced the ability of the

Inconel 718 particles to initiate the necking process [40], thus leading to poor sintering as seen in Fig. 6.4.

The TGA of the binders, as shown in Figure 3.4, suggested that the burnout of the MMW polyvinyl alcohol was more sensitive to the change in temperature and the burnout was gradual compared to the LMW and MMW polyvinyl alcohol, leading to reduced porosity.

6.2.3 Role of HIP on reducing porosity

Fig. 6.5 and 6.6 represents the micrographs of the transverse cross sectional area of parts that were sintered in an argon purged environment and N_2/H_2 mixture followed by argon respectively, then post-processed in a HIP environment.

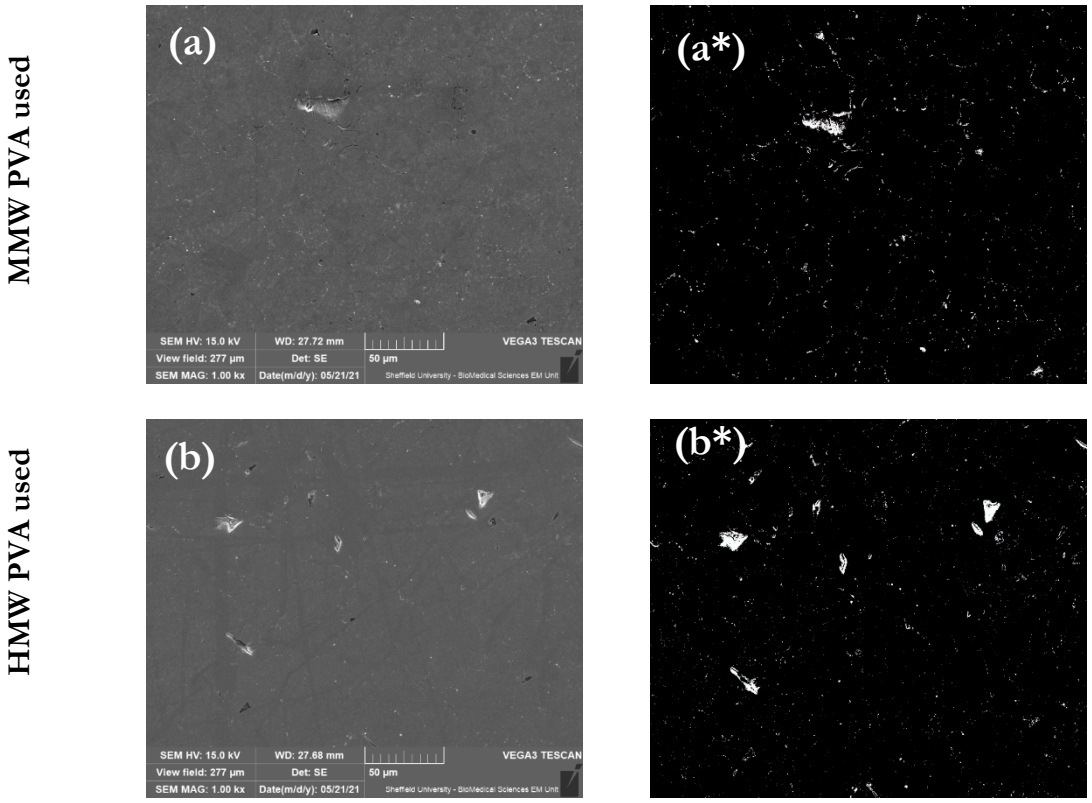

Fig 6.5 SEM micrographs and porosity mapping of tensile specimens sintered solely in an argon environment and then HIP'ed: (a&a*) MMW; porosity of 1.04% (b&b*) HMW; porosity of 1.35%

The corresponding porosity maps have also been represented as per convention followed throughout this chapter. The parts that were printed using MMW and HMW PVA in the feedstock and the liquid binders were sent for HIP as the high levels of porosity seen in the parts printed using LMW PVA were unsatisfactory enough to not proceed ahead with any further post-processing. There was a extensive reduction in porosity in the sintered parts along with an increase in the contiguousness of the sintered surface. Comparing with the data represented in Fig. 6.3, there was a reduction of porosity in the parts printed using MMW and HMW PVA by 4.3% and 8.42%. The HIP based post-processing seemed to have an equalising effect on the porosity of the specimens, with both the specimens printed using different binders having the same porosity. The porosity of the samples after completion of HIP is at par with other studies involving commercial systems and binders where Inconel was processed using sintering procedures which are more complicated to carry out [41].

The trend of reduction in porosity was not replicated in samples sintered in the N_2/H_2 gas mixture Porosity remained unaffected in the specimens sintered in the N_2/H_2 gas mixture after being post-processed in HIP environment. The presence of Cr_2N phase can be blamed for this, but there is no literature which has reported the behaviour of a sintered part with nitrogen uptake in a HIP environment.

6.3 Chapter Summary

Chapter 6 focuses on the process response of porosity which is a major metric of part quality. It is a phenomenon which is observed in all additively manufactured parts and in other, more conventional manufacturing processes like casting and joining processes like welding and brazing. A porosity specific literature review revealed the differences in the mechanism of pore formation between different additive manufacturing techniques like PBF techniques and Binder Jetting. Existing studies also reported the prevalence of using HIP as a post-processing measure to reduce porosity. The mechanism of porosity in Binder Jetting was found to be very similar to parts made

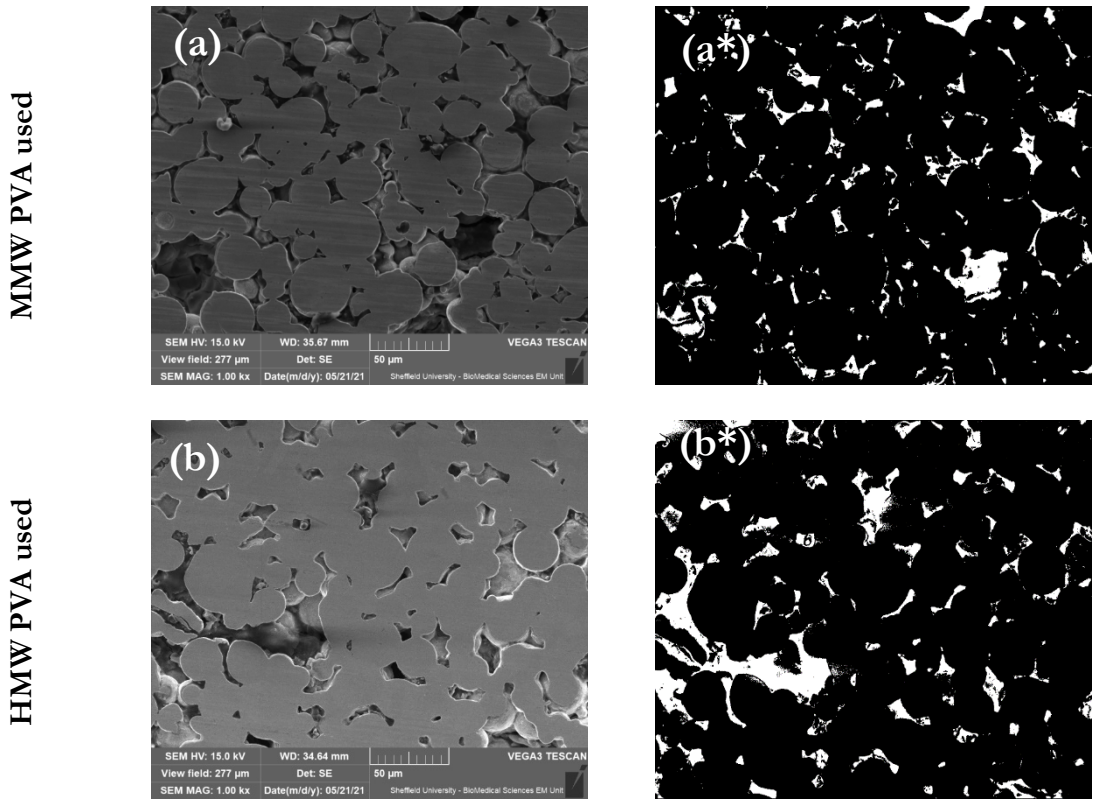

Fig 6.6 SEM micrographs of transverse sections of tensile specimens and corresponding porosity mapping, sintered solely in an N_2/H_2 mixture followed by an argon purged environment, HIP'ed: (a&a*) MMW; porosity of 11.05% (b&b*) HMW; porosity of 10.20%

by MIM, due to the important role played by the sintering step in both processes. The role of mode of binder deposition on part quality was hence investigated to understand the role played by the jetting action of the inkjet printhead device. The repeatability and consistency of the deposition of droplets by the printhead was credited for the better densification of the printed parts in comparison to parts that were built using a manual deposition of binder.

The role of sintering environment on the quality and composition of the part is extensive as was established in Section 2.5, Chapter 2. Samples sintered in two different environments, 99.98% argon throughout and a combination of N_2/H_2 mixture, followed by argon in the sintering stage provided very contrasting levels of porosity. The N_2/H_2 environment induced nitrogen uptake by

the chromium present in the alloy to form Cr_2N which stunted the sintering process, causing very poor densification in the specimens sintered in the N_2/H_2 atmosphere. The 99.98% argon atmosphere during sintering led to very low levels of specimen porosity with the samples printed using MMW PVA based binder and feedstock reporting a value of 5.34% porosity.

HIP improved the porosity of the parts sintered in 99.98% argon substantially with the porosity reported as going below 2%. However, post-processing could not improve the lack of sintering in the specimens that were sintered in the N_2/H_2 environment.

An aspect which was not explored in this thesis was the effect of porosity on the fatigue life of printed parts of Inconel 718. Muhammad et al. reported that randomly distributed pores in the bulk of the SS 316L specimens manufactured by BJT, did not contribute to failure induced by cyclic loading [42]. The phenomenon of interconnected porosity was observed to be more detrimental to the fatigue life of BJT specimens as they helped in the propagation of macro-cracks during fatigue testing leading to failure [42-45]. Once crack initiation occurs due to cyclic loading, their propagation is hastened due to the nature of interconnected porosity.

References:

1. ASTM. ASTM 52900 (2021). Additive manufacturing – General Principles – Fundamentals and vocabulary. West Conshohocken, US: ASTM International. 2021: 1-14.
2. Katayama S, Seto N, Mizutani M, Matsunawa A. Formation mechanism of porosity in high power YAG laser welding. In International Congress on Applications of Lasers & Electro-Optics 2000 Oct (Vol. 2000, No. 1, pp. C16-C25). Laser Institute of America.
3. Katayama S. Laser welding of aluminium alloys and dissimilar metals. Welding International. 2004, 18(8):618-625.
4. Matsunawa A, Mizutani M, Katayama S, Seto N. Porosity formation mechanism and its prevention in laser welding. Welding international. 2003 Jun 1;17(6):431-7.

5. Yadroitsev I, Gusarov A, Yadroitsava I, Smurov I. Single track formation in selective laser melting of metal powders. Journal of Materials Processing Technology. 2010 Sep 1;210(12):1624-31.
6. Gunenthiram V, Peyre P, Schneider M, Dal M, Coste F, Koutiri I, Fabbro R. Experimental analysis of spatter generation and melt-pool behavior during the powder bed laser beam melting process. Journal of Materials Processing Technology. 2018 Jan 1; 251:376-86.
7. Hojjatzadeh SM, Parab ND, Guo Q, Qu M, Xiong L, Zhao C, Escano LI, Fezzaa K, Everhart W, Sun T, Chen L. Direct observation of pore formation mechanisms during LPBF additive manufacturing process and high energy density laser welding. International Journal of Machine Tools and Manufacture. 2020 Jun 1; 153:103555.
8. Kasperovich G, Haubrich J, Gussone J, Requena G. Correlation between porosity and processing parameters in TiAl6V4 produced by selective laser melting. Materials & Design. 2016 Sep 5; 105:160-70.
9. Gordon JV, Narra SP, Cunningham RW, Liu H, Chen H, Suter RM, Beuth JL, Rollett AD. Defect structure process maps for laser powder bed fusion additive manufacturing. Additive Manufacturing. 2020 Dec 1; 36:101552.
10. Sung HW, Ha TK, Ahn S, Chang YW. Powder injection molding of a 17-4 PH stainless steel and the effect of sintering temperature on its microstructure and mechanical properties. Journal of Material Processing Technology. 2002 Dec 20; 130-131: 321-327.
11. Machaka R, Ndlangamandla P, Seerane M. Capillary theological studies of 17-4 PH MIM feedstocks prepared using a custom CSIR binder system. Powder Technology. 2018 Feb 15; 326: 37-43.
12. Hayat MD, Goswami A, Matthews S, Li T, Yuan X, Cao P. Modification of PEG/PMMA binder by PVP for titanium metal injection moulding. Powder Technology. 2017 June 15; 315: 243-249.

13. Hayat MD, Zhang H, Karumbaiah KM, Singh H, Xu Y, Qu X, Ray S, Cao P. A noel PEG/PMMA based binder composition for void-free metal injection moulding of Ti components. Powder Technology. 2021 Apr 10; 382: 431-440.
14. Wei F, He X, Ruijie Z, Yang S, Qu X. The effects of filling patterns on the powder-binder separation in powder injection molding. Powder Technology. 2014 Apr 6; 256: 367-376.
15. Butkovic S, Saric E, Mehmedovic. Porosity distribution in metal injection molded parts. Advanced Technologies & Materials. 2021 June 25; 46(1): 7-10.
16. Loh, NH, German, RM. Statistical analysis of shrinkage variation for powder injection molding. Journal of Material Processing Technology. 1996 May 27; 59(3): 278-284.
17. Luo TG, Qu XH, Qin ML, Ouyang ML. Dimension precision of metal injection molded pure tungsten. International Journal of Refractory Metals and Hard Materials. 2009 May; 27(3): 615-620.
18. Mirzababaei S, Pasebani S. A review on binder jet additive manufacturing of 316L stainless steel. Journal of Manufacturing and Materials Processing. 2019 Sep;3(3):82.
19. Ziaee M, Tridas EM, Crane NB. Binder-Jet printing of fine stainless-steel powder with varied final density. JoM. 2017 March; 69: 592-596.
20. Du W, Ren X, Pei Z, Ma C. Ceramic binder jetting additive manufacturing: a literature review on density. Journal of Manufacturing Science and Engineering. 2020 Apr 1;142(4):040801.
21. Mostafaei A, Toman J, Erica LS, Hughes ET, Krimer YL, Chmielus M. Microstructural evolution and mechanical properties of differently heat-treated binder jet printed samples from gas-and water-atomized alloy 625 powders. Acta Materialia. 2017 Feb 1; 124: 280-289.
22. Mostafaei A, De Vecchis PR, Nettleship I, Chmielus M. Effect of powder size distribution on densification and microstructural evolution of binder-jet 3D-printed alloy 625. Materials & Design. 2019 Jan 1; 162: 375-383.

23. Kim FH, Kim FH, Moylan SP. Literature review of metal additive manufacturing defects. Gaithersburg, MD, USA: US Department of Commerce, National Institute of Standards and Technology; 2018 May 17.
24. Lou X, Song M, Emigh PW, Othon MA, Andresen PL. On the stress corrosion crack growth behaviour in high temperature water of 316L stainless steel made by laser powder bed fusion additive manufacturing. Corrosion Science. 2017 Nov 1; 128:140-53.
25. Hedayati R, Yavari SA, Zadpoor AA. Fatigue crack propagation in additively manufactured porous biomaterials. Materials Science and Engineering: C. 2017 Jul 1; 76:457-63.
26. Edwards P, O'conner A, Ramulu M. Electron beam additive manufacturing of titanium components: properties and performance. Journal of Manufacturing Science and Engineering. 2013 Dec 1;135(6).
27. Brennan MC, Keist JS, Palmer TA. Defects in Metal Additive Manufacturing Processes. Journal of Materials Engineering and Performance. 2021 Jul;30(7):4808-18.
28. Åsberg M, Fredriksson G, Hatami S, Fredriksson W, Krakhmalev P. Influence of post treatment on microstructure, porosity, and mechanical properties of additive manufactured H13 tool steel. Materials Science and Engineering: A. 2019 Jan 10; 742:584-9.
29. Chen C, Xie Y, Yan X, Yin S, Fukanuma H, Huang R, Zhao R, Wang J, Ren Z, Liu M, Liao H. Effect of hot isostatic pressing (HIP) on microstructure and mechanical properties of Ti6Al4V alloy fabricated by cold spray additive manufacturing. Additive manufacturing. 2019 May 1; 27:595-605.
30. Moussaoui K, Rubio W, Mousseigne M, Sultan T, Rezai F. Effects of Selective Laser Melting additive manufacturing parameters of Inconel 718 on porosity, microstructure, and mechanical properties. Materials Science and Engineering: A. 2018 Sep 26; 735:182-90.
31. Kaletsch A, Qin S, Herzog S, Broeckmann C. Influence of high initial porosity introduced by laser powder bed fusion on the fatigue strength of Inconel 718 after post-processing with hot isostatic pressing. Additive Manufacturing. 2021 Nov 1; 47:102331.

32. Kumar A, Bai Y, Eklund A, Williams CB. Effects of hot isostatic pressing on copper parts fabricated by binder jetting. Procedia Manufacturing. 2017 July 17; 10: 935-944.
33. Kumar AY, Bai Y, Eklund A, Williams CB. The effects of hot isostatic pressing on parts fabricated by binder jetting additive manufacturing. Additive Manufacturing. 2018 Dec; 24: 115-124.
34. Kumar AY, Wang J, Bai Y, Huxtable ST, Williams CB. Impacts of process-induced porosity on material properties of copper made by binder jetting additive manufacturing. Materials & Design. 2019 Nov 15; 182: 108001.
35. Mostafaei, A, De Vecchis PR, Kimes KA, Elhassid D, Chmielus M. Effect of binder saturation and drying time on microstructure and resulting properties of sinter-HIP binder-jet 3D-printed WC-Co composites. Additive Manufacturing. 2021 October; 46: 102128.
36. Mariani M, Goncharov I, Mariani D, De Gaudenzi GP, Popovich A, Lecis N, Vedani M. Mechanical, and microstructural characterisation of WC-Co consolidated by binder jetting additive manufacturing. International Journal of Refractory Metals and Hard Materials. 2021 Nov; 100: 105639.
37. Dahmen T, Henriksen NG, Dahl KV, Lapina A, Pedersen DB, Hattel JH, Christiansen TL, Somers MAJ. Densification, microstructure, and mechanical properties of heat-treated MAR-M247 fabricated by Binder Jetting. Additive Manufacturing. 2021 March; 39: 101912.
38. Martin E, Natarajan A, Kottilingam S, Batmaz R. Binder jetting of 'Hard-to-Weld' high gamma prime nickel-based superalloy RENE 108. Additive Manufacturing. 2021 March; 39: 101894.
39. Eid KF, Panth M, Sommers AD. The physics of water droplets on surfaces: exploring the effects of roughness and surface chemistry. European Journal of Physics. 2018 Feb 9; 39(2):025804.

40. Saha D, Apelian D. De-lubrication during sintering of P/M compacts: operative mechanism and process control strategy. Worcester, US: Worcester Polytechnic Institute, April 2005. 46p. Report No.: 01-2.
41. Nandwana P, Elliott AM, Siddel D, Merriman A, Peter WH, Babu SS. Powder bed binder jet 3D printing of Inconel 718: Densification, microstructural evolution and challenges☆. Current Opinion in Solid State and Materials Science. 2017 Aug 1;21(4):207-18.
42. Muhammad W, Batmaz R, Natarajan A, Martin E. Effect of binder jetting microstructure variability on low cycle fatigue behaviour of 316L
43. Lai WJ, Ojha A, Luo Z. Effect of Surface Roughness on Fatigue Behavior of 316L Stainless Steel Produced by Binder Jetting Process. In TMS 2022 151st Annual Meeting & Exhibition Supplemental Proceedings 2022 (pp. 164-176). Springer, Cham.
44. Borujeni SS, Shad A, Venkata KA, Günther N, Ploshikhin V. Numerical simulation of shrinkage and deformation during sintering in metal binder jetting with experimental validation. Materials & Design. 2022 Apr 1; 216:110490.

CHAPTER 7:

MECHANICAL PROPERTIES OF SINTERED PARTS

'Do you test it on animals or is it like, cruelty free?' – a Year 6 student at an outreach programme

7.1. Introduction

The aim of additively manufactured components is to compete with their conventionally manufactured counterparts and if possible, replace the conventional manufacturing process. When components have structural and load bearing applications, it is very important to ensure that the printed parts have the mechanical capability to withstand the load bearing environment. Mechanical testing is often conducted on these additively manufactured specimens to evaluate their suitability as replacements of conventionally manufactured counterparts. Mechanical testing often involves measuring and calculating properties like elasticity modulus, tensile strength, hardness, and fatigue behaviour and ensuring that these values are within the safe limits, depending on the application and nature of intended use of the components.

The review of the different studies on mechanical properties of components fabricated by different AM techniques by Lewandowski and Seifi concluded that mechanical properties of parts printed using SLM, EBM and DED methods reported properties similar to those manufactured using casting, forging and metal injection moulding [1]. The review also noticed that the most research on mechanical testing of AM parts involved tensile and compression testing of specimens and the most materials tested were titanium, nickel, and aluminium alloys along with stainless steels. Li et al., focused on the mechanical properties of Binder Jetted components and compared the yield strength and ultimate tensile strength (UTS) with parts manufactured using cold working. The properties were reported to be consistently lower than the cold rolled counterparts.

Porosity is a process response which is inherent of the Binder Jetting process, as has been seen in Chapter 5. Porosity and lack of fusion has been seen as a common reason for compromised mechanical properties. Zwiren and Murphy compared the mechanical properties of conventionally sintered parts with those fabricated using Binder Jetting and concluded that the conventionally sintered parts had lower porosity and higher value of ultimate tensile strength, when sintered at 1260°C. The powder metallurgy samples were compacted at a pressure of 830 MPa which was credited for reducing the porosity significantly, which in turn resulted in the samples having higher values of ultimate tensile strength [3]. Binder Jetted parts made of steels were often strengthened by infiltration with brass and bronze to improve the mechanical properties [4-7]. Elliott et al. improved the tensile strength of Binder Jetted parts made of austenitic stainless steel by using stainless steel nanoparticles [8]. Nandwana et al. stated that infiltration of parts printed using Inconel 718 was considered counterproductive given that a lot of applications require a homogenous microstructure [9].

Mechanical properties like hardness and behaviour under tensile testing can often be explained from the presence or absence of certain phases in the microstructure. As discussed in Section 2.3 in Chapter 2, Inconel 718 is a precipitation strengthened nickel alloy which has an austenitic matrix {γ} in which intermetallic phases like $Ni_3(Al, Ti)$ {γ'}, tetragonal Ni_3Nb {γ"} and orthorhombic Ni_3Nb {δ} are precipitated to provide the mechanical strength that Inconel 718 is known for. There are other tetragonally close packed phases like Fe (Cr, Mo) {σ} and Laves phases that are deleterious for the mechanical properties of the material [10-11]. The presence of carbides like NbC, TiC and Ti(CN) are also detected in the form of small inclusions which promote grain boundary stabilisation and can provide a secondary strengthening mechanism via dispersion into the main γ phase matrix [12].

There has been extensive research on additive manufacturing of Inconel 718, especially with focus on SLM of Inconel 718 [13-16]. The study of formation of Laves phase during welding of Inconel

718 was done by Radhakrishna and Rao et al [17]. They concluded that post-weld heat treatment was essential for reversing the effect of formation of Laves phase. The studies of Popovich et al. concluded that freshly printed SLM specimens of Inconel 718 had dendritic Laves phase and carbide rich zones which dissolved into the γ phase matrix after lengthy post processing including HIP and an eight-hour heat treatment process [18]. The formation of Laves rich zones in the freshly printed samples resulted in lower tensile strength as compared to cast and wrought counterparts [18]. Quantitative studies revealed that the distribution of Laves phase was concentrated at the bottom of the build and it declined with the deposition of layers which slowed down the cooling rate [19]. The tensile strength also was directly affected by this varying distribution of Laves phase. Li et al focused on the effect of heat treatment strategies like solution ageing and double ageing on the hardness of specimens of Inconel 718, printed using SLM [20]. They concluded that freshly printed specimens had segregated Laves phase and carbides presence which underwent homogenisation after heat treatment. However, they found that the hardness of the heat-treated specimens was higher than the freshly printed samples because the hardness was derived from the strengthening of γ" phase by the dissolution of Nb back into the matrix phase. They did not associate the hardness of the specimens with the presence of the Laves phases.

7.2. Results & Discussions

7.2.1 Results

Figure 7.1 (a) to (c) represent the tensile testing results of the printed parts using PVA based liquid binders of different molecular weights and sintered in two different purging environments. It was observed that specimens sintered in an argon environment had a higher ultimate tensile strength (UTS) irrespective of the nature of binder used. The UTS of the samples printed using LMW PVA binder and feedstock were 126 MPa and 97 MPa when sintered solely in argon and in a mixture of N_2/H_2 and argon, respectively. These values were the poorest reported amongst all the samples. When MMW PVA was used as the binder base and part of the modified feedstock, the ultimate

tensile strength was seen to improve. They were measured to be 237 MPa and 170 MPa when sintered in argon and the gas mixture, respectively. Ultimate tensile strength reported for HMW PVA binder and feedstock were 196 MPa and 172 MPa.

The measured values of ultimate tensile strength were low in comparison to other studies which did mechanical testing of Inconel 718 parts manufactured using conventional methods like casting and forging; and other competing additive manufacturing techniques like SLM [21].

Figure 7.2 is a graphical summary of the tensile testing of specimens that were post processed using HIP. Post processing was performed on the two samples that had the highest ultimate tensile strengths, which were the samples printed using MMW and HMW PVA binders and feedstock, both sintered solely in 99.98% argon environment. The post processing drastically elevates the ultimate tensile strength of both the samples. The slope of the MMW PVA specimen is steeper in comparison to the HMW PVA. The specimen which was printed using HMW PVA present in the feedstock and binder underwent a larger change in strain for marginally lower values of stress which is indicative of more ductile behaviour in comparison to the MMW PVA sample. The stress-strain plot of the MMW PVA sample was very similar to brittle materials like glass [22], with a plot being a straight line which ends in brittle fracture. The discrepancy of material responses between the specimens printed using HMW and MMW PVA can be attributed to the human errors introduced into the specimens during the printing process, especially during the manual spreading of feedstock. Slippage between the specimen and the jaws of the UTM was observed during tensile testing of the specimen which was printed using HMW PVA. The specimen printed using MMW PVA based binder and feedstock reported an ultimate tensile strength of 1010 MPa and the HMW PVA specimen had an ultimate tensile strength of 880 MPa. The results of the printed specimens after HIP were better than their cast counterparts and were comparable to the tensile strengths of Inconel 718 specimens printed using SLM [21].

Figure 7.3 (a) and (b) represents the macro hardness data of the sintered and HIPed samples, respectively. In Fig. 7.3 (a), it was observed that the hardness of the samples printed using MMW and HMW base binders and feedstock have similar levels of hardness. The sample printed using MMW PVA based binder and feedstock had the highest hardness when sintered solely in argon. The hardness of the samples printed using LMW binders and feedstock were measured to be the lowest

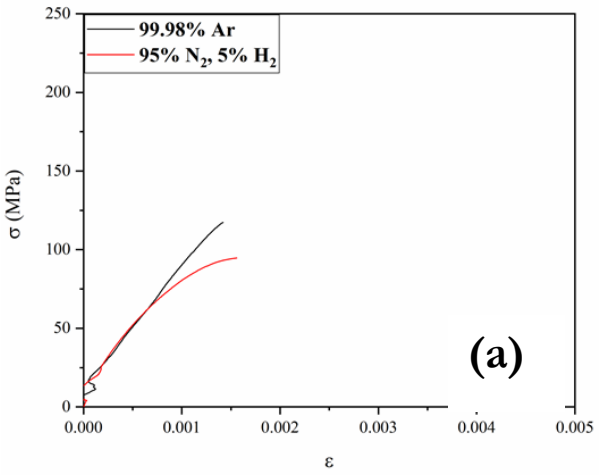

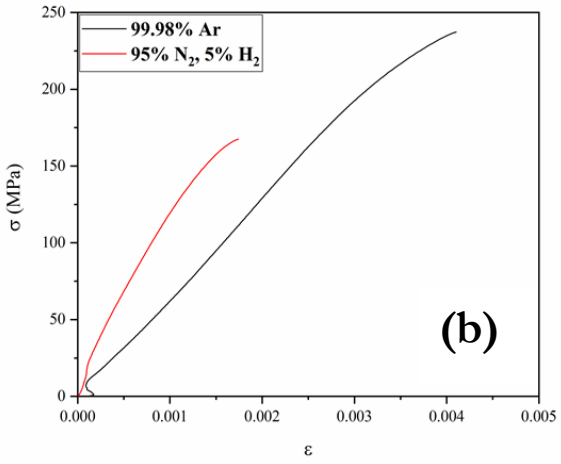

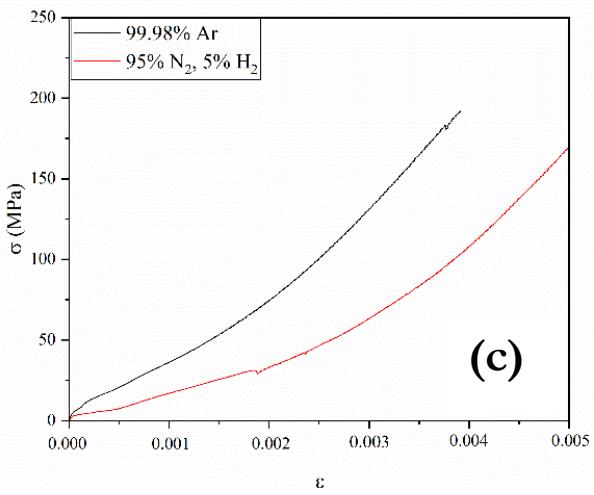

Fig 7.1 Stress vs Strain plots of Inconel 718 tensile specimens printed using different PVA based binders and feedstock: (a) LMW (b) MMW (c) HMW

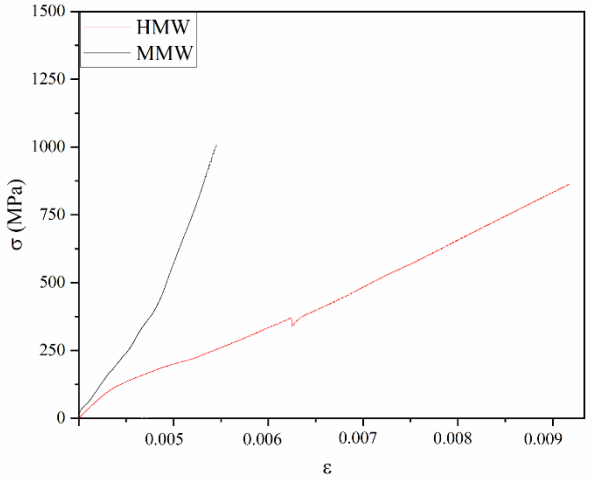

Fig 7.2 Stress vs Strain plot of Inconel 718 tensile specimens sintered in 99.98% argon and post processed using HIP.

The hardness of the samples was observed to increase after they were post processed using HIP and it was observed that the sample printed using MMW based binder and feedstock which was sintered in argon still had the highest value of hardness. The effect of HIP was not that pronounced on the samples printed using LMW based binder and feedstock.

The hardness of the printed and sintered samples was consistently lower than values reported by studies on SLM of Inconel 718 [23-24]. However, the specimens printed using MMW based binder

and feedstock had a higher value of hardness in comparison to reported values in studies which focused on BJT of nickel superalloys [25].

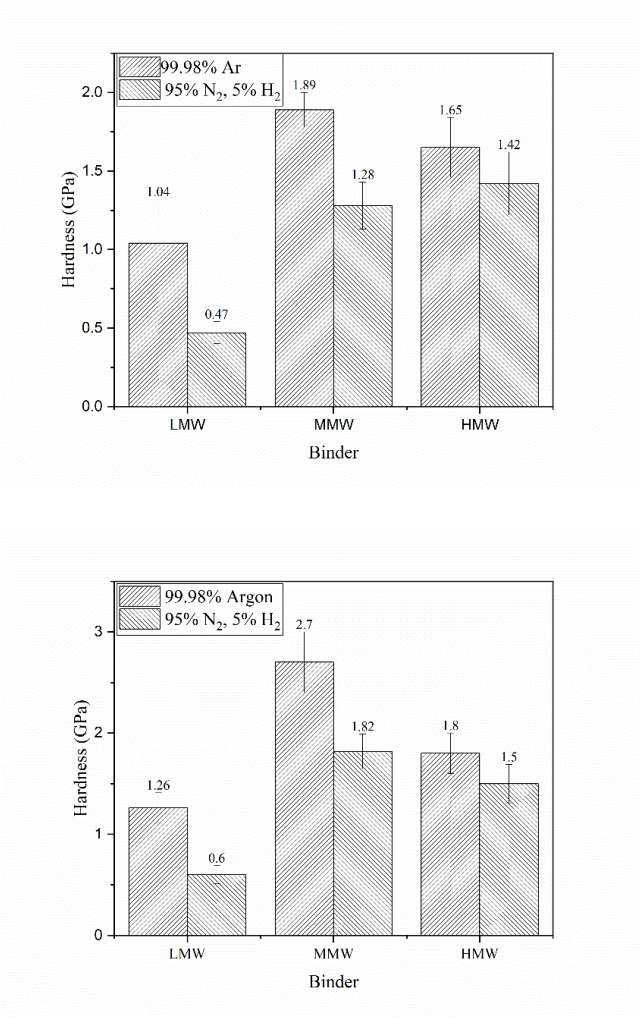

Fig 7.3 Variation in hardness in specimens: (a) freshly sintered (b) sintered + HIP

7.2.2 Phase Analysis and Mechanical Properties

Figure 7.3 represents the X ray diffraction (XRD) based phase analysis of specimens processed in different sintering environments including post-processing strategies like HIP. These specimens were printed using MMW based binder and feedstock. The XRD scans revealed that none of the specimens contained Laves phases or any other TCPs which are usually deleterious to the mechanical properties of the printed parts, as discussed in Table 2.1. This contrasts with samples

printed using SLM, which tend to have Laves phases distributed within the microstructure, as discussed in section 7.1 earlier. Stevens et al. mapped the distribution of Laves phases in specimens printed out of Inconel 718, using SLM and concluded that the regions having a higher percentage of Laves phase had higher values of hardness, thus attributing hardness to Laves phase content in specimens printed using SLM [26]. Kotzem et al. processed Inconel 718 using EBM and observed that ageing of the specimens after sintering led to the dissolution of the Laves phases in the γ matrix, reducing the hardness [27]. Laves phases in Inconel 718 lower the ductile-brittle transition temperature to 0.6 T_m to 0.8 T_m, where T_m is the melting point of the alloy [28-29]. Laves phases like Fe_2Nb, which has C14 Strukturbericht designation type has one feasible shear planes at (1120) when maintained at ambient temperature [30]. This inhibits plastic deformation, hence its association with brittle behaviour. The absence of Laves and δ phase is the cause of low hardness reported in Fig. 7.3 in comparison with counterparts manufactured using SLM or more conventional alternatives like casting. There was evidence of nitrogen uptake in the specimens sintered in a N_2/H_2 environment. The nitrogen reacted with the chromium present in the alloy to form Cr_2N and as discussed in Section 6.2.2 in Chapter 6, it interferes with the necking phenomenon in between two particles during the sintering process which leads to incomplete fusion, increased porosity, and subsequently bad mechanical properties. The nitrogen uptake is not reduced after HIP, and it remains present in the microstructure. The specimens which were sintered in an argon environment and underwent HIP process had γ" phase present in the microstructure as well. The γ" phase has a secondary strengthening effect on the matrix which would explain improvement in mechanical properties from a compositional standpoint.

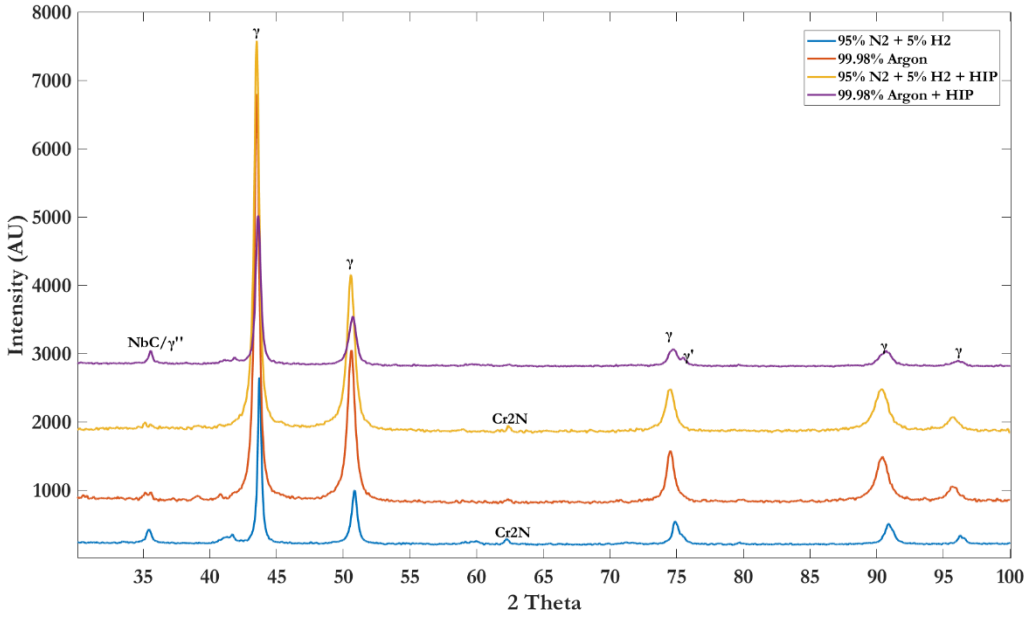

Fig 7.4 Phase analysis of samples printed with MMW PVA based binder and feedstock with different sintering and post-processing strategies.

7.3 Chapter Summary

Chapter 7 is the final results-oriented chapter, and it focuses on the mechanical testing which was performed to gauge the mechanical properties of the specimens and investigate the role of variables like molecular weight of PVA used in the binders and the feedstock, sintering environment, and post-processing steps like HIP. After Chapter 6, it was obvious that the specimens sintered in an N_2/H_2 environment would not perform well during mechanical testing due to the high values of porosity and lack of sintering. Tensile testing of the specimens confirmed better UTS of specimens sintered in 99.98% argon over the specimens which had nitrogen uptake due to presence of N_2 in the sintering environment. Specimens printed using MMW PVA binder and feedstock and sintered solely in an argon environment had the highest values of UTS. However, the values of UTS of all the sintered specimens were very low in comparison to Inconel 718 parts printed using competing methods like SLM. The UTS was improved in both MMW and

HMW PVA based specimens sintered solely in argon by a factor of 4.26 and 4.48. It was interesting to observe that the HMW specimen improved marginally more than the MMW counterpart, but it was the specimen printed using MMW PVA binder and feedstock which had the highest value of UTS, which also was in a similar range of UTS reported by other Binder Jetting studies on Inconel 718.

XRD assisted phase analysis revealed that the none of the samples has δ and Laves phases present in its microstructure, which lowered the hardness of the specimens in general. The samples sintered in an N_2/H_2 environment had Cr_2N present in the microstructure which confirmed nitrogen uptake as the reason due to which the specimens sintered in the N_2/H_2 environment had poor sintering and mechanical properties.

References

1. Lewandowski JJ, Seifi M. Metal additive manufacturing: a review of mechanical properties. Annual Review of Materials Research. 2016 Jul 1; 46:151-86.
2. Li M, Du W, Elwany A, Pei Z, Ma C. Metal binder jetting additive manufacturing: a literature review. Journal of Manufacturing Science and Engineering. 2020 Sep 1;142(9).
3. Zwiren A, Murphy TF. Comparison of binder jetting additive manufacturing to press and sinter 316L stainless steel. Cinnaminson, US: GKN Hoeganaes, 2018; 17p.
4. Doyle M, Agarwal K, Sealy W, Schull K. Effect of layer thickness and orientation on mechanical behavior of binder jet stainless steel 420+ bronze parts. Procedia Manufacturing. 2015 Jan 1; 1:251-62.
5. Sachs E, Allen S, Cima M, Wylonis E, Guo H. Production of injection molding tooling with conformal cooling channels using the three dimensional printing process. Polymer Engineering & Science. 2000 May, 40(5): 1232-1247.
6. Crane NB, Wilkes J, Sachs E, Allen SM. Improving accuracy of powder based SFF processes by metal deposition from a nanoparticle dispersion. Rapid Prototyping Journal. 2006 Oct 1.

7. Cordero ZC, Siddel DH, Peter WH, Elliott AM. Strengthening of ferrous binder jet 3d printed components through bronze infiltration. Additive Manufacturing. 2017 May; 15: 87-92.
8. Elliott A, Al Salihi S, Merriman AL, Basti MM. Infiltration of nanoparticles into porous binder jet printed parts. American Journal of Engineering and Applied Sciences. 2016 Jan 1;9(1).
9. Nandwana P, Elliott AM, Siddel D, Merriman A, Peter WH, Babu SS. Powder bed binder jet 3D printing of Inconel 718: Densification, microstructural evolution and challenges☆. Current Opinion in Solid State and Materials Science. 2017 Aug 1;21(4):207-18.
10. Belan J. GCP and TCP phases presented in nickel-base superalloys. Materials Today: Proceedings. 2016 Jan 1;3(4):936-41.
11. Rae CM, Karunaratne MS, Small CJ, Broomfield RW, Jones CN, Reed RC. Topologically close packed phases in an experimental rhenium-containing single crystal superalloy. Superalloys. 2000; 2000:767-76.
12. Li RB, Yao M, Liu WC, HE XC. Isolation and determination for δ, γ' and γ'' phases in Inconel 718 alloy. Scripta Materialia. 2002; 46: 635-638.
13. Kruth JP, Leu MC, Nakagawa T. Progress in additive manufacturing and rapid prototyping. Cirp Annals. 1998 Jan 1;47(2):525-40.
14. Kruth JP, Levy G, Klocke F, Childs TH. Consolidation phenomena in laser and powder-bed based layered manufacturing. CIRP annals. 2007 Jan 1;56(2):730-59.
15. Osakada K, Shiomi M. Flexible manufacturing of metallic products by selective laser melting of powder. International Journal of Machine Tools and Manufacture. 2006 Sep 1;46(11):1188-93.
16. Qi H, Azer M, Ritter A. Studies of standard heat treatment effects on microstructure and mechanical properties of laser net shape manufactured Inconel 718. Metallurgical and Materials Transactions A. 2009 Oct;40(10):2410-22.
17. Radhakrishna CH, Prasad Rao K. The formation and control of Laves phase in superalloy 718 welds. Journal of Materials Science. 1997 Apr;32(8):1977-84.

18. Popovich VA, Borisov EV, Popovich AA, Sufiiarov VS, Masaylo DV, Alzina L. Impact of heat treatment on mechanical behaviour of Inconel 718 processed with tailored microstructure by selective laser melting. Materials & Design. 2017 Oct 5; 131:12-22.
19. Zhang B, Wang P, Chew Y, Wen Y, Zhang M, Wang P, Bi G, Wei J. Mechanical properties, and microstructure evolution of selective laser melting Inconel 718 along building direction and sectional dimension. Materials Science and Engineering: A. 2020 Sep 9; 794:139941.
20. Li X, Shi JJ, Wang CH, Cao GH, Russell AM, Zhou ZJ, Li CP, Chen GF. Effect of heat treatment on microstructure evolution of Inconel 718 alloy fabricated by selective laser melting. Journal of Alloys and Compounds. 2018 Oct 5; 764:639-49.
21. Popovich VA, Borisov EV, Popovich AA, Sufiiarov VS, Masaylo DV, Alzina L. Functionally graded Inconel 718 processed by additive manufacturing: Crystallographic texture, anisotropy of microstructure and mechanical properties. Materials & Design. 2017 Jan 15; 114:441-9.
22. Zemanova A, Schmidt J, Šejnoha M. Evaluation of tensile strength of glass from combined experimental and numerical analysis of laminated glass. WIT Transactions on The Built Environment. 2018 Dec 3; 175:29-39.
23. Amato KN, Gaytan SM, Murr LE, Martinez E, Shindo PW, Hernandez J, Collins S, Medina F. Microstructures, and mechanical behaviour of Inconel 718 fabricated by selective laser melting. Acta Materialia. 2012 Mar 1;60(5):2229-39.
24. Gong X, Wang X, Cole V, Jones Z, Cooper K, Chou K. Characterization of microstructure and mechanical property of Inconel 718 from selective laser melting. In: International Manufacturing Science and Engineering Conference 2015 Jun 8 (Vol. 56826, p. V001T02A061). American Society of Mechanical Engineers.
25. Mostafaei A, Behnamian Y, Krimer YL, Stevens EL, Luo JL, Chmielus M. Effect of solutionizing and aging on the microstructure and mechanical properties of powder bed binder jet printed nickel-based superalloy 625. Materials & Design. 2016 Dec 5; 111:482-91.

26. Stevens EL, Toman J, To AC, Chmielus M. Variation of hardness, microstructure, and Laves phase distribution in direct laser deposited alloy 718 cuboids. Materials & Design. 2017 April 5; 119: 188-198.
27. Kotzem D, Arold T, Niendorf T, Walther F. Influence of specimen position on the build platform on the mechanical properties of as-built aged electron beam melted Inconel 718 alloy. Materials Science & Engineering A. 2020; 772: 138785.
28. Livingston JD. Laves-Phase Superalloys? Physica Status Solidi. 1992; 131:415-423.
29. Kumar KS. Laves phase-based materials: microstructure, deformation modes and properties. MRS Online Proceedings Library (OPL). 1996;460.
30. Chisholm MF, Kumar S, Hazzledine P. Dislocations in complex materials. Science. 2005 Feb 4;307(5710):701-3.

CHAPTER 8: SUMMARY, CONCLUSIONS & FUTURE WORK

'*In conclusion, I would like to conclude that I have concluded my thesis'* – **author after realising that he has finished writing the thesis.**

This chapter recaptures the findings which were discussed in Chapters 4, 5, 6 and 7 along with some possibilities of future work which can be explored in other studies.

8.1 Conclusions

In **Chapter 4**, the FT4 based rheological evaluation of the pure Inconel 718 and the different modified feedstocks has shown that the addition of granular PVA improved the permeability of the feedstocks in comparison to the virgin Inconel 718. An increase in permeability translated into better powder spreadability which would improve the printing procedure. The feedstock with MMW PVA granules was found to have the highest value of permeability among all the candidates. However, The VFR flow test, which is a measure of powder stability did not provide a clear trend. The shear test showed high values of shear stress for the MMW and HMW PVA based feedstocks which was contrary to the trends which were obtained from the permeability tests.

The temperature-based variation of surface tension and dynamic viscosity of the binders was found to be low enough to ensure that there is no substantial change of properties over a range of 30°C. The Z number was calculated for the binders at 30°C and it was concluded from their values that the binders could be reliably dispensed from the printhead device.

The powder-binder interaction was evaluated in **Chapter 5** where the static sessile drop testing method was used to measure the contact angle between the droplet of binder and the powder bed. The performance of the PVA based binders was benchmarked initially against a solid Inconel 718 substrate and it was concluded that the PVA based binders had high contact angles which was

indicative of their poor wetting with the solid substrate. However, when the solid substrate was substituted with the powder bed, it was seen that the droplets had better lateral spreading and vertical infiltration action. The MMW PVA based binder had the lowest contact angle with the powder bed having the corresponding MMW PVA based feedstock. The MMW and HMW based PVA binders had better wettability compared to a commercial binder which was tested against virgin Inconel 718. The MMW PVA based binder had the overall best interaction with the corresponding feedstock because of its optimum polymeric chain length which caused intra-chain crosslinking which allowed the aqueous component of the binder to infiltrate the powder bed without any hindrance. The permeability results from Chapter 4 were also taken into consideration, where the MMW PVA had exhibited the highest value of permeability, which would have decreased the chance of agglomerates and introduces spacing between adjacent metal powder particles, which gave the liquid binder a better chance to penetrate the powder bed.

Porosity was evaluated as a process response in the sintered specimens in **Chapter 6**. The literature concluded that the mechanism of pore formation in Binder Jetting was like that in metal injection moulding. The role of the jetting action by the printhead device on part quality by comparing it with manual binder deposition and it was found out that the reliable dispensing action of the printhead led to better powder-binder interaction which led to better sintering and consequently lower porosity and a contiguous surface. Manual deposition of the binder on the powder bed led to poor binder penetration and consequently high porosity characterised by a lack of fusion between the particles.

The role of the sintering environment was also seen on porosity, and it was observed that porosity was lower when the printed parts were sintered in a 99.98% argon purged environment. The porosity levels were calculated to be 7.21, 5.34 and 9.77% for parts that were printed using LMW, MMW and HMW PVA based binder and feedstock, respectively. The porosity of the MMW and HMW specimens reduced further to 1.04 and 1.35%, respectively when they were post-processed

using HIP, which reduced the porosity to levels which were reported in literature using commercial binders and systems. Specimens were also pre-sintered in an environment of 95% N_2 + 5% H_2 and then sintered in 99.98% argon. The pre-sintering in a nitrogenous environment caused the chromium present in the alloy to react with the nitrogen to form Cr_2N, which interfered with the 'necking' process, thus resulting in parts having poor porosity. Post-processing of these parts did not lower the porosity to a level which was comparable to results reported in available literature.

Chapter 7 discussed the results of tensile and hardness testing of the specimens which were printed using different PVA based binders and sintered in the two previously mentioned environments. Tensile testing of the samples revealed that the ones sintered in 99.98% argon environment had better UTS than the specimens that were sintered in a nitrogenous environment. This was due to the uptake of nitrogen in the form of Cr_2N which stunted the sintering process, thus weakening the parts. The UTS of the sintered samples, irrespective of nature of binder or sintering environment used was very poor in comparison to values reported by available reports. The hardness of the specimens was also found to lower than their counterparts manufactured using SLM, as reported in literature. Post-processing of the specimens sintered in 99.98% argon led to a substantial improvement in the mechanical properties, with the samples printed using MMW PVA based binder and feedstock reporting a post HIP UTS of 1010 MPa, which was comparable to other reports of Binder Jetting of nickel superalloys.

The XRD assisted phase analysis detected the presence of Cr_2N in specimens sintered in a N_2/H_2 environment, which confirmed the phenomenon of nitrogen uptake by the chromium present in the Inconel 718 composition. It also detected a lack of δ and Laves phases in the microstructure of all the sintered specimens. This was considered as a positive over other competing AM methods like SLM, which has consistently reported the formation of Laves phases in the microstructure which are detrimental for the mechanical strength of the parts. However, δ phase is also

responsible for imparting hardness to the parts, which explained the relatively low hardness of the specimens.

8.2 Proposed Areas of Future Work

The future work can be further classified into two parts, experiments which were planned but could not be executed due to delays brought upon by the CoVID 19 pandemic and work which can be done to develop this body of work further.

8.2.1 Powder-binder interaction

The original work plan included an experimental approach to the powder-binder interaction which involved study of the infiltration process of the binder into the powder bed. The extent of the lateral spreading and vertical penetration of the binder could be experimentally mapped using a fluorescent dye which could be mixed with the binders and could be monitored in a dark room using an ultraviolet light source. The findings along with that obtained from the sessile drop testing would have been a better study of the powder-binder interaction.

Numerical simulation of the powder-binder interaction was out of the scope of the work which has been undertaken. However, the expertise of a simulation expert may be solicited to numerically model the above-mentioned experiment and consider different parameters like permeability and inter-particle spacing and the correlate the infiltration behaviour of the binder with experimental results. It can also efficiently investigate controllable factors like temperature of the binder and the powder bed which might positively affect the binder penetration. Promising numerical simulations can pave the way for an experimental study.

8.2.2 Evaluation of Porosity

The current work has evaluated the porosity of the processed parts using image processing of micrographs of their polished surfaces. This process has been carried out in multiple studies and is considered a reliable technique for preliminary porosity studies. A parallel study of porosity

could be conducted using X ray microtomography (MicroCT) as a tool. The 3D imaging technique can also investigate 3D porosity distribution, pore size and morphology; and study interconnected pores which cannot be studied using image processing, which is a 2D technique, and hence was out of scope for the current work.

8.2.3 Sintering environment, post processing and mechanical testing strategies,

The application of Inconel 718 include use in gas turbines blades and aeronautical components which are exposed to high operating temperatures. Mechanical and thermal fatigue are issues which were not studied in this work because of time constraints brought upon by the pandemic. An extensive experimental fatigue and creep study of specimens printed using MMW PVA based binders and feedstock and sintered in 99.98% argon purged environment would provide a more comprehensive picture of the feasibility of adopting PVA based binders for processing niche superalloy powders using BJT.

The effect of different sintering environments has been seen in this body of work. However, vacuum sintering could not be performed on the specimens due to lack of time. Vacuum sintering is an industry standard in the metal injection moulding and BJT industry and can be done for specimens printed using MMW PVA binder and feedstock.

HIP was used as the main post-processing strategy in this body of work. However, HIP is an expensive post-processing strategy that would limit the extent to which PVA binders can be adopted to only niche industries, where product quality is paramount, and price is only secondary. The efficiency of post-processing strategies like solution ageing and annealing on improving part quality may be investigated further in future studies.

8.3 Concluding Remarks

The body of work which has been described in this thesis strived to investigate the feasibility of using PVA based binders to process a niche alloy using BJT. It has been demonstrated for the first time in the current work that an aqueous PVA based binder can be used in a standard inkjet system for binder jetting of a very niche and less investigated strategic alloy Inconel 718. The combination of an aqueous PVA binder of medium molecular weight and modified feedstock, as an innovative approach, has provided similar strength, hardness, and porosity in Inconel 718 upon post-processing via HIP, when compared to commercial binder jetting system.

The future work section has emphasised on the need to back this work up with more investigation of a fundamental nature with greater supplementary characterisation to be able to see the entire picture and realise the potential of this methodology.

Appendix I: Gibbs Free Energy Calculations

The Appendix I is relevant for the calculations which have been mentioned in Section 5.2.3, where the Gibbs free energy (ΔG_m) was calculated to ascertain if the PVA granules would dissolve readily when exposed to the liquid PVA binder.

The Gibbs free energy is expressed in the form of the Flory-Huggins equation, as is provided by Equation 5.2. The equation is mentioned below as:

$$\Delta G_m = RT[n_1 \ln \phi_1 + n_2 \ln \phi_2 + n_1 \phi_2 \chi_{12}$$

Where, $\Delta G_m, R, T, n_1, n_2, \phi_1, \phi_2, \chi_{12}$ are the Gibbs free energy, universal gas constant, quantity of solvent in moles, quantity of solute in moles, solvent volume fraction, solute volume fraction and mixing parameter, respectively.

Universal gas constant, R = 8.314 J mol^{-1} K^{-1}

Operating temperature, T = 303 K

Mixing parameter, χ_{12} = 0.32

Density of PVA at 303 K = 1.19 g/cc

For LMW PVA,

n_1 = 9.99 x 10^{-12} mol; ϕ_1 = 0.042

n_2 = 1.06 x 10^{-8} mol; ϕ_2 = 0.958

Substituting the values in the Flory-Huggins equation,

$$\Delta G_m^{LMW} = 8.314 \times 303 \times [(9.99 \times 10^{-12}) \times ln\,(0.042) \times (1.06 \times 10^{-8}) \times ln\,(0.958) + (9.99 \times 10^{-12} \times 0.958 \times 0.32)]$$

$$\Longrightarrow \Delta G_m^{LMW} = -(0.07 \times 10^{-6})\,J$$